Aus dem Institut für Zahn-, Mund- und Kieferheilkunde (CC3)
Abt. Orale Struktur- und Entwicklungsbiologie
der Medizinischen Fakultät Charité – Universitätsmedizin Berlin

DISSERTATION

Concerning the lack of a muscular antagonist to the lateral pterygoid

Morphogenetic and morphological investigations of the murine temporomandibular joint and masticatory muscles from stages E13.25 to P4

zur Erlangung des akademischen Grades
Doctor medicinae dentariae (Dr. med. dent.)

vorgelegt der Medizinischen Fakultät
Charité – Universitätsmedizin Berlin

von

Esther María Fernández Rubio

aus Madrid

Datum der Promotion: 17.09.2021

TABLE OF CONTENTS

LIST OF FIGURES

LIST OF TABLES

1 ABSTRACT

During physiological function of the temporomandibular joint, we have to rely only on elastic structures (in particular the bilaminar zone) for repositioning of the articular disc. A real muscle, however, would be functionally more reasonable. In patients, a decrease of this elasticity is possibly one of the reasons for temporomandibular joint malfunctions, which affect between 16% and 36% of the population (March 2020).

This thesis assesses the morphogenesis of the murine (*Mus musculus*) temporomandibular joint with particular regard to the masticatory muscles, to throw light on this topic. To that end, a collection of 11 murine heads ranging from prenatal stages E13.25 to E20 was used and early postnatal stages P0 to P4, which were prepared as histological sections (thickness 8-10 µm) and stained conventionally (HE, TRAP, Safranin O/Fast green, Trichrome and Alcian blue) in order to examine them with light microscopy. Next, the temporomandibular joint and selected surrounding structures, along with the masticatory muscles, were three-dimensionally reconstructed using analySIS® software. Subsequently, specific morphometric analyses were performed.

The evaluation of the results led to the following conclusions:

1. The mechanical aspect of developmental processes has been brought more into focus again by recent research groups. Our morphometric study serves as a contribution towards testing the descriptions of mechanical forces explained by Blechschmidt, who maintained that muscles arise from mesenchymal tissue, which is stretched under the direct mechanical forces of the developing skull. The anterior region of the temporomandibular joint, where most of the masticatory muscles are situated, increases sixfold in size from stages E14.5 to P4, whereas the posterior region, where instead any muscle formation, the bilaminar zone was observed, only increases by twofold in size. This could be one of the reasons for the lack of an antagonist to the lateral pterygoid muscle.
2. Some ambiguities in the knowledge of fundamental embryology regarding the masticatory muscles of the mouse, such as the regions of insertion and the number of bellies, were clarified.
3. Taken together, the present investigation provides a comprehensive view of the morphogenesis and morphology of the mouse temporomandibular joint and the selected neighboring structures, and it enables this model organism to be used for further studies.

2 ZUSAMMENFASSUNG

Während der physiologischen Funktion des Kiefergelenks, müssen wir uns nur auf elastische Strukturen (insbesondere die bilaminäre Zone) zur Repositionierung des Discus articularis verlassen. Ein echter Muskel wäre jedoch funktionell sinnvoller. Bei Patienten ist eine Abnahme dieser Elastizität möglicherweiser einer der Gründe für Funktionsstörungen des Kiefergelenks, die zwischen 16% und 36% der Bevölkerung betreffen (März 2020).

Es wurden in der vorliegenden Arbeit die Morphogenese des Kiefergelenks der Maus (*Mus musculus)* unter besonderer Berücksichtigung der Kaumuskulatur untersucht. 11 Mäuseköpfe der prenatalen Stadien E13.25-E20 und der frühen postnatalen Stadien P0-P4 wurden verwendet. Hierzu wurden die histologische Schnittserien (Dicke 8-10 µm) präpariert und konventionell (HE, TRAP, Safranine O/Fast green, Trichrom und Alcianblau) gefärbt. Nach mikroskopischer Analyse des vorliegenden Materials wurden das rechte Kiefergelenk und benachbarte Strukturen, sowie die Kaumuskulatur mit Hilfe der Software analySIS® dreidimensional rekonstruiert. Anschließend wurden spezifische morphometrische Analysen durchgeführt.

Folgende Ergebnisse konnten gewonnen werden:

1. Der mechanische Aspekt von Entwicklungsprozessen stellt wieder ein aktuelles Forschungsgebiet der Grundlagenforschung dar. Unsere morphometrischen Befunde dienen als Beitrag zur Prüfung der Hypothese von Blechschmidt, der mechanische Kräfte (insbesondere Dehnung durch den sich entwickelnden Schädel) als Ursache für die Differenzierung von Muskulatur aus mesenchymalen Gewebe annahmen. Der vordere Bereich des Kiefergelenks, in dem sich der Hauptanteil der Kaumuskulatur befindet, vergrößert sich von Stadium E14.5 auf P4 um das Sechsfache, während sich der hintere Bereich, in dem keine Muskelbildung, sondern die bilaminäre Zone zu beobachten ist, nur zweimal vergrößert. Dies könnte einer der Gründe für das Fehlen eines Antagonisten des Musculus pterygoideus lateralis sein.
2. Einige Unklarheiten in der Kenntnis der grundlegenden embryologischen Entwicklung bezüglich der Kaumuskulatur der Maus, wie zum Beispiel die Insertionsregionnen und die Anzahl der Bäuche, könnten geklärt werden.
3. Insgesamt bietet die vorliegende Untersuchung einen umfassenden Überblick über die Morphogenese und Morphologie des Kiefergelenks der Maus und der ausgewählten Nachbarstrukturen und ermöglicht es, diesen Modellorganismus für weitere Untersuchungen zu nutzen.

3 INTRODUCTION

3.1 The temporomandibular joint of the mouse

3.1.1 Phylogeny

The temporomandibular joint is a unique structure in mammals since it differs from other synovial joints in its development, structure, function, biomechanical properties and molecular genetics. The complex embryological development and anatomy makes the study of its phylogeny necessary for a better understanding.

Non-mammalians have a primary jaw joint composed by the articular, which is formed by the most proximal part of Meckel's cartilage and is situated in the lower jaw, and by the quadrate that is located in the skull. In 1837, Reichert proposed that these two bones passed into the mammalian middle ear as the malleus and the incus (Reichert, 1837) (Fig. 1). In 1912, Gaupp extended Reichert's theory and explained that during evolution the incorporation of the primary jaw joint into the mammalian middle ear was possible due to the formation of a new jaw joint, known as the temporomandibular joint, that was unique to mammals and articulated the upper and lower jaws (Gaupp, 1912). Other explanations have been given, but Reichert's theory has recently been confirmed by developmental and molecular biology, as well as by the evidence from fossil records and by the study of marsupials, who use the joint between the malleus and incus as the primary jaw joint in the first weeks after birth (Anthwal et al., 2013).

The formation of the temporomandibular joint has been explained in terms of morphological, functional, and dietary hypotheses. The first of these is based on fossil records that are said to show how areas of insertions of the jaw-closing musculature moved into an anterior position. As a result, the forces in the primary jaw joint decreased, while increasing in the dentary. Hence, a new joint between the dentary and the squamosal formed (Crompton, 1963). The functional hypothesis claimed that since sound is transmitted in fish through water, terrestrial animals were forced to evolve a better system. In this way, they developed structures close to the ground, i.e. the middle ear (Pirlot, 1976). The advent of a temporomandibular joint was also linked to a change in tooth shape and the kind of mastication since some mammal-like reptiles increased their food requirements and their joint was not able to resist the forces (Kermack, 1972).

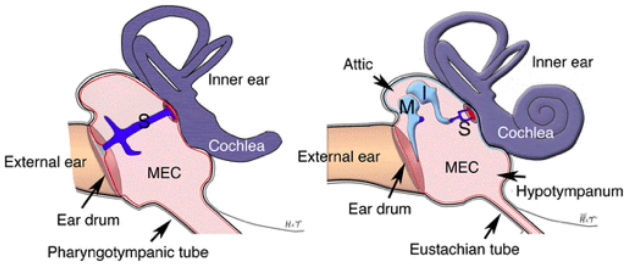

a **b**

Fig. 1: Schematic representation of the middle ear in non-mammals and mammals.

a: Schematic of a non-mammal middle ear formed by only one ossicle, which is known as stapes in reptiles and as columella in birds.

b: Schematic of a mammal middle ear with three ossicles, in particular malleus, incus and stapes.

S: stapes, M: malleus, I: incus, MEC: middle ear cavity.

Depiction obtained from Tucker (2017).

3.1.2 Prenatal development

The temporomandibular joint is a bilateral synovial articulation that displays several specific features: it develops late in embryonic life (Purcell et al., 2009), and unlike most other joints that originate from segmentation, i.e. due to the separation of a common mesenchymal primordia, the temporomandibular joint is classified as an appositional joint, which means that the two mesenchymal primordia (previously separated) move closer (Radlanski, 2018). Besides that, its articular structures are covered by fibrous rather than hyaline cartilage and the two bones of the joint do not articulate with each other directly, rather a disc interposes between them (Purcell et al., 2009). Moreover, it is the only joint in the body whose end point, i.e. the teeth, are distant from the joint itself (Ohshima et al., 2011).

As in humans, the temporomandibular joint of the mouse develops in three stages (Mérida Velasco et al., 1999; Liang et al., 2016). First, the “initiation or appearance stage” when the condylar and glenoid blastemas appear. Next, the “growth or cavitation stage” with the formation of the articular disc, the joint cavities, the synovial membrane, and the secondary cartilage of the condylar process. Finally, the “maturation or completion stage” when all structures grow and the vascular network develops.

Thus, the temporomandibular joint consists of multiple tissues, including the condylar head of the mandible, the glenoid fossa of the temporal bone, the articular disc placed between these bones that divides the joint space into two cavities, the capsule, and associated muscles, tendons, and ligaments (Fig. 2). As mentioned above, the development of the joint starts with the appearance of two mesenchymal condensations, the condylar and glenoid blastemas. The first one appears between stage E12.75 (Tsuchikawa et al., 2010) and stage E15 (Ohshima, 2011) and

is situated superior to Meckel's cartilage, inferior to the trigeminal ganglion and anterior to the primordia of the middle ear ossicles. It undergoes endochondral ossification and develops secondary cartilage from the periosteum of the ossifying mandible (Shibata et al., 2013). The glenoid blastema derives from the otic capsule and it is located posterior to the zygomatic arch. It forms between stage E13 (Tsuchikawa et al., 2010) and stage E14.5 (Gu et al., 2014; Liang et al. 2016) and subsequently ossifies primarily through intramembranous bone formation (Liang et al. 2016). The articular disc appears first as a mesenchymal condensation around stage E15.5 (Liang et al. 2016) and stage E18 (Frommer, 1964; Tsuchikawa et al., 2010) between the condylar and the glenoid blastemas, and it matures into fibrocartilage in the late fetal stages. The formation of the superior or upper joint cavity starts around stage E16 (Ohshima et al., 2011) with the expansion of the joint space and is completed one day after its first appearance. The inferior or lower joint cavity forms around stage E18 (Ohshima et al., 2011) due to apoptosis and is also completed one day after its first appearance. The lateral pterygoid attaches to the articular disc, the neck of the condyle and the joint capsule. Therefore, the temporomandibular joint is fully-formed between stage E16 (Tsuchikawa et al., 2010) and stage E20 (Frommer, 1964), with the formation of the fibrous capsule, the tendon of the lateral pterygoid muscle and various ligaments.

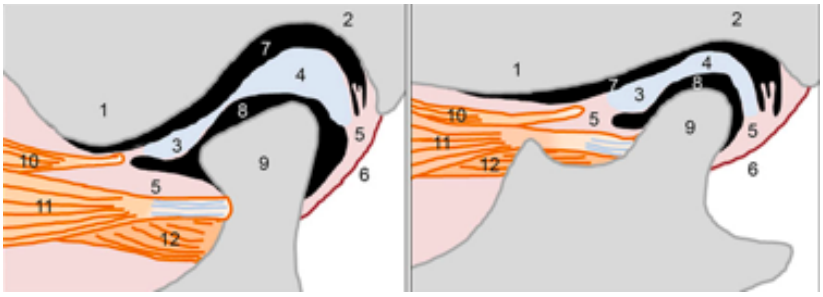

Fig. 2: Schematic representation of the temporomandibular joint in humans and mice.

The main morphological differences between human and mouse temporomandibular joints are: the lack of articular eminence, the glenoid fossa being quite flat, the lateral pterygoid being less voluminous, the superior joint cavity forming first, and the articular disc rarely becoming fibrocartilaginous.

a: Human temporomandibular joint.

b: Mouse temporomandibular joint.

1: articular eminence, 2: glenoid fossa, 3: anterior band of the articular disc, 4: posterior band of the articular disc, 5: bilaminar zone; 6: posterior portion of the joint capsule, 7: superior joint cavity, 8: inferior joint cavity, 9: condyle, 10 and 11: superior head of the lateral pterygoid, 12: inferior head of the lateral pterygoid.

Depiction obtained from Suzuki & Iwata (2016).

3.2 The masticatory muscles of the mouse

Unlike most other mammals, rodents have only one incisor and three molars in each quadrant separated by a large diastema and, as a result, they have two feeding modes: gnawing at the incisors and chewing at the molars. However, due to a mismatch, these teeth cannot be in occlusion at the same time, so they are forced to make rapid anterior-posterior movements (Abe et al., 2008; Suzuki & Iwata, 2016). Hence, the masticatory musculature of rodents has become highly specialized (Cox & Jeffery, 2011). These muscles arise from the skull and insert into the mandible and are classified into two functional groups: the jaw-opening or jaw-depressors, namely the digastric, and the jaw-closing or jaw-adductors, which comprise the masseter, the temporalis, and the lateral and medial pterygoids. The present study will focus on this last group.

3.2.1 Morphology and functions

There is no consensus in the nomenclature of the masticatory muscles, mainly due to the method employed to define them. Classically, they have been classified based on their bony attachments, tendinous architecture, and innervation (Druzinsky et al., 2011). The two publications that have specifically examined the anatomy of the masticatory musculature in the *Mus musculus* used the following nomenclature: Patel (1978) divided them into superficial masseter and deep masseter (subdivided into anterior and posterior), temporalis (subdivided into anterior, posterior and zygomaticus), and pterygoids (external and internal). Baverstock et al., (2013) classified them into superficial masseter, deep masseter and zygomaticomandibularis (subdivided into anterior, posterior and infraorbital), temporalis (subdivided into medial and lateral), and pterygoids (external and internal).

The masseter is the largest masticatory muscle in rodents and produces the strongest bite forces (Hiiemae & Houston, 1971; Satoh, 1998; Baverstock et al., 2013). Most of the authors divided it into three parts referred to as: superficial masseter, deep masseter and zygomaticomandibularis (Turnbull, 1970, Cox & Jeffery, 2011; Baverstock et al., 2013); or as superficial masseter, lateral masseter and medial masseter (Wood, 1965; Hautier & Saksiri, 2009); or as a combination of both systems (Sato & Iwaku, 2004, 2006, 2009; Druzinsky et al., 2011).

The superficial masseter runs from a small process of the maxilla, inferior to the infraorbital foramen, and it inserts on both the lateral and medial sides of the angular process. These attachments are situated directly beneath the attachment of the deep masseter, from the angular process to a position inferior to the first molar. It shows a posterior elongation into the medial surface of the mandible, called *pars reflecta*, just anterior to the attachment of the medial

pterygoid (Baverstock et al., 2013). The superficial masseter is the main transitional mover of the mandible by pulling it forward and upward (Hiiemae & Houston, 1971; Patel 1978).

The deep masseter is the largest masticatory muscle and unlike other rodents (Cox & Jeffery, 2011) it is reported as one single muscle in the mouse (Baverstock et al., 2013). It originates in the inferolateral surface of the zygomatic arch and attaches into the lateral surface of the mandible from the angular process to a point inferior to the first molar, superior to the superficial masseter and inferior to the zygomaticomandibularis (Baverstock et al., 2013). The contraction of the deep masseter pulls the mandible forward and upward (Hiiemae & Houston, 1971; Patel, 1978).

The zygomaticomandibularis is a slim and short muscle. Several authors do not recognize it as a separate muscle of the deep masseter (Hiiemae & Houston, 1971; Byrd, 1981; Satoh, 1997; Patel, 1978), while others do (Turnbull, 1970; Cox & Jeffery, 2011; Baverstock et al., 2013). It is divided into three different parts; the anterior zygomaticomandibularis, which is the largest part of the three, arises from the posteromedial border of the zygomatic arch. Its insertion is located posterior to the deep masseter, from a point anterior to the first molar towards the coronoid process to the mandibular notch, where it meets the attachment of the posterior zygomaticomandibularis (Patel, 1978). This last one is the smallest of the three parts of the zygomaticomandibularis. It originates from the posterolateral border of the zygomatic arch and inserts between the condylar and coronoid processes (Patel, 1978). Finally, the infraorbital zygomaticomandibularis, also called maxillomandibularis (Schumacher, 1961; Turnball, 1970), runs from a concavity of the maxilla inferior to the nasal bone, medial to the zygomatic process of the maxilla, anterior to the orbit and posterior to the premaxillary-maxillary suture. It attaches on the lateral side of the mandible anterior to the first molar and posterior to the attachment of the superficial masseter. It extends also on the medial surface of the zygomatic process of the maxilla (Patel, 1978).

The temporalis is the second largest masticatory muscle in mice, but the largest in carnivores. It is the only retractive muscle in rodents and also plays an important role in jaw elevation (Hiiemae & Houston, 1971). It is divided into two parts known as medial and lateral (Baverstock et al., 2013), or as anterior and posterior (Turnbull, 1970; Hiiemae & Houston, 1971; Druzinsky et al., 2011), that function independently (Hiiemae & Houston, 1971) since the medial fasciculus pulls the mandible upward and backward, while the lateral retracts the mandible (Patel, 1978). The medial part arises from a large area on the lateral side of the floor of the temporal fossa that extends posterior to the occipitoparietal suture and anterior to the posterior boundary of the first molar. It also expands into the zygomatic process of the temporal bone. The medial part inserts

into the medial surface of the mandible, anterior to the lateral pterygoid and posterior to the *pars reflecta* of the superficial masseter. It extends anterior to the dental ridge and posterior to the mandibular notch. This muscle covers the medial surface of the coronoid process. The lateral part of the temporalis originates anterior to the medial part and runs laterally to it to attach into the tip and into a small area of the lateral surface of the coronoid process (Baverstock et al., 2013).

The lateral pterygoid is smaller than its medial counterpart. The contraction of this muscle pulls the condyle forward from the glenoid fossa (Hiiemae, 1967; Patel, 1978) since it arises from the cranial base and inserts into the medial surface of the condylar process (Baverstock et al., 2013).

The medial pterygoid pulls the mandible forward, upward and medially (Hiiemae, 1967; Patel, 1978). Its origin accounts for half the size of that of the lateral pterygoid. It arises in the cranial base, medial to its counterpart, and inserts into the angular process, posterior to the superficial masseter to almost meet its *pars reflecta* anteriorly (Baverstock et al., 2013).

3.2.2 Craniofacial myogenesis

There is a great variety of approaches to explain the development of the masticatory muscles. Many of them are based on molecular and cellular regulatory mechanisms, especially through genome manipulation and *in vitro* organ culture techniques (Chai & Maxson, 2006). Although these fields are not able to explain the morphology, research on muscle morphogenesis also requires the understanding of tissue interaction, cell movement, signaling, and transcriptional regulation. For this purpose, it has been considered necessary a brief description of the molecular players responsible for it.

Myogenesis is a process of several steps that allows for the differentiation of mesenchymal cells into myoblasts. Although the cell types within the head and the trunk are identical, the program controlling the first stages of masticatory myogenesis differs from those in the trunk and limbs (Noden & Francis-West, 2006). Keeping with the cephalocaudal sequence of fetal development, the craniofacial muscles are the first to develop in the body (Sperber, 1989; Noden, 1991). The cranial paraxial mesoderm, which is formed of seven incompletely segmented structures, called somitomeres (Yamane, 2005), together with neural crest cells, migrate into the branchial arches (Noden & Francis-West, 2006). Next, myogenesis of the masticatory muscles starts in the mesodermal core of each branchial arch. The cranial paraxial mesoderm gives rise to the craniofacial muscles, some skeletal elements and blood vessels, whereas the cranial neural crest forms the tendons, connective tissue and elements of the nervous system. In some cases, a myogenic condensation forms within a single somitomere, moves to its terminal site and finally

gives rise to a single muscle. In other cases, a common premuscle mass gives rise to several muscles (Sperber, 1989; Noden, 1991).

Regarding the morphology, it should be pointed out that although some signals are present in the mesenchyme to guide the orientation of muscle fibers prior to differentiation of connective tissue (and therefore, prior to the formation of the definitive attachments), myoblasts are not preprogrammed regarding the geometry of the tissue they will form and they depend greatly on the local environment. Conversely, connective tissue precursors contain detailed instructions about their final shape (Noden, 1991).

Myf5 and MyoD are the two key regulatory factors in branchiomeric myogenesis. Later, myogenic differentiation is marked by myogenin when myoblasts differentiate into contractile cells. In the next mature stages, proteins such as desmin and myosin are synthetized (Shi et al., 2008). There are some transcription factors that operate before the onset of MyoD and Myf5 such as Tbx1, Pitx2, Tcf21 (Capsulin) and Msc (MyoR). Furthermore, muscle development in the branchial arches is also controlled by transcriptional and signaling factors from other sites due to the interaction between the mesodermal core of the branchial arches and tissues, cells and autocrine sources. Of interest are Wnt, bone morphogenetic protein (BMP) and fibroblast growth factor (FGF) (Kelly, 2010).

3.3 The bilaminar zone

3.3.1 Definition and nomenclature

The bilaminar zone is situated in the posterior portion of the temporomandibular joint. Classically, its boundaries have been set at the posterior band of the articular disc and the posterior portion of the joint capsule (Bernick, 1962). However, some authors have included it as part of the disc (Rees, 1954; Siéssere et al., 2004) and others as part of the capsule (Zenker, 1956; Schmolke, 1994; Rodríguez et al., 1999; Mérida Velasco et al., 2007). Piette (1995) even affirmed that in the rat the bilaminar zone extended all around the articular disc.

The lack of consensus about this region also affects the nomenclature since it has been referred as bilaminar zone (Rees, 1954), trilaminar zone (Smeele, 1988), retroarticular pad (DuBrul, 1988), retroarticular plastic pad (Zenker, 1956), and retrodiscal fat pad (Murakami & Hoshino, 1982).

3.3.2 Histology

Yamamoto et al., (2014a) compared the bilaminar zone in small (12-14 weeks of gestation) and large (30-37 weeks of gestation) human fetuses and concluded that while this region was composed almost exclusively of mesenchymal tissue and veins in the small ones, connective tissue fibers had differentiated in the large fetuses, but the characteristic bilaminar arrangement was not present yet. In postnatal stages, the bilaminar zone is composed of a superior (superior stratum) and an inferior (inferior stratum) layer of connective tissue with a highly vascularized middle region (Leonardi et al., 2012). The superior layer runs from the posterior portion of the articular disc to the posterior wall of the mandibular fossa and the squamotympanic suture (Rees, 1954; Siéssere et al., 2004, Mérida Velasco et al., 2007; Leonardi et al., 2012). It is made of loose connective tissue that contains elastic fibers (Rees, 1954; Benigno et al., 2001). The inferior layer runs from the posterior portion of the articular disc to the posterior part of the condyle (Rees, 1954; Siéssere et al., 2004; Mérida Velasco et al., 2007, Leonardi et al., 2012) and is composed of loose connective tissue with few elastic fibers (Rees, 1954; Benigno et al., 2001). The intermediate layer, also known as the genu vasculosum or retrodiscal pad, is limited anteriorly by the attachment of the short fibers to the articular disc and posteriorly by the long fibers from the temporal bone to the mandible (Dixon, 1962; Siéssere et al., 2004). This region is thoroughly vascularized and innervated and it also contains loose connective tissue, collagen fibers, and vascular spaces. It is irrigated by superficial temporal arteries and by branches of the maxillary artery, in particular the anterior tympanic artery and deep auricular artery (Benigno et al., 2001; Siéssere et al., 2004, Mérida Velasco et al., 2007), and it is innervated by sensorial terminations of the auriculotemporal nerve (Dixon, 1962; Siéssere et al., 2004). The retrodiscal pad contains also lubricin, the major component of the synovial fluid (Rizzolo & Madeira, 2005; Leonardi et al., 2012) and adipose tissue (Benigno et al., 2001).

3.3.3 Functions

The bilaminar zone experiences tension as it is pulled anteriorly by the articular disc (Scapino, 1991), and this results in a great number of functions, such as the restriction of pathological anterior disc displacement (Siéssere et al. 2004) through the opposition of the action of the lateral pterygoid (Rizzolo & Madeira, 2005). In addition, it provides nutrients, water (Kino et al., 1993) and blood (Sano, 2000) to the temporomandibular joint. It also acts as a cushion of mechanical stress by absorbing joint sounds during temporomandibular joint motion (Wish-Baratz et al., 1993), including masticatory movements (Piette, 1995).

3.4 Aims of this investigation

Once the current state of research has been reviewed, the goals of the present work will be enumerated:

1. To evaluate and describe the morphogenesis and the morphology of the temporomandibular joint and related structures of the mouse from prenatal stage E13.25 to postnatal stage P4. Is the mouse a relevant model for the study of temporomandibular joint development as compared to its human development?
2. Assuming that the surrounding structures have developmental influences, to evaluate and describe the morphogenesis and the morphology and of those that may have an effect on the formation of the temporomandibular joint. What are the developmental temporospatial relationships between them and the joint components?
3. To evaluate and describe the development of the masticatory muscles of the mouse, including a systematic volume measurement.
4. To evaluate and describe the morphogenesis of the bilaminar zone of the mouse.

Prepared with the previous information, we can test the hypothesis of Blechschmidt, wherein the dilation of the mesenchymal tissue due to growth of the skeletal primordia is necessary for the development of muscles, by measuring and comparing the proportions of the anterior and posterior regions of the temporomandibular joint of the mouse. Can this hypothesis explain the lack of an antagonist to the lateral pterygoid?

4 MATERIALS AND METHODS

4.1 Materials

A total of 11 heads (1 per stage) of mice (species *Mus musculus*, C57Bl/6J strain) were used for this study. They belong to the Radlanski Collection[1] and range from stages E13.25 to P4. The time interval between each specimen varies: half a day or one day between the smallest embryos (stages E13.25 to E17) and two days between the largest embryos (stages E18 and E20) and the postnatal stages (stages P0 to P4). Any mouse with deformities or developmental abnormalities in the examined regions was excluded. The main characteristics of these laboratory mice are shown in Table 1.

The age of the specimens was defined based on the ejection of the vaginal plug from the mother. Therefore, the day of plug discovery was designated as stage E0. Subsequently, mice were decapitated and tissue preparation and staining were performed (veterinary approval was given by LAGeSo T0110/11) according to standard laboratory procedures (Mulisch & Welsch, 2010) explained as follows. Specimens were fixed in formalin 4% (Fa. Herbeta Arzneimittel, Berlin, Germany) and Histochoice (Amresco®, Solon, Ohio) and decalcified with ethylenediaminetetraacetic acid (EDTA) (Fa. Herbeta Arzneimittel, Berlin, Germany) for 3-8 weeks depending on the size of the mice. Dehydration followed with an increasing concentration series of ethanol until 100%. After clearing the preparations with xylene (Fa. J.T. Baker, Netherlands), they were embedded in low-melting paraffin (Sigma Paraplast® Regular, Steinheim, Germany) at 50-60°. Next, they were cut as serial sections of 8 µm and 10 µm (depending on the stage) in frontal and horizontal planes with a microtome (Leica, Reichert-Jung RM 2065, Nußloch, Germany). Standard staining was performed with hematoxylin-eosin (HE). Some additional staining methods used at selected sections were TRAP (tartrate-resistant acid phosphatase), Safranin O/Fast green, Trichrome (Masson-Goldner, Van Gieson modified according to Domagk and modified elastic tissue-Masson trichrome) and Alcian blue (Mulisch & Welsh, 2010). Mounting was carried out using Eukitt® (O. Kindler GmbH, Freiburg, Germany) or with Kaiser's glycerol gelatine (Fa. Merck, Darmstadt, Germany).

[1] Charité-Universitätsmedizin, Berlin, Campus Benjamin Franklin, Center for Dental, Oral and Maxillofacial Sciences, Department of Craniofacial Developmental Biology.

Table 1: Features of the specimens used.

	EDTA	Paraffin	Section-thickness	Section-plane	HE	TRAP	Safranin O Fast Green	Trichrome	Alcian Blue
E13.25 52-11[2]	3 weeks	x	8 µm	Frontal	x			x (Domagk)	
E13.5 20-08	3 weeks	x	8 µm	Frontal	x	x			
E14.5 27-08	3 weeks	x	8 µm	Frontal	x	x		x (Domagk)	
E15 35-08	6 weeks	x	8 µm	Frontal	x	x		x (Domagk)	
E16 45-08	6 weeks	x	8 µm	Frontal	x	x	x	x (Domagk)	
E17 51-08	7 weeks	x	8 µm	Frontal	x	x	x	x (Domagk)	
E18 102-11	7 weeks	x	10 µm	Frontal	x				x
E20 115-08	8 weeks	x	8 µm	Frontal	x	x			x
P0 65-08	8 weeks	x	8 µm	Hori-zontal	x	x			
P2 70/08	8 weeks	x	10 µm	Frontal	x	x		X (Domagk, Elastic)	
P4 73/08	8 weeks	x	8 µm	Frontal	x	x		X (Domagk, Elastic)	

[2] The number under the developmental stage indicates the serial number of each mouse.

4.2 Methods

4.2.1 Preliminary remarks

The complex task of 3D reconstruction requires training. For this reason, the testing of reconstructions and morphometric analysis of the segment of a murine mandible and a dental primordium was performed under the supervision of experienced departmental staff. This allowed us to go through the fundamental sequence of steps involved and to learn the most important 3D commands to create a completely reconstructed 3D model.

4.2.2 3D Reconstruction technique

The visualization under light microscopy (Stemi SV11 Zeiss; Zeiss Universal, Oberkochen, Germany) of the histological serial sections at magnification x2.5 and x4 was performed prior to the 3D reconstructions. This permitted us to select histological sections without any damage such as folds, cracks, and deformations. Moreover, during development, anatomical structures change both qualitatively and quantitatively, and light microscopy visualization allowed us to select embryos without any malformation in the examined regions and to determine that the staging of the embryos was accurate.

The serial sections were photographed and digitized using an Olympus Scanning-System VS120 (Olympus, Tokyo, Japan) microscope at magnification x10. The distance between each image was 10-50 μm depending on the interest of region examined. Therefore, approximately 100-150 serial sections were digitized for each embryo and were saved in the TIFF format. For the subsequent 3D reconstruction, each image was required to not exceed 150 MB for technical reasons, thus compression with Photoshop CS4 software (Adobe Systems Software, Ireland) was carried out. All images for each embryo were transferred into a personal computer forming a stack and the analySIS® 5.0 software (OSIS, Münster, Germany) was used for the 3D reconstruction process. This consists of several steps, in particular arrangement, calibration, scaling, definition of the height distance, alignment, segmentation and visualization, in order to obtain a 3D model. All these steps, starting with the definition of a workspace to finally creating a 3D model, are explained as follows. Images were arranged within the stack by sorting them into the right order from anterior to posterior. Next, they were calibrated and scaled on both x- and y-axes, and the distance between images was defined. The planes of the stack have to be arranged in such a way that the structures are positioned accurately in relation to one another, so it was therefore mandatory to align the planes involved. AnalySIS® provided a semi-automatic single-point alignment for horizontal and vertical displacement that was used in the first place, and a manual alignment that was performed using some fiducial markers, such as Meckel's

cartilage, the eyes or the tongue (Gaunt & Gaunt, 1978; Radlanski et al., 2003) (Fig. 3). Some adjustments in the alignment were necessary during the reconstruction process when the surface of the 3D model was wrongly shaped or not smooth enough.

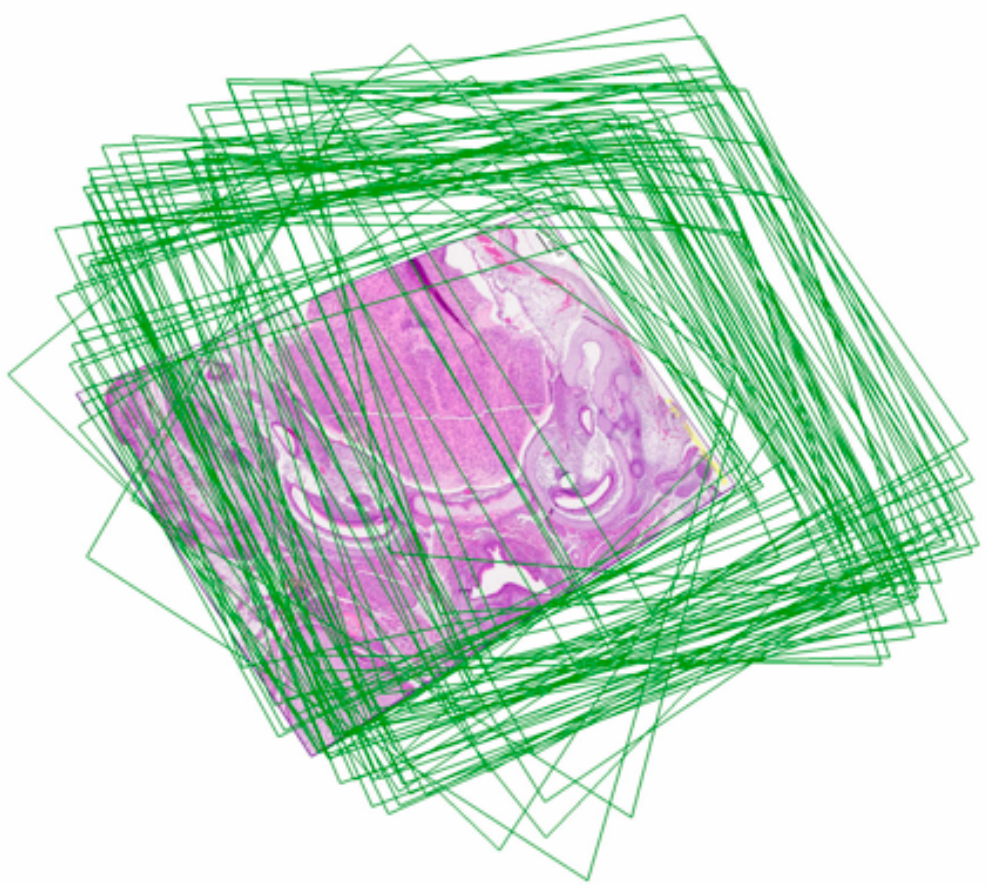

Fig. 3: Visualization of the stack after single-point alignment and manual alignment with analySIS® 5.0 software (OSIS, Münster, Germany).

The histological section constitutes the most posterior plane. Above it are situated the rest of the approximately 150 photographed sections, which are represented here as green contours. The distance between these sections oscillates between 10 µm and 50 µm depending on the interest of region examined.

Histological section through the middle ear of the mouse at stage E15.

Frontal plane, HE staining.

The manual segmentation took place in two different steps. First, the contours of the selected structures (mandible, masticatory muscles, etc.) were identified at higher magnifications based on anatomical and histological characteristics. Second, they were manually delineated using the 3D command of the software (Fig. 4). Polygons were thus defined and subsequently linked to each other via the segmentation process and triangulation method. The linkage of the separate polygons resulted in a single, unified 3D model (Fig. 5).

The reconstructed anatomic structures were colored to be distinguished better on the 3D models and the selected color code was applied systematically throughout all of the reconstructions (Table 2).

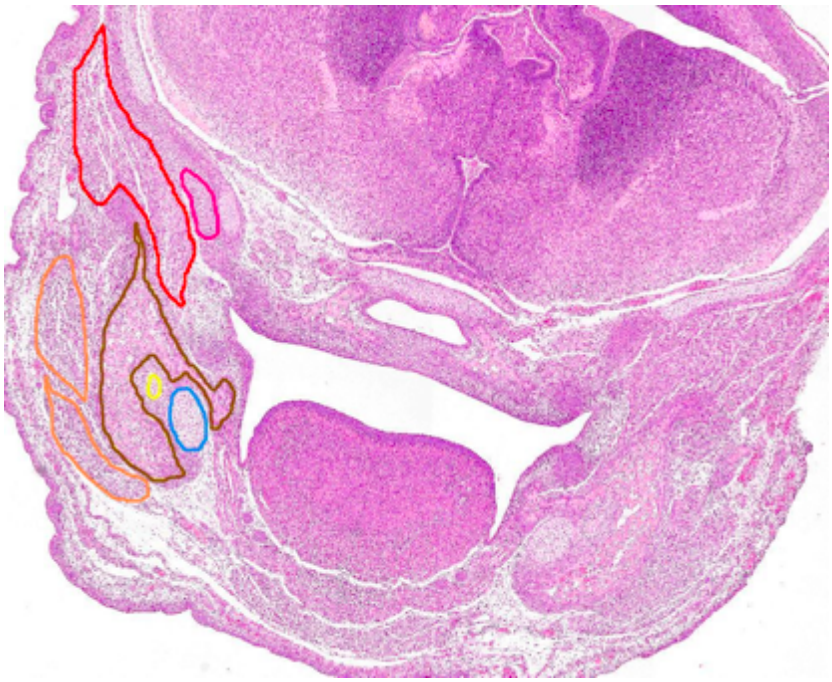

Fig. 4: Visualization of some histological structures that were manually delineated with analySIS® 5.0 software (OSIS, Münster, Germany).

The manual segmentation permits to define polygons on places in the stack. Afterwards, they are combined with each other to form a linkage.

Histological section through the head region of a mouse at stage E15.

Frontal plane, HE staining.

Mandible (brown), inferior alveolar nerve (yellow), Meckel's cartilage (blue), masseter (orange), temporalis (red), lateral pterygoid (pink).

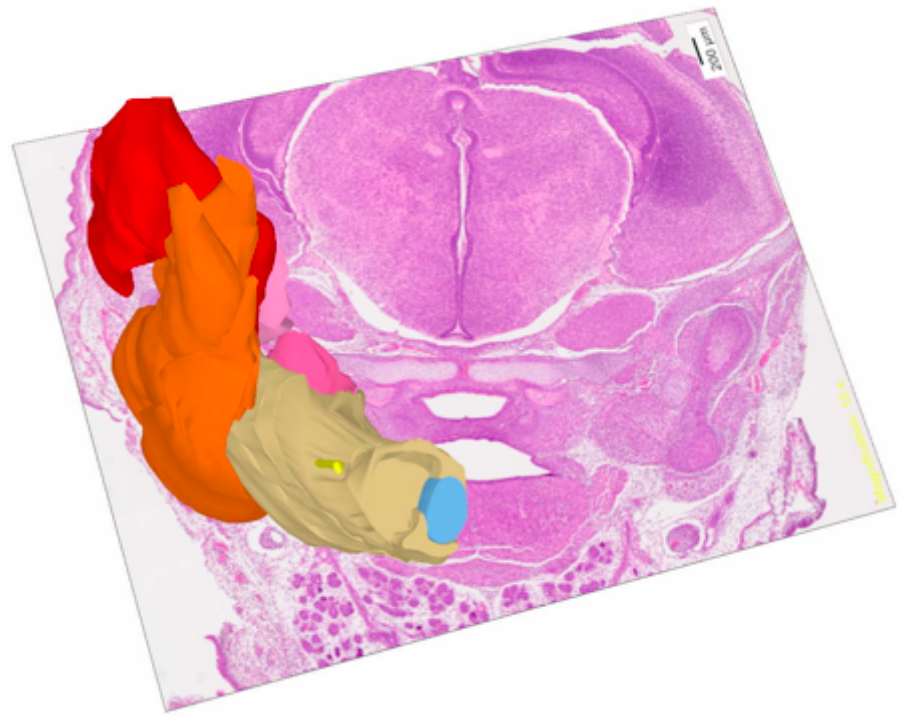

Fig. 5: Visualization of a 3D model obtained with analySIS® 5.0 software (OSIS, Münster, Germany) from histological sections.

The 3D model was created after the processes of arrangement, calibration, scaling, definition of the height distance, alignment, and segmentation.

Histological section of a mouse at stage E15 with superimposed 3D reconstruction of the mandible, Meckel's cartilage, the inferior alveolar nerve and the masticatory muscles.

Frontal plane, HE staining.

For color code, see Table 2.

Table 2: Color code used for the anatomical structures of the 3D reconstructions.

Modified according to Blechschmidt (1963).

Color	Anatomical structure	analySIS-HSL			RGB		
		Hue	**Satura-tion**	**Light-ness**	**Red**	**Green**	**Blue**
Bones							
	Maxilla, Mandible	28	146	161	222	191	120
	Sphenoid	28	146	151	211	171	91
	Temporal bone, Zygomatic bone	28	146	171	-	-	-
Cartilage (endochondral ossification)							
	Sphenoidal cartilage	133	240	183	106	207	255
	Temporal cartilage	137	240	160	85	183	255
Cartilage							
	Meckel's cartilage	138	185	158	101	174	235
	Condylar and angular cartilage	130	230	151	70	206	251
Ear							
	External acoustic meatus	160	0	120	127	127	127
	Pharyngotympanic tube	160	0	181	192	192	192
	Cochlear cartilage	133	240	142	47	187	255
	Incus cartilage	138	185	(125)	38	142	227
	Stapes cartilage	138	184	105	26	120	198
	Malleus cartilage	138	185	158	101	174	235
Eye							
	Lens	160	0	0	0	0	0
	Bulbus oculi	160	0	240	255	255	255
Nerves and ganglions							
	Nerve and ganglion	40	240	120	255	255	0
Blood vessels							
	Artery	0	240	110	234	0	0
	Vein	160	240	155	74	74	255
Muscles							
	Superficial masseter	13	240	135	255	104	32
	Deep masseter	13	240	120	255	83	0
	Lateral pterygoid	219	201	182	245	141	196
	Medial pterygoid	224	234	164	253	96	158
	Temporalis	0	240	110	255	0	0
	Stylomandibular	14	237	168	254	156	103
Glands							
	Lacrimal gland	120	240	62	0	128	128
	Parotid gland	120	240	58	0	128	128

The right side of each mouse was 3D reconstructed. The left side was histologically analyzed during the whole process, which resulted in no noticeable discrepancies with the opposite side. The most anterior and inferior parts of the masseter defined the anterior and inferior boundaries of the reconstructions, respectively. The posterior margin was defined by the external acoustic meatus, and the superior margin by the most superior part of the temporalis. Therefore, from lateral to medial, the anatomical structures reconstructed in the present study were: parotid and lacrimal gland, masticatory muscles, maxilla, zygomatic bone, temporal bone, sphenoid bone, mandible (including Meckel's cartilage and the inferior alveolar nerve), the most relevant components of the temporomandibular joint in order to answer the research questions of the present investigation (namely condyle and condylar cartilage, glenoid fossa, articular disc, and superior and inferior joint cavities), as well as some vessels found in the bilaminar zone, and some components of the middle ear. Other structures, such as the eyeball, lens, tympanic cavity, external acoustic meatus, pharyngotympanic tube, cochlea, tympanic ring, and superior and inferior first and second molars, were also reconstructed for spatial orientation purposes, but a detailed description has been omitted.

All anatomical and histological structures were named in accordance with the international standardized anatomical terminology of location, *Terminilogia Anatomica* (IFAA, 1998). Therefore, terms such as "top /bottom", "front/back" and "right/left" have been avoided and "anterior/posterior", "superior/inferior" and "medial/lateral" have been used instead.

4.2.3 Morphometric analyses

When explaining the 3D reconstruction technique in the previous section, scaling the images was one of the steps mentioned. Doing this correctly has allowed us to measure muscle volume, to perform unilateral measurements and to calculate the distance between some specific landmarks.

1. For the first purpose, the "Volume & Surface area" command was selected in the analySIS® 5.0 software (OSIS, Münster, Germany)**.** The embryos at stages E13.25, E13.5, and E17 were excluded from these calculations due to the different reasons explained in the discussion.
2. The unilateral measurements differed between those carried out in the superior-inferior plane and those in the anterior-posterior plane. The first ones were carried out to calculate the distance between the condylar cartilage and articular disc, and were performed using the "Distance" command in the analySIS® 5.0 software (OSIS, Münster, Germany). The measurements in the anterior-posterior plane could be easily performed on the histological sections since the distance between the images had been defined at the beginning of the 3D reconstruction process. Those

measurements were the extension of the condylar and angular cartilages and the extension of the parotid and lacrimal gland.

3. Finally, the distance between some landmarks was calculated in order to elucidate the dilation of the tissue anterior and posterior to the temporomandibular joint, as follows. First, our 3D models were positioned using a plane that passed through the inferior margin of the orbit and the superior margin of the incus. Next, the landmarks were determined (Fig. 6):

- ➢ Anterior distance: From the anterior margin of the condylar cartilage to the mental foramen.
- ➢ Posterior distance: From the posterior margin of the condylar cartilage to the anterior surface of the incus.

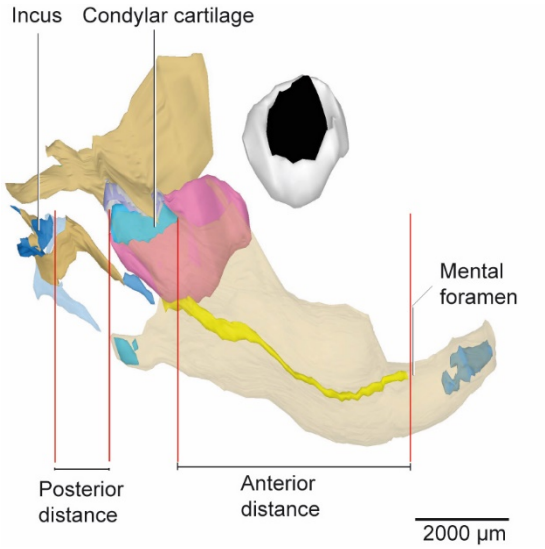

Fig. 6: Visualization of the landmarks that were established to calculate the dilation of the tissue anterior and posterior to the temporomandibular joint.

The 3D model was first horizontally positioned along the orbitale and the most superior border of the incus. Subsequently, the anterior distance was defined between the anterior surface of the condylar cartilage and the mental foramen of the mandible. The posterior distance had its boundaries at the posterior surface of the condylar cartilage and at the anterior surface of the incus. Those landmarks are marked here as red lines.

Partial 3D reconstruction of some components of the right temporomandibular joint.

Mouse at stage P4.

5 RESULTS

5.1 Preliminary remarks

In order to better understand the craniofacial development, the morphogenesis of the right temporomandibular joint of the mouse and some selected structures was described. Specifically, the focus was set on the masticatory musculature in relation to the joint by detailing the critical period of the muscle formation, and its appearance, extension and development. The morphogenesis of structures that are anatomically in close relationship with the joint, in particular the parotid and lacrimal glands, the maxilla, the zygoma, the temporal bone, the sphenoid, the mandible, the bilaminar zone and the middle ear ossicles, was also described. The present section also includes 3D reconstruction depictions obtained from histological serial sections of eleven mice ranging from stages E13.25 to P4.

Since this investigation includes an accurate characterization of the masticatory muscles, it has to be mentioned that conventional staining methods only allow the detection of the bulk of the muscles. The origins and attachments, as well as the fasciae, which must be present at a certain stage of development, remain unidentifiable. Hence, in the 3D reconstructions, only the contractile region of the musculature could be delimited.

After the descriptions, a depiction of every stage brought to the same scale was also carried out in order to show the size increase and change of proportions during development. Some tables and diagrams from the morphometric analyses are also presented at the end of this chapter for a better comprehension of the results.

5.2 Morphology

5.2.1 Stage E13.25

The main tissue at this developmental stage was mesenchyme, which showed regions of increased cell populations, i.e. mesenchymal condensations, such as the frontonasal, the maxillary and the mandibular. Many blood vessels were distributed along these mesenchymal populations, though some of them seemed to be discontinuous, however.

At stage E13.25 any component of the temporomandibular joint could be visualized. Nevertheless, other structures related to our region of interest, such as the palate shelves, situated at each side of the tongue, the trigeminal ganglion and the trigeminal nerve were recognized. The whole oronasal cavity was occupied by the developing tongue (Fig. 7).

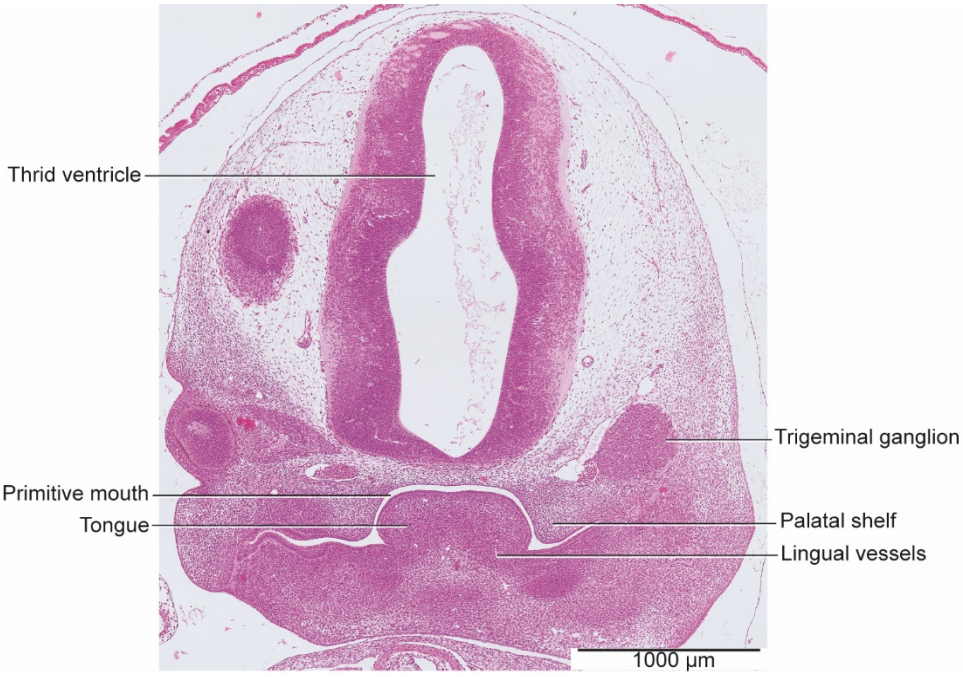

Fig. 7: Stage E13.25 (52-11). Histological section of the head of the mouse through the future temporomandibular region.

No muscles or bone structures were discernible in this section of this developmental stage.

Frontal plane, HE staining.

5.2.2 Stage E13.5

At this prenatal stage, much of the mesenchyme tissue had differentiated at some regions to give rise to structures of our interest.

The muscle primordium of the masseter, composed of premyoblasts, was located lateral to the ossification center of the mandible. There was no insertion on it, instead, the space between muscle and bone was occupied by connective tissue (Fig. 10b).

As a component of the parotid gland, only its developing duct could be visualized and it showed a cylindrical form (Fig. 9).

A mesenchymal cell population inferior to the trigeminal ganglion was identified as the primordium of the maxilla. The palate shelves had developed downwards on each side of the tongue, which occupied almost the whole oronasal cavity (Fig. 8).

The body of the sphenoid was composed of cartilaginous tissue (Fig. 9).

The formations of the first ossification centers of the mandible were detected lateral to the inferior alveolar nerve and medial to the primordium of the masseter. The nerve, imposed as a well-developed structure, was located lateral to Meckel's cartilage and it arose from the trigeminal ganglion, which had duplicated in size compared to the previous stage. By outline, Meckel’s cartilage could be divided into three parts; the posterior third was wider than the central one and the anterior increased in diameter towards its anterior end (Fig. 10a, b).

Any component of the temporomandibular joint or the bilaminar zone could be identified at this stage.

Some parts of the outer, middle and inner ear had developed so far that they could be distinguished, such as the external acoustic meatus, the pharyngotympanic tube, the mesenchymal condensation of the cochlea and the tympanic cavity. However, there were no primordia of the middle ear ossicles, and Meckel's cartilage had not reached into the tympanic cavity with its posterior end (Fig. 9).

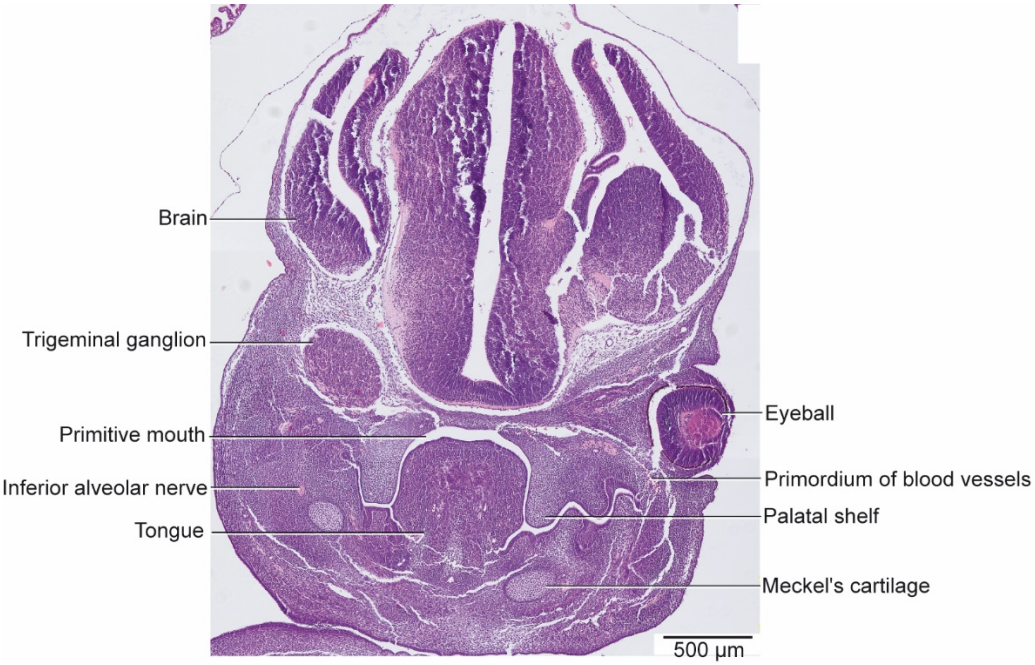

Fig. 8: Stage E13.5 (20-08). Histological section of the head through the center of the trigeminal ganglion.
Frontal plane, HE staining.

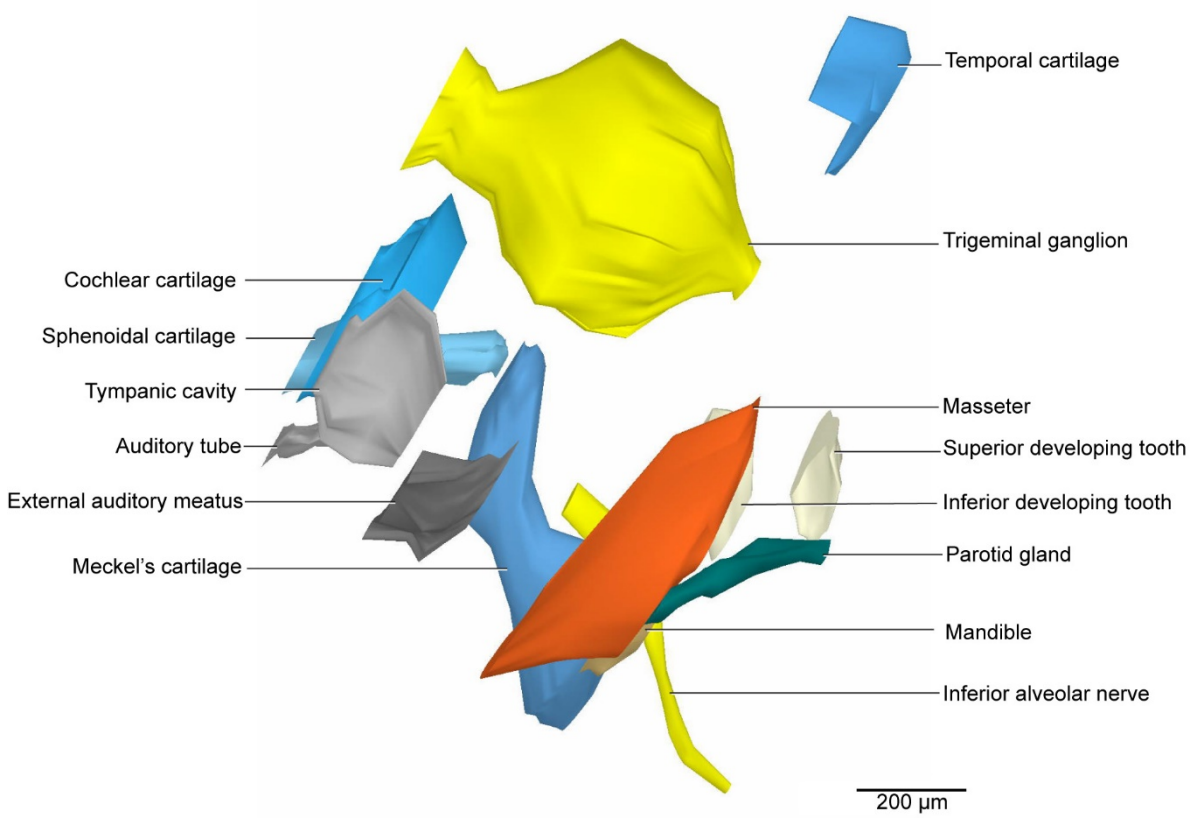

Fig. 9: Stage E13.5 (20-08). 3D partial reconstruction of the region of the right half of the head where the temporomandibular joint and the masticatory muscles will later develop.
Lateral view.

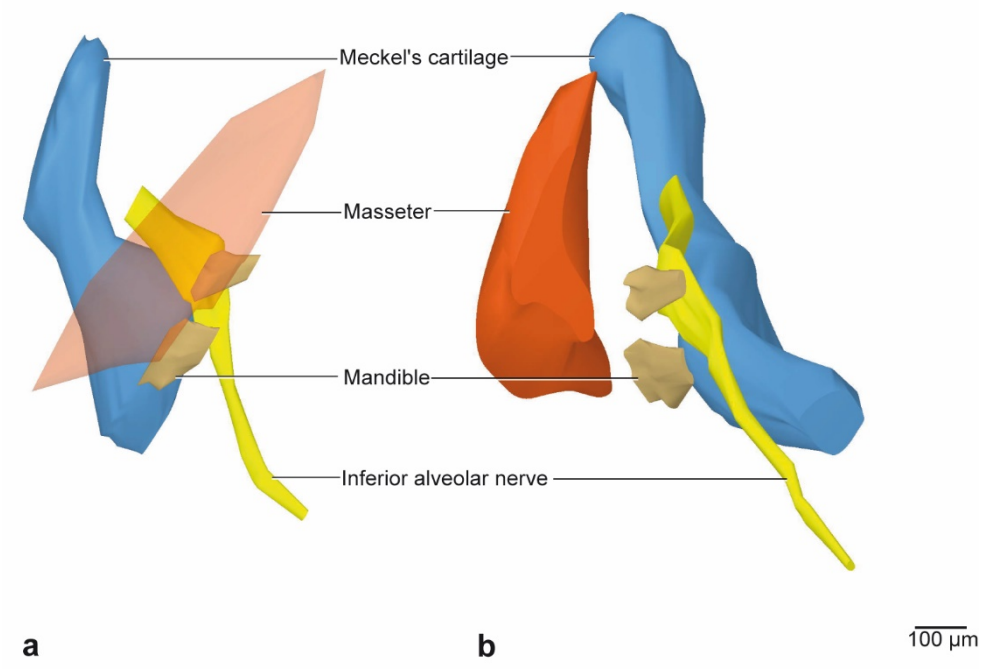

Fig. 10: Stage E13.5 (20-08). 3D reconstruction of the right half of the mandible and masseter muscle.

a: Masseter made transparent to visualize the extension of the mandible and Meckel's cartilage. Lateral view.

b: Visualization of the distance between the mandible and masseter. Anterior view.

5.2.3 Stage E14.5

The masseter (Fig. 11a, b and Fig. 12) had its origin at the mesenchyme around the temporal process of the zygomatic bone and the zygomatic process of the maxilla. The superficial masseter inserted into the mesenchymal tissue of the lateral, medial and inferior surface of the angular process, sharing this attachment with the medial pterygoid. Furthermore, it showed an insertion into the inferior third of the lateral surface of the ramus of the mandible and into the masseteric tuberosity. The attachment of the deep masseter was found directly superior to the superficial masseter, inserting into the superior two thirds of the lateral surface of the ramus of the mandible. These two bellies run side by side, and the tissue characteristics between the developing muscle and the bone insertions were clearly discernible at this stage. As the muscle fibers were in the stage of differentiation, their direction could not be identified, but at least the myoblasts within the mesenchyme were observed running obliquely in posterolateral direction. The muscle extended in a triangular shape, with the apex in the anterior part of the maxilla and the base in the posterior part of the mandible. The masseter accounted for 57% of the total masticatory muscle mass.

The temporalis (Fig. 11a, b and Fig. 12) originated from a large mesenchymal area on the lateral surface of the skull. The attachment to the mandible was seen in the region of the coronoid process, which was just visible as a small protuberance, and to the corresponding medial surface of the mandible. An additional insertion existed at the mesenchymal tissue of the medial surface also of the mandible at this level. The myoblasts followed a determinate direction depending on the part of the muscle: those situated in the anterior third run straight vertical, those in the center run with a slight oblique inclination downward and those in the posterior third run anteriorly downward. The form of the temporalis was also triangular with the apex located inferior to the mandibular notch and the base at the lateral surface of the skull. Since any layer could be visualized, so it was therefore described as a single muscle. It comprised 25% of the overall masticatory muscle mass.

The lateral pterygoid (Fig. 11b and Fig. 12) had its origin was at the mesenchyme surrounding the cartilage of the lateral surface of the lateral pterygoid process and the greater wing of the sphenoid bone. It inserted at the medial surface of the condylar mesenchyme and at the neck of the mandible and some myoblasts reached the mesenchymal condensation situated between the condylar process and the glenoid fossa. The myoblasts in the mesenchyme followed a posterolateral direction. Unlike the masseter and the temporalis, this muscle inserted with less space between muscle and bone as seen in the histological sections. The lateral pterygoid showed a parallelogram shape with no compartments inside, despite the three regions of

insertion. At this developmental stage, the muscle accounted for 6% of the whole masticatory muscle mass.

The medial pterygoid (Fig. 11b and Fig. 12) originated from the mesenchyme of the cartilaginous medial surface of the lateral pterygoid process of the sphenoid bone. It attached at the mesenchymal periosteum of the medial and the inferior surface of the angular process, where the masseter also inserted. The attachment was tight with less space between bone and muscle. The myoblasts of the muscle run obliquely in a posterolateral direction. The shape of the medial pterygoid could be described as rectangular and a significant septum divided it into a superior and an inferior head. Both together accounted for 12% of the whole masticatory muscle mass.

The parotid, classified as a major salivary gland, was situated on either side of the mouth. It was located lateral to the masseter, posterior to the ramus of the mandible, and inferior to the angular process. It was composed of excretory ducts, including the major one called Stensen's duct, and a body. Stensen's duct emerged from the most anterior and superior part of the gland and ran in an anterior-superior direction to open into the oral cavity at the level of the first maxillary molar. The body was surrounded by a capsule of connective tissue and it occupied an extension of 456 μm in the anterior-posterior direction.

The exocrine lacrimal gland was located superior to the masseter and lateral to the temporalis. It was formed by a duct that opened into the eye, and a body that occupied an extension of 160 μm in the anterior-posterior direction.

The maxilla (Fig. 11a), situated in the midface, was imposed as an immature bone with a large vascular network and vascular spaces. The intramembranous ossification had started and a thick layer of mesenchyme surrounded it. The body and three processes, in particular the zygomatic, frontal, and palatine, could be observed and the origin of the masseter was located at the first one.

The largest part of the zygomatic bone (Fig. 11a) observed at this stage was its temporal process, which was located lateral to the mandible and the maxilla, and inferior and anterior to the temporal bone. It was composed of immature bone with large mesenchymal tissue around it, and it also served as the origin for the masseter.

The temporal bone (Fig. 13a, c) was located at the sides and base of the skull. Two parts of this structure could be clearly visualized at this developmental stage: the squamous part with the glenoid fossa, and posteriorly to it, the petrous part. Both were composed of intramembranous bone, which was surrounded by a thick layer of mesenchymal tissue. The glenoid fossa was situated posterior to the zygomatic process and its shape was markedly flattened. A large distance of approximately 200 μm separated the glenoid fossa from the condyle. The temporal

fossa, which was formed among others by the squamous part of the temporal bone, served as site of origin for the temporalis.

The sphenoid bone (Fig. 12) was situated at the base of the skull. It had developed a central body, two pairs of greater and lesser wings on either side and also two pterygoid processes on either side. The sphenoid was composed of cartilaginous parts, except for the medial pterygoid process, which was located lateral to the pharynx and contained osteoid-like tissue at its superior region and secondary cartilage in its middle zone. A mesenchymal condensation of the tensor veli palatini was detected lateral to the medial pterygoid process. The sphenoid was also the site of origin of the lateral and medial pterygoids.

Both the body and ramus of the mandible (Fig. 13a-d) showed almost the same length, and they exposed an extended vascular network. The three processes of the mandible (condylar, angular and coronoid) were composed of highly vascularized mesenchymal tissue. The developing condylar process was located anterior to the primordia of the middle ear ossicles and lateral to Meckel's cartilage, and it showed a convexity at its superior edge. The angular process was situated inferiorly and laterally to Meckel's cartilage, and its inferior border was found to be concave. The coronoid process was seen as a very slight mesenchymal protuberance superior and lateral to Meckel's cartilage. This last structure was surrounded by the mandibular bone and was straight except for a slight curvature in the middle. At the posterior end of Meckel's cartilage the malleus became discernible (Fig. 14a, b). The inferior alveolar nerve (Fig. 13a-d) ran medial to the body of the mandible but was not completely encircled by it. It gave off the mental nerve, which passed through the mental foramen situated at about the level of the anterior border of the mandibular molar primordium.

At this developmental stage, the components of the temporomandibular joint (Fig. 13a-d) were very immature. The glenoid fossa was flattened, and no secondary cartilage could be found on the condylar process. Between these two structures, the mesenchyme showed a circumscribed condensation, namely the articular disc, and the distance between it and the condylar process was approximately 107 μm.

For the first time, the bilaminar zone (Fig. 13a, b and Fig. 16) could be identified between the posterior border of the region where the temporomandibular joint was developing and the anterior surface of the middle ear primordia. The main tissue found in this zone was loose mesenchyme with an extended network of voluminous vascular spaces surrounding the retromandibular vein. Lateral to this last structure, a few sinusoidal waveform collagen bundles were noted running in a vertical direction. Other structures that could be identified were arterioles and the auriculotemporal nerve, as well as adipose tissue and parotid gland tissue. The

visualization of the typical two laminae of collagen fibers was not possible with our histological methods.

The three middle ear ossicles, i.e., malleus, incus and stapes, (Fig. 15) were visible as cartilaginous primordia at this stage. The malleus and the incus were discerned as two separated structures, whereas the malleus was the posterior extension of Meckel's cartilage.

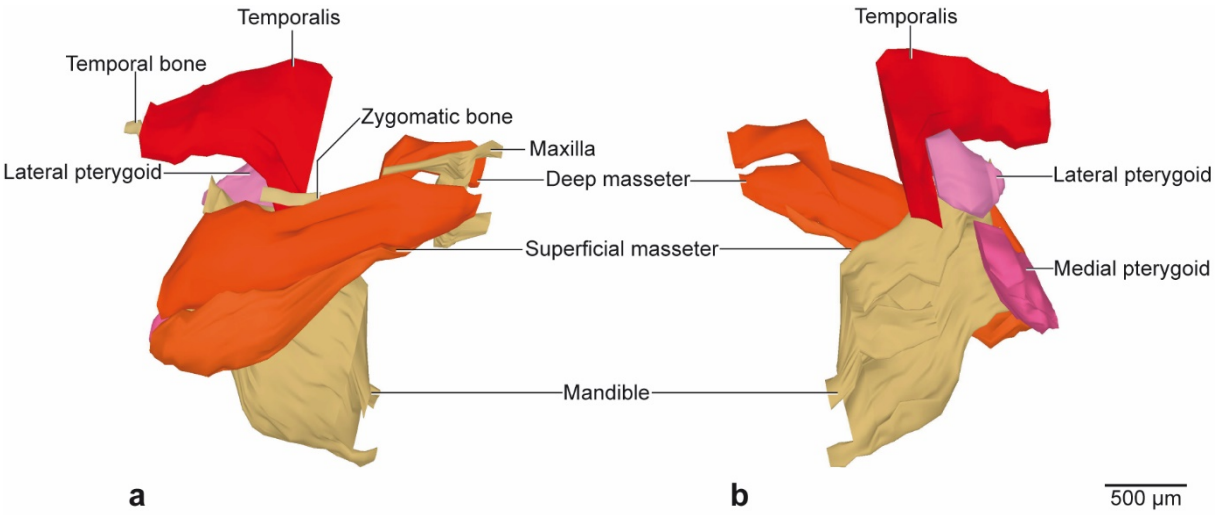

Fig. 11: Stage E14.5 (27-08). 3D reconstruction of the right half of the mandible and masticatory muscles.
In this stage, all the masticatory muscles were observed for the first time and they already showed their species-specific form and location.
a: Extension and attachments of the masseter and temporalis. Lateral view.
b: Extension and attachments of the lateral and medial pterygoids. Medial view.

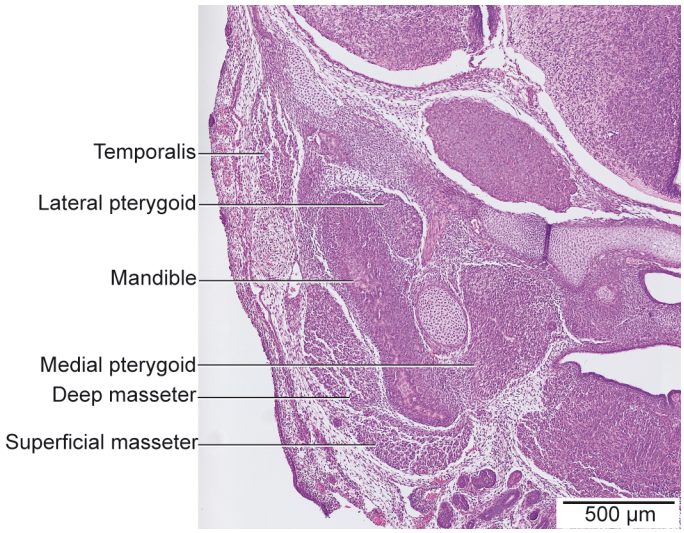

Fig. 12: Stage E14.5 (27-08). Histological section of the right half of the mandible through the condyle indicating the anatomical arrangement of the masticatory muscles.
Frontal plane, HE staining.

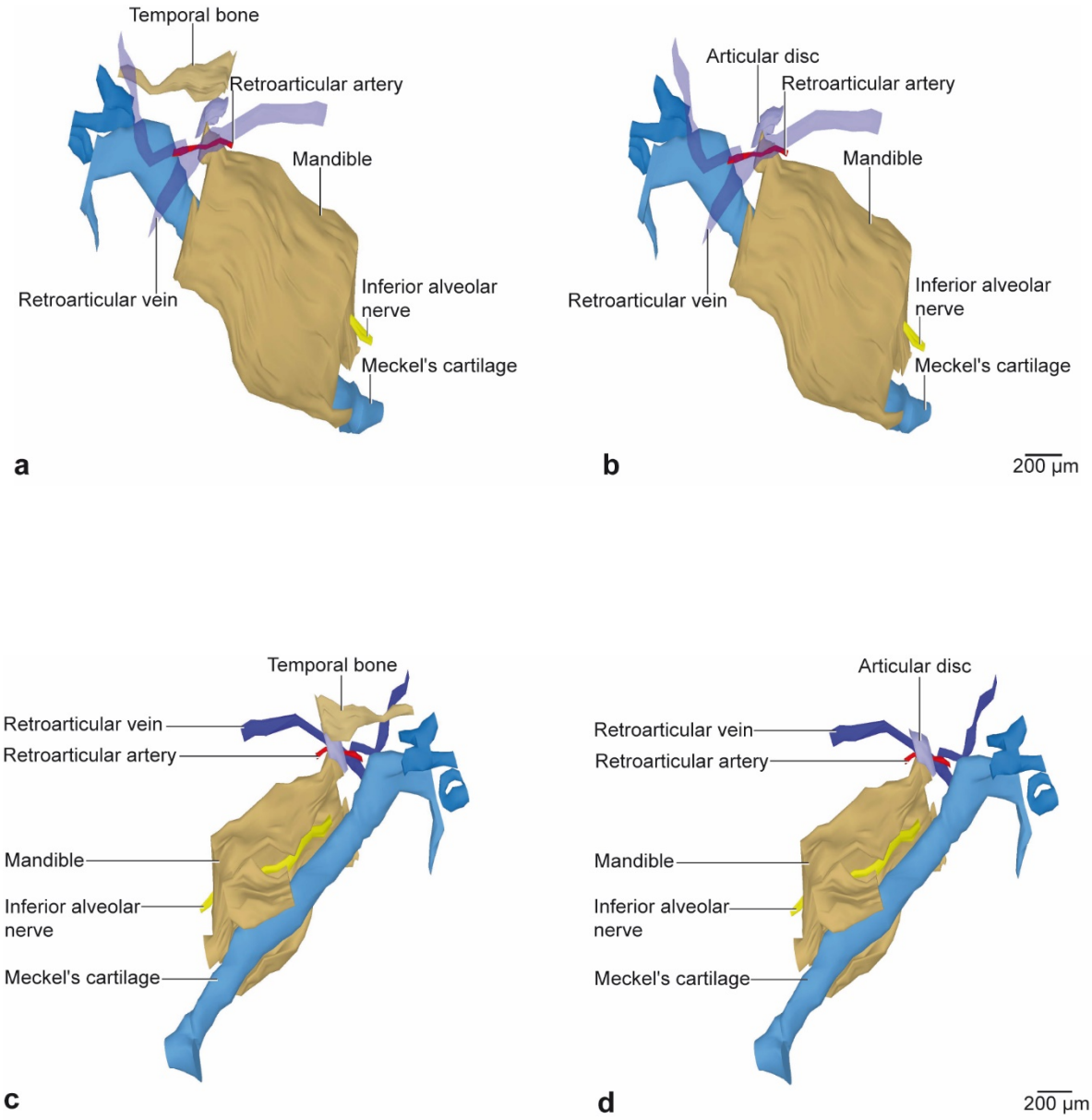

Fig. 13: Stage E14.5 (27-08). Partial 3D reconstruction of some components of the right temporomandibular joint and the region of the bilaminar zone.

a: Temporomandibular joint region with its temporal bone. Retromandibular vein made transparent to visualize the content and extension of the bilaminar zone. Lateral view.

b: Temporomandibular joint region, temporal bone removed to visualize the articular disc. Retromandibular vein made transparent to visualize the content and extension of the bilaminar zone. Lateral view.

c: Temporomandibular joint region with its temporal bone. Medial view.

d: Temporomandibular joint region, temporal bone removed to visualize the articular disc. Medial view.

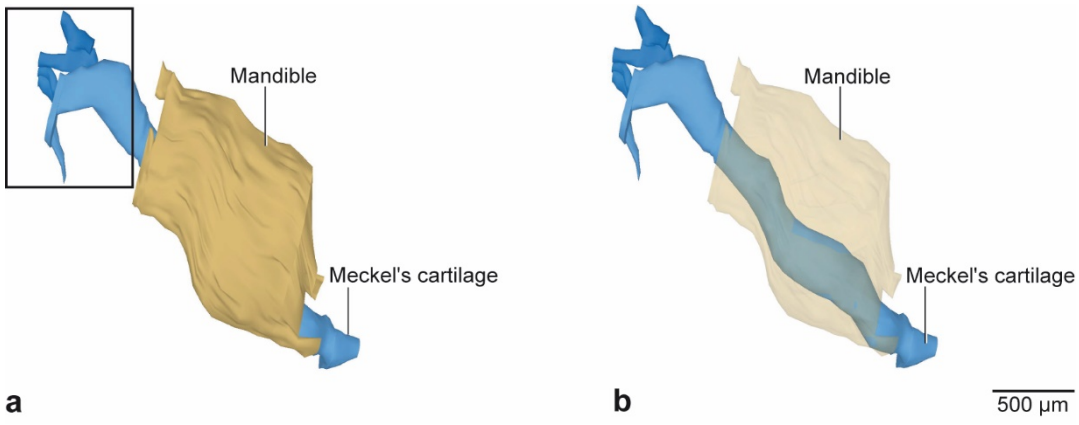

Fig. 14: Stage E14.5 (27-08). 3D reconstruction of the right half of the mandible, Meckel's cartilage and primordia of the middle ear ossicles.

a: Lateral view. Box: See Fig. 15.

b: Same view with mandible made transparent. Lateral view.

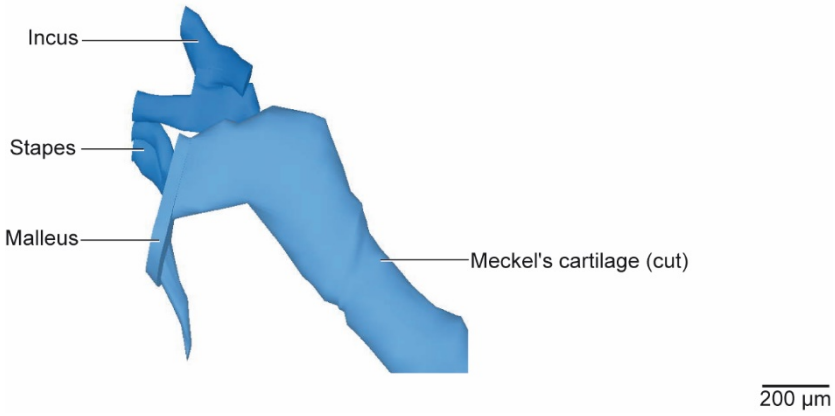

Fig. 15: Stage E14.5 (27-08). 3D reconstruction of a detailed view of the right primordia of the middle ear ossicles.

Lateral view.

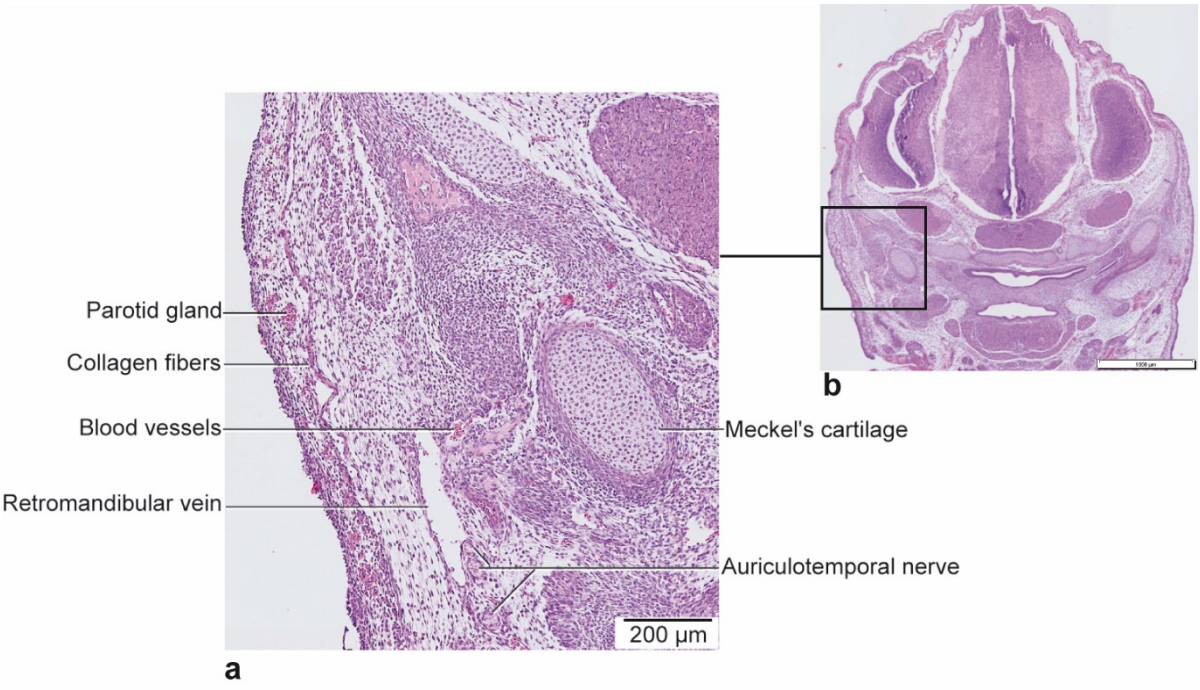

Fig. 16: Stage E14.5 (27-08). Bilaminar zone.

a: Histological section through the right bilaminar zone. Frontal plane, HE staining.

b: Survey of the whole section.

5.2.4 Stage E15

The masseter (Fig. 17a, b and Fig. 18) originated from the mesenchymal tissue of the ossified temporal process of the zygomatic bone and from the zygomatic process of the maxilla. The superficial masseter attached at the mesenchyme of the lateral, medial and inferior surfaces of the angular process, lateral to the medial pterygoid. It also inserted at the inferior third of the lateral surface of the ramus of the mandible and at the masseteric tuberosity. The deep masseter attached at the superior two thirds of the ramus of the mandible. As at the previous stage, the tissue characteristics between muscle and bone were easily distinguishable at the insertion regions. Muscle fibers were in the transition to differentiate, and meanwhile myoblasts in the mesenchyme ran obliquely in posterolateral direction. The masseter showed a triangular form with the apex situated at the anterior part of the maxilla and the base at the posterior edge of the mandible. At this stage, the superficial masseter overlapped the inferior third of the deep masseter and both bellies comprised 56% of the total masticatory muscle mass.

The temporalis (Fig. 17a, b and Fig. 18) extended from the lateral surface of the osseous temporal fossa and it attached to the mesenchyme around the apex of the coronoid process. Furthermore, it showed an insertion at the anterior part of the mandibular notch and at the medial surface of the mandible. The muscle fibers were in the transition to differentiate, and the myoblasts were arranged following a straight vertical direction in the anterior part of the muscle, a slight oblique anterior inclination in the center, and an anterior direction in the posterior part of the muscle. As in the previous stage, the shape of the temporalis was triangular, with the apex at the mandibular notch and the base at the lateral surface of the skull. This non-compartmentalized muscle accounted for 26% of the total masticatory muscle mass.

The lateral pterygoid (Fig. 17b and Fig. 18) extended from the mesenchyme of the cartilaginous and ossified portion of the greater wing and mesenchyme of the cartilaginous lateral surface of the lateral pterygoid process of the sphenoid bone. It attached to the medial surface of the condylar mesenchyme, to the neck of the mandible and to the anterior border of the mesenchymal articular disc. The myoblasts ran posterolaterally while the muscle fibers were in the transition to differentiate. The lateral pterygoid showed a parallelogram-like form. Despite the three regions of insertion, the three corresponding heads could not be morphologically visualized. It comprised 7% of the overall masticatory muscle mass.

The medial pterygoid (Fig. 17b and Fig. 18) originated from the mesenchyme of the cartilaginous medial surface of the lateral pterygoid process of the sphenoid bone. The attachment of this muscle was found at the medial and inferior borders of the angular process, sharing this insertion with the superficial masseter. An additional attachment was found at the

mesenchyme of the medial surface of the mandibular ramus. Histological methods allowed us to visualize an oblique arrangement of the myoblasts in the posterolateral direction. The two heads of this muscle extended in a rectangular shape and accounted for 11% of the total muscle mass.

The parotid gland was situated lateral and posterior to the masseter, and anterior to the external acoustic meatus. It comprised an excretory duct and a body. The duct lacked curvature and it followed an anterior direction to open into the oral cavity opposite to the primordium of the first maxillary molar. The body and its surrounding capsule increased in posterior-superior extension compared to the previous stage, and it occupied 696 μm in the anterior-posterior direction.

The lacrimal gland was situated superior to the masseter and lateral to the temporalis. It had extended posteriorly compared to stage E14.5, showing for the first time its characteristic almond shape. It comprised a duct and a body, which occupied an extension of 520 μm in the anterior-posterior direction.

The maxilla (Fig. 17a) was located at the midface. At this developmental stage, its intramembranous ossification had gone further, the body appeared more voluminous and the frontal process had extended superiorly. The palatine and the zygomatic process could be also visualized, and the latter served as origin for the masseter.

The temporal process of the zygomatic bone (Fig. 17a) was located lateral to the mandible and the maxilla, and inferior and anterior to the temporal bone. It was composed of three cylindrical-like shaped structures, which extended 920 μm in the anterior-posterior direction. Additionally, the origin of the masseter could be observed at this structure.

The temporal bone (Fig. 19a, c), located at the sides and base of the skull, appeared more voluminous at this stage due to the progression of intramembranous ossification at the squamous part. The glenoid fossa was quite shallow and the distance between this structure and the condyle was approximately 408 μm, larger than in the previous stage. The temporalis originated from the temporal fossa of the squamous part.

The sphenoid (Fig. 18) was composed of a central body, greater and lesser wings on either side and lateral and medial pterygoid processes also on either side. It was situated at the base of the skull. All components were cartilaginous, with the exception of the superior part of the greater wing where bone had been differentiated via endochondral ossification. In addition, bone tissue had extended and cartilage differentiation was more evident in the medial pterygoid process, which first became connected to the body. The tensor veli palatini could be clearly visualized and was situated medially to the medial pterygoid process. The site of origin of the lateral and medial pterygoids could also be observed at the lateral pterygoid process.

At stage E15, the body of the mandible (Fig. 19a-d) had clearly increased in size compared to the ramus. Secondary cartilage was detected for the first time at the entire condylar process and it showed its characteristic conical shape. The extension occupied by the condylar cartilage was approximately 464 μm in the anterior-posterior direction. The size of the secondary cartilage in the angular process, also observed for the first time at this stage, was 400 μm in the anterior-posterior direction. Three layers could be identified in both secondary cartilages, which from superior to inferior were: the fibroblastic/polymorphic tissue layer, the flattened chondrocytes zone, and the zone of hypertrophic chondrocytes. The coronoid process was larger at this stage, and as a result the mandibular notch could be clearly visualized between the condylar and coronoid processes. Meckel's cartilage was thinner and straight except for a curvature at the level of the posterior border of the condylar process. It was still a continuous structure indivisible from the malleus (Fig. 20a, b). The mandible surrounded the inferior alveolar nerve (Fig. 19a-d) and it left an ovoid-like shaped foramen for the mental branch. At this developmental stage the nerve was completely encircle by bone.

The temporomandibular joint (Fig. 19a-d). was composed of the slight convex glenoid fossa of the temporal bone, the condylar process of the mandible with its secondary cartilage and the mesenchymal tissue between these two structures. The distance between the condyle and this mesenchymal condensation was approximately 408 μm.

The bilaminar zone (Fig. 19a, b and Fig. 22) was mainly composed of loose mesenchyme and the number of blood vessels and vascular spaces around the retromandibular vein had increased compared to the previous stage. Some other structures found at the bilaminar zone were small arteries, the auriculotemporal nerve at the medial border of the retromandibular vein, adipose tissue and parotid gland tissue. Some sinusoidal waveform collagen bundles running vertical and lateral to the retromandibular vein were also identified.

The middle ear ossicles, i.e. malleus, incus and stapes, (Fig. 21) were composed of cartilaginous tissue. The malleus had increased in volume at its posterior portion and appeared separated from the incus as at stage E14.5. There were no remarkable changes in the incus and stapes compared to the previous stage.

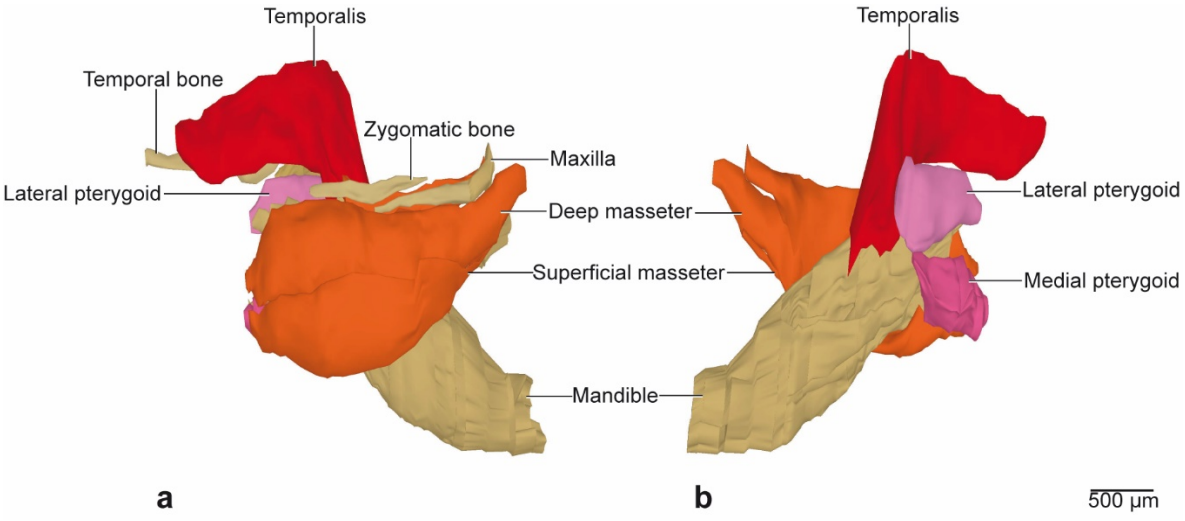

Fig. 17: Stage E15 (35-08). 3D reconstruction of the right half of the mandible and masticatory muscles.

a: Extension and attachments of the masseter and temporalis. Lateral view.

b: Extension and attachments of the lateral and medial pterygoids. Medial view.

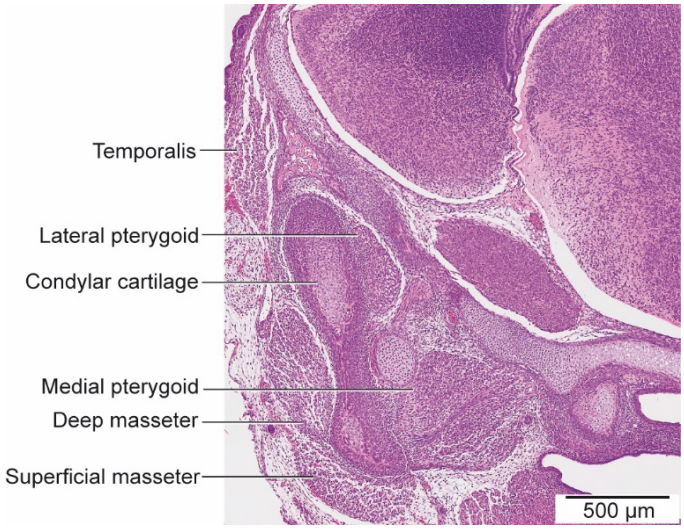

Fig. 18: Stage E15 (35-08). Histological section of the right half of the mandible through the condyle indicating the anatomical arrangement of the masticatory muscles.

Frontal plane, HE staining.

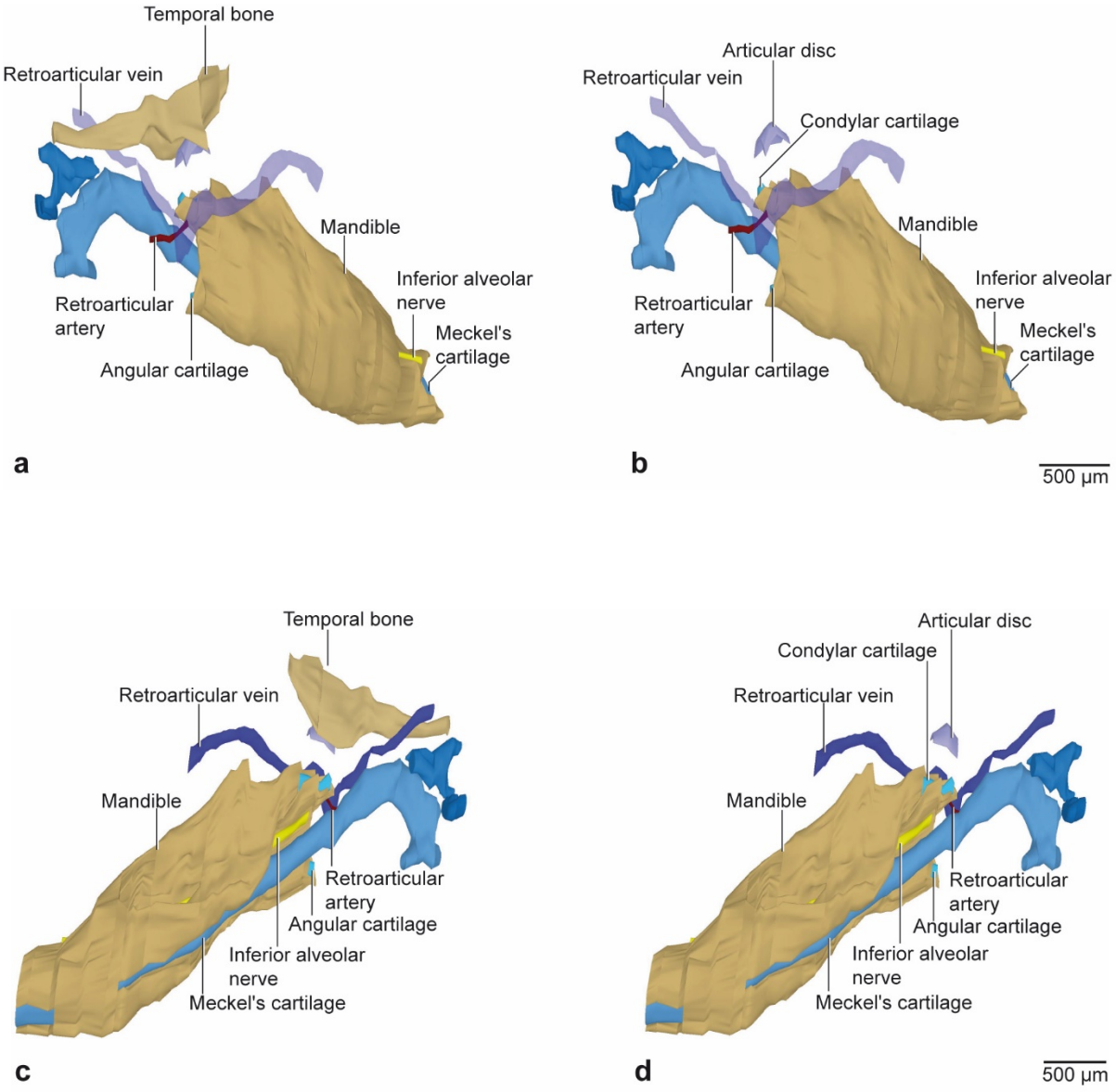

Fig. 19: Stage E15 (35-08). Partial 3D reconstruction of some components of the right temporomandibular joint and the region of the bilaminar zone.

a: Temporomandibular joint region with its temporal bone. Retromandibular vein made transparent to visualize the content and extension of the bilaminar zone. Lateral view.

b: Temporomandibular joint region, temporal bone removed to visualize the articular disc. Retromandibular vein made transparent to visualize the content and extension of the bilaminar zone. Lateral view.

c: Temporomandibular joint region with its temporal bone. Medial view.

d: Temporomandibular joint region, temporal bone removed to visualize the articular disc. Medial view.

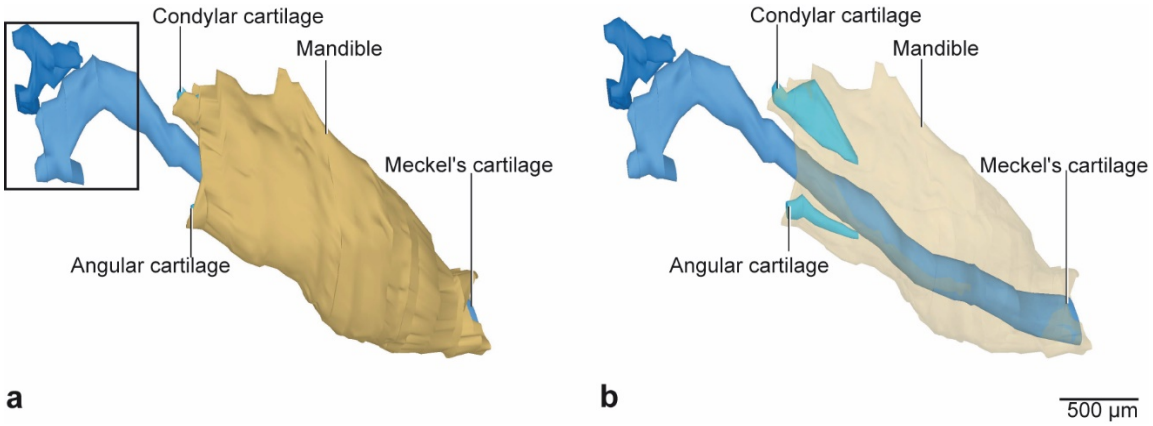

Fig. 20: Stage E15 (35-08). 3D reconstruction of the right half of the mandible, Meckel's cartilage and middle ear ossicles.

a: Lateral view. Box: see Fig. 21.

b: Same view with mandible made transparent. In this developmental stage the condylar and angular cartilages could be observed for the first time. Lateral view.

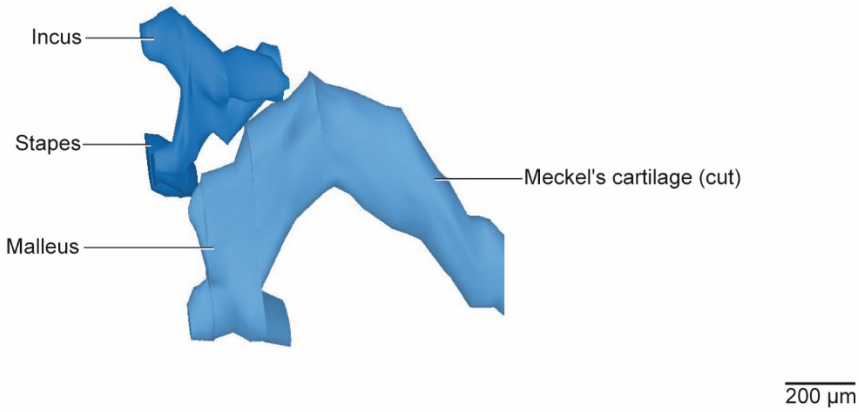

Fig. 21: Stage E15 (35-08). 3D reconstruction of a detailed view of the right middle ear ossicles.

Lateral view.

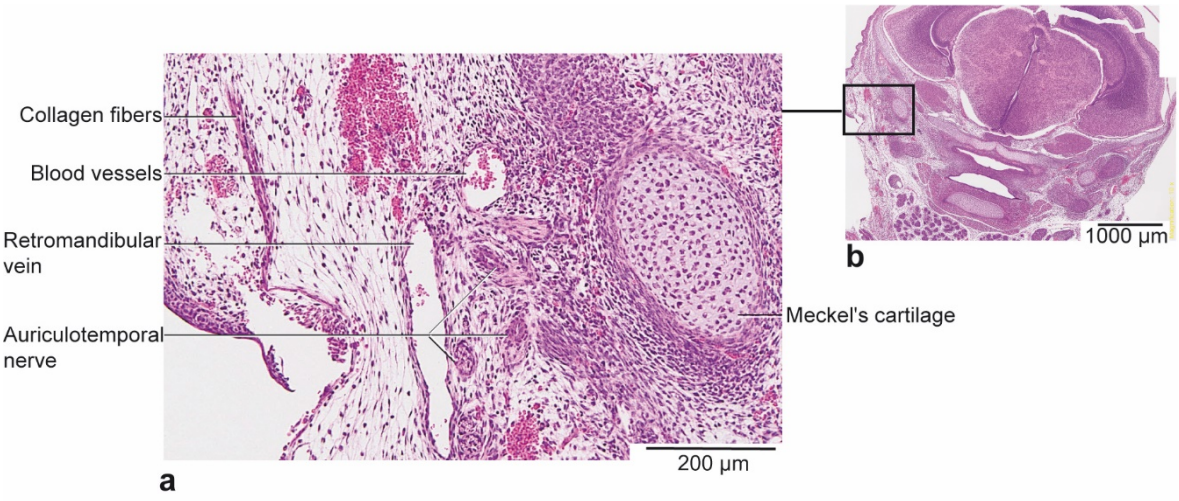

Fig. 22: Stage E15 (35-08). Bilaminar zone.

a: Histological section through the right bilaminar zone. Frontal plane. HE staining.

b: Survey of the whole section.

5.2.5 Stage E16

The zygomatic bone had extended in the anterior and posterior direction at this developmental stage, and this provided us a more accurate visualization of the masseter (Fig. 23a, b and Fig. 24): the superficial head arose from the anterior two thirds of the inferior lateral border of the zygomatic arch and from the zygomatic process of the maxilla. The deep head originated from the posterior third of the inferior lateral border and from the entire medial surface of the zygomatic arch. The attachment of the superficial head was found at the lateral, medial and inferior surfaces of the angular process, sharing this insertion area with the medial pterygoid. It also inserted at the inferior third of the lateral surface of the ramus of the mandible and at the masseteric tuberosity. The deep head was attached at the superior two thirds of the lateral surface of the ramus of the mandible. At this developmental stage some muscle fibers were observed for the first time, which run obliquely in the posterolateral direction. The masseter showed a more voluminous and rounded triangular shape than in the previous stages. Its apex was found at the anterior part of the maxilla, while the base was situated at the posterior border of the mandible. The superficial masseter overlaid two thirds of the deep masseter, and together they accounted for 55% of the overall masticatory muscle mass.

The temporalis (Fig. 23a, b and Fig. 24) arose at the lateral border of the temporal fossa and inserted into the mesenchyme of the coronoid process, the anterior part of the mandibular notch and at the corresponding medial surface of the mandible. The anterior fibers run straight vertically, the central fibers with an oblique anterior inclination, and the posterior fibers anteriorly downwards. The muscle showed a triangular form with the apex at the mandibular notch and the base at the temporal fossa. It had no specific boundaries inside and comprised 25% of the total masticatory muscle mass.

The lateral pterygoid (Fig. 23b and Fig. 24) had its origin at the ossified superior part and cartilaginous inferior part of the greater wing of the sphenoid. Furthermore, it also originated from the cartilaginous lateral surface of the lateral pterygoid process of this bone. It attached to the medial surface of the mesenchymal tissue of the condylar process and to the neck of the mandible. A further insertion was identified at the mesenchyme of the articular disc. The muscle fibers, which could be visualized for the first time at this stage, followed a posterolateral direction. The muscle extended in a parallelogram-like shape and no morphological divisions could be identified despite the different regions of attachment. The lateral pterygoid accounted for 9% of all the masticatory muscle mass.

The medial pterygoid (Fig. 23b and Fig. 24) originated at the cartilaginous region of the medial part of the lateral pterygoid process of the sphenoid bone. The attachment was located at the

mesenchyme of the medial and inferior surface of the angular process, sharing this site with the superficial masseter, and at the medial surface of the mandibular ramus. As its counterpart, the muscle fibers of the medial pterygoid run obliquely in a posterolateral direction. A fascia divided this rectangular-like shaped muscle into a superior and inferior head and both together accounted for 11% of the masticatory muscle mass.

The parotid gland was located lateral and posterior to the masseter and anterior to the cochlea. The excretory duct left the anterior-superior border of the gland and ran straight to open into the oral cavity at the level of the primordium of the first maxillary molar. The body of the parotid gland had superiorly, anteriorly and posteriorly increased in size compared to the previous stage and extended for 1240 μm in the anterior-posterior direction.

The lacrimal gland was situated superior to the masseter and lateral to the condylar process. It was formed by a duct, which ran anteriorly to reach the eyeball, and a body, which showed no changes in its dimension compared to the previous stage and extended 400 μm in the anterior-posterior direction.

The maxilla (Fig. 23a) was a voluminous bone situated at the middle third of the face. Compared to the previous stage, the frontal and palatinal processes were larger. The zygomatic process maintained its size and served as origin for the masseter.

The intramembranous ossification of the zygomatic bone (Fig. 23a) had also progressed further. At this developmental stage, two parts with a cylindrical-like shape were distinguished. One of them had reached the zygomatic process of the temporal bone to form the zygomatic arch that served as origin for the masseter.

The temporal bone (Fig. 25a, c) was located at the lateral wall and at the base of the skull. The extension and degree of ossification had progressed in the squamous and petrous regions. The concavity of the glenoid fossa at its inferior border was defined and a thin layer of collagen tissue surrounded it. The distance between it and the condyle had reduced slightly compared to the previous stage, and it was approximately 361 μm. At the anterior border of the glenoid fossa, the articular tubercle could be seen for the first time as a very slightly rounded eminence. Also for the first time, the zygomatic process could be observed as an extension of the most anterior part of the squamous region, and it articulated with the zygomatic bone to form the zygomatic arch. The temporalis arose from the temporal fossa, also located in the squamous part.

The sphenoid (Fig. 24) was located at the base of the skull and consisted of a central body, greater and lesser wings on either side of the bone, and two pterygoid processes, also on either side. The superior half of the greater wing had ossified, and calcified bone tissue formed the major part of the medial pterygoid process. At the same time, the number of cartilage cells in the

last- mentioned region had clearly decreased. The lateral pterygoid process was entirely cartilaginous, and regarding the body, the connection between it and the medial pterygoid process was more evident at this developmental stage. The attachment of the tensor veli palatini to the medial pterygoid process was evident, as well as the site of origin of the lateral and medial pterygoids at the lateral process.

Regarding the mandible (Fig. 25a-d), the secondary cartilage of the condylar and angular processes was more voluminous than in the previous stage and occupied an extension of 584 μm and 648 μm, respectively, in the anterior-posterior direction. The layers of the secondary cartilage were: the fibroblastic/polymorphic tissue layer, the flattened chondrocytes zone, and the zone of hypertrophic chondrocytes. The endochondral ossification had started in both regions. The coronoid process was also larger, ran straight superiorly and was continuous with the ramus of the mandible. Due to the increase in size in both the condylar and coronoid processes, the mandibular notch had become more pronounced. Meckel's cartilage (Fig. 26a, b) was seen for the first time to not be a continuous structure, since it had started to degenerate at the level of the anterior border of the first molar tooth bud. The posterior segment of Meckel's cartilage was observed as a straight structure, except for a slight inferior curvature at the level of the posterior border of the condylar cartilage. The inferior alveolar nerve (Fig. 25a-d) passed along the medial aspect of the mandible and ran superiorly to Meckel's cartilage following the same anterior direction. The nerve crossed through the mental foramen, which was located between the two segments of Meckel's cartilage.

The temporomandibular joint (Fig. 25a-d) consisted of the condylar process, the convex-shaped glenoid fossa, and the articular disc composed of mesenchymal tissue, among other structures. At this stage the distance between the condylar cartilage and the articular disc was approximately 145 μm.

In the bilaminar zone (Fig. 25a, b and Fig. 28), the loose mesenchyme could be found in less proportion than in the previous stages. However, the number of blood vessels and vascular spaces had increased and they surrounded the retromandibular vein, which was more voluminous. Numerous bundles of straight collagen fibers ran in a vertical direction lateral to the retromandibular vein, in which vicinity the masseter could be noted. Some other structures found in the bilaminar region were arterioles, the auriculotemporal nerve, fat tissue and parenchyma of the parotid gland.

The incudomalleolar and incudostapedial joints between the incus and the malleus and between the incus and the stapes, respectively, were visualized for the first time. All structures were composed of cartilaginous tissue (Fig. 27).

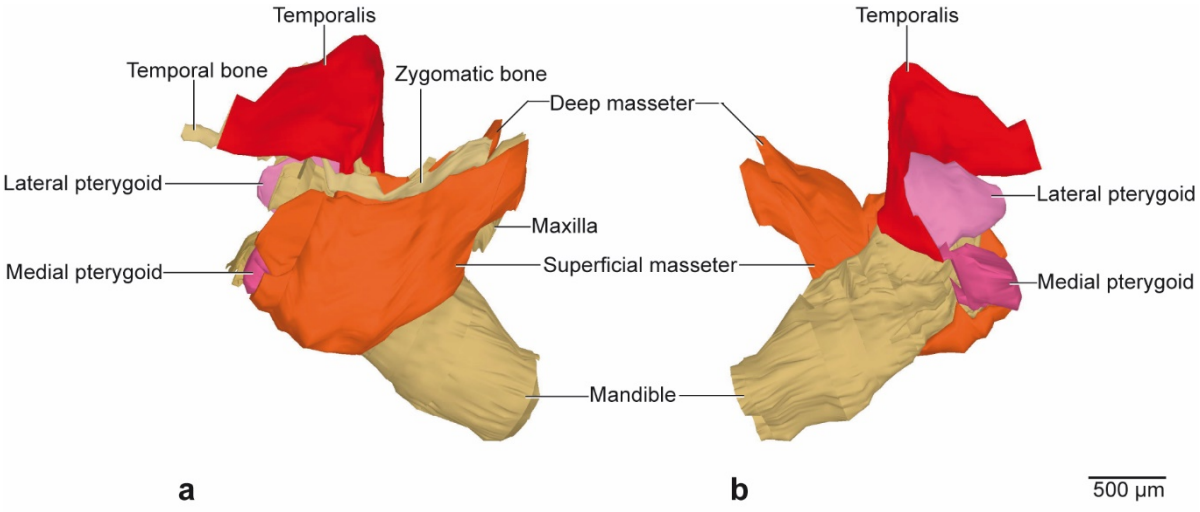

Fig. 23: Stage E16 (45-08). 3D reconstruction of the right half of the mandible and masticatory muscles.

a: Extension and attachments of the masseter and the temporalis. Lateral view.

b: Extension and attachments of the lateral and medial pterygoids. Medial view.

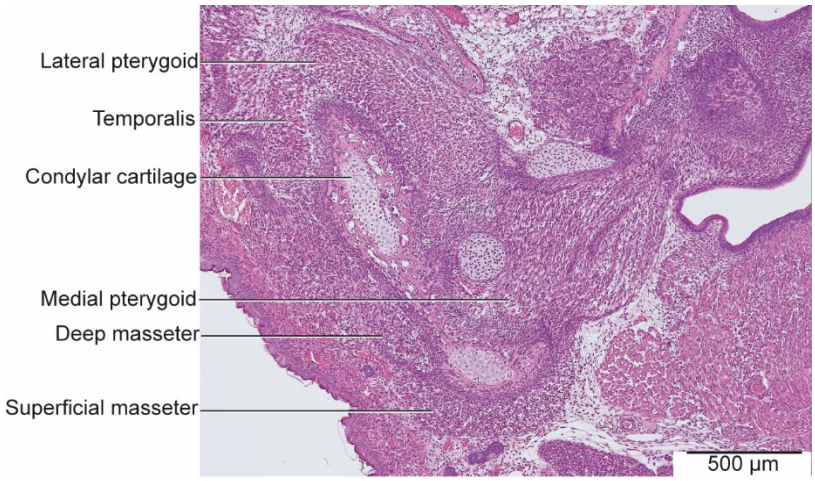

Fig. 24: Stage E16 (45-08): Histological section of the right half of the mandible through the condylar cartilage indicating the anatomical arrangement of the muscles.

Frontal plane, HE staining.

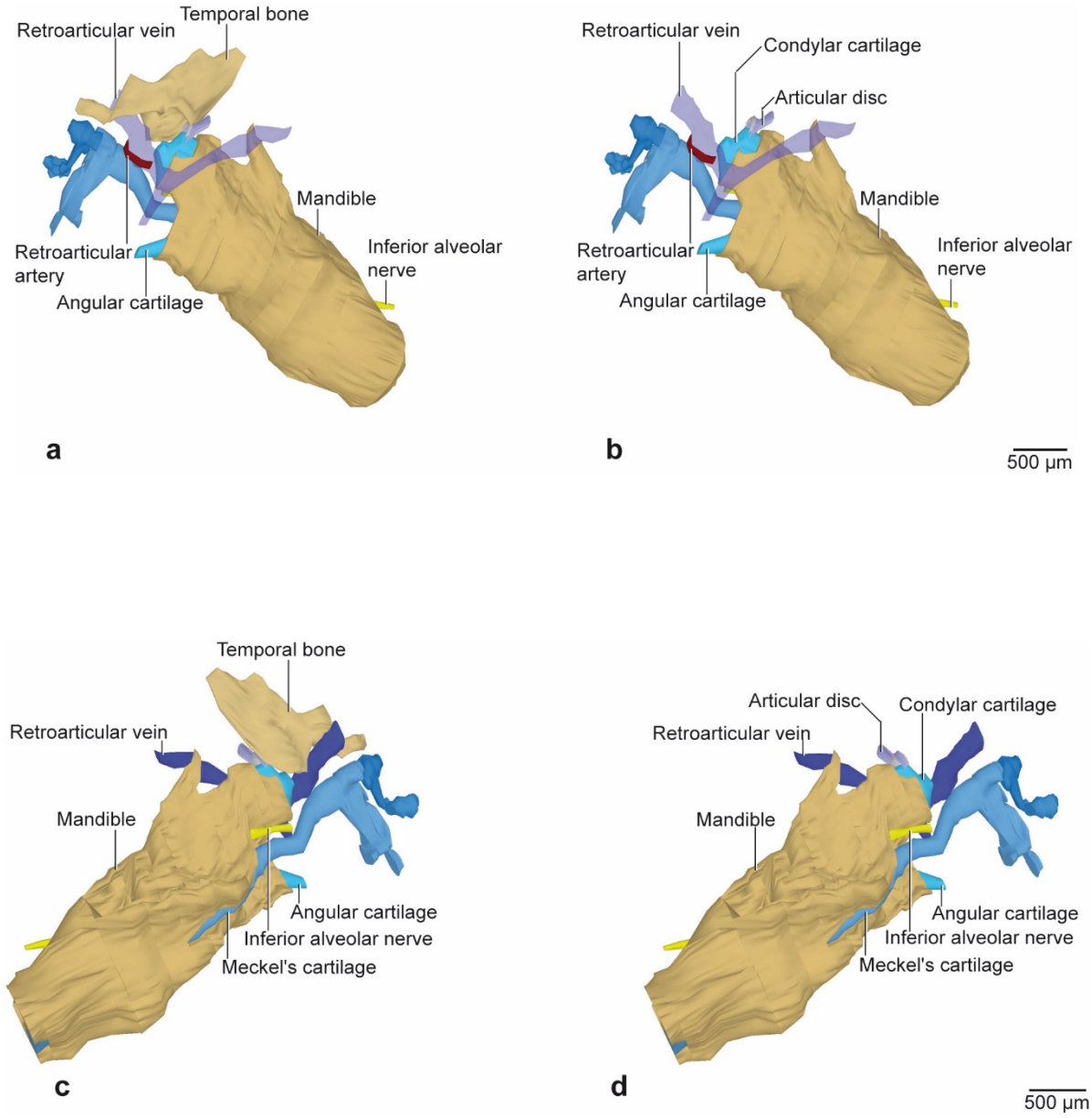

Fig. 25: Stage E16 (45-08). Partial 3D reconstruction of some components of the right temporomandibular joint and the region of the bilaminar zone.

a: Temporomandibular joint region with its temporal bone. Retromandibular vein made transparent to visualize the content and extension of the bilaminar zone. Lateral view.

b: Temporomandibular joint region, temporal bone removed to visualize the articular disc. Retromandibular vein made transparent to visualize the content and extension of the bilaminar zone. Lateral view.

c: Temporomandibular joint region with its temporal bone. Medial view.

d: Temporomandibular joint region, temporal bone removed to visualize the articular disc. Medial view.

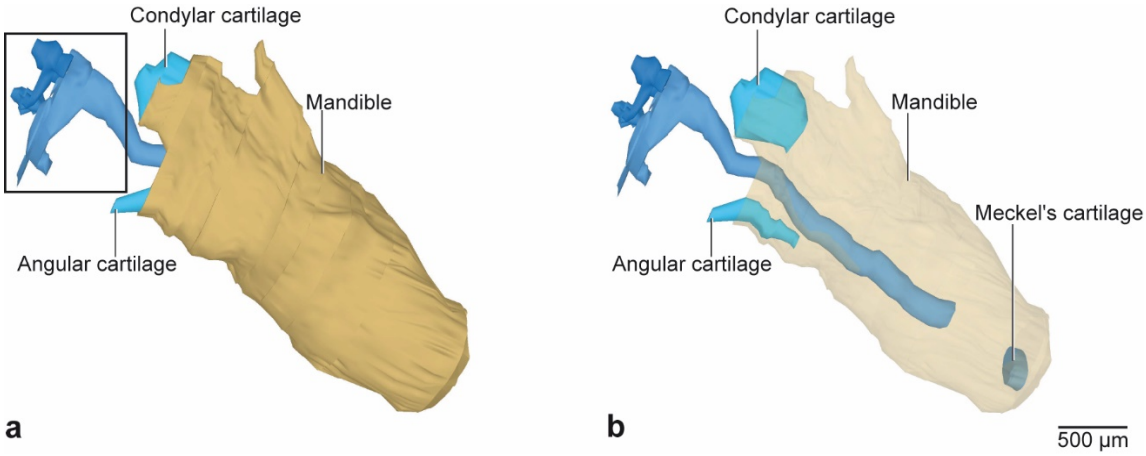

Fig. 26: Stage E16 (45-08). 3D reconstruction of the right half of the mandible, Meckel's cartilage and middle ear ossicles.

a: In this stage, the condylar cartilage is larger than in the previous stage and its shape has become round. Lateral view. Box: see Fig. 27.

b: Same view with mandible made transparent. For the first time Meckel's cartilage was seen not to be a continuous structure. A small portion of Meckel's cartilage was visible at the most anterior part of the mandible. Lateral view.

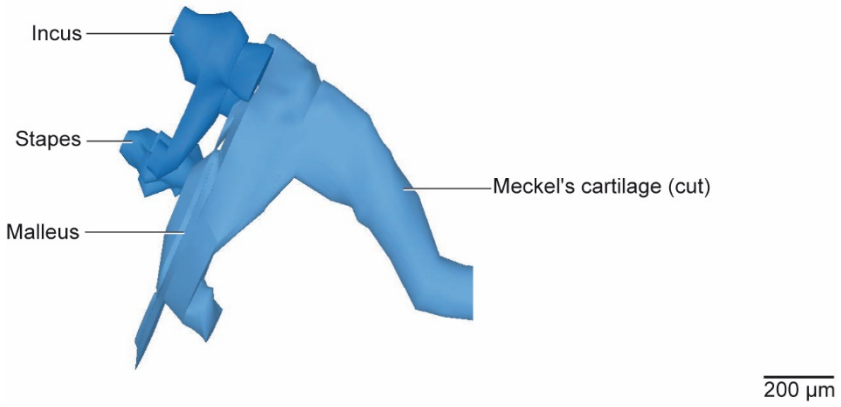

Fig. 27: Stage E16 (45-08). 3D reconstruction of a detailed view of the right middle ear ossicles.

Lateral view.

The incudomalleolar and incudostapedial joints could be observed for the first time.

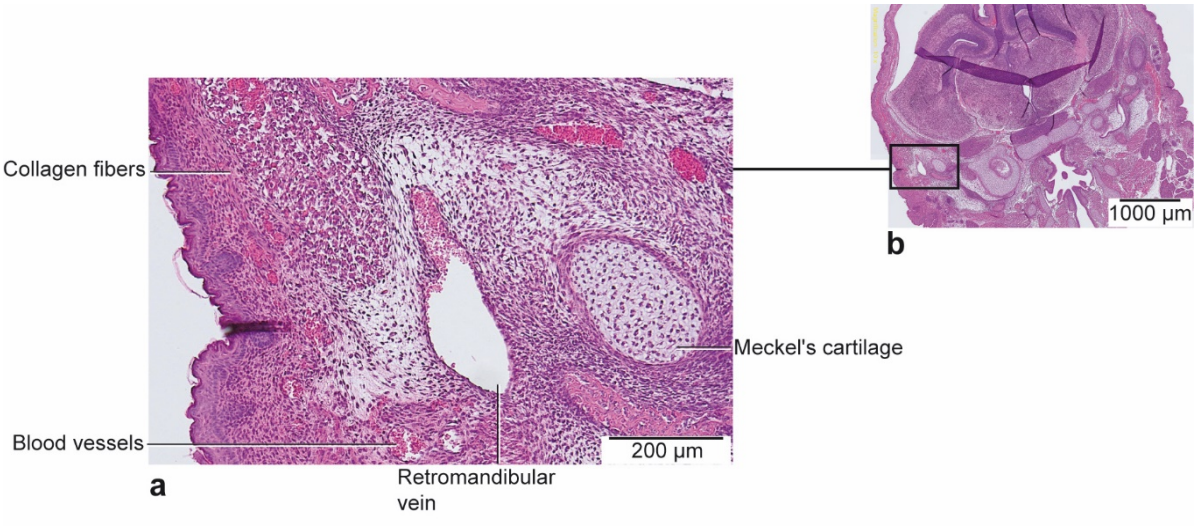

Fig. 28: Stage E16 (45-08). Bilaminar zone.

a: Histological section of the region through the right bilaminar zone. Frontal plane, HE staining.

b: Survey of the whole section.

5.2.6 Stage E17

Regarding the masseter (Fig. 29a, b and Fig. 31), the superficial belly had its origin at the anterior two thirds of the inferior lateral border of the zygomatic arch and at the zygomatic process of the maxilla, while the deep belly originated from the posterior third of the inferior border of the lateral surface of the zygomatic arch, and also from its entire medial surface. The superficial masseter attached to both the lateral border of the angular process and the inferior third of the lateral surface of the ramus of the mandible. It also inserted at the masseteric tuberosity of the mandible. The deep masseter had its attachment at the superior two thirds of the lateral border of the ramus of the mandible, just superior to the superficial masseter. The masseter showed a triangular-like shape with the apex in the maxilla and the base in the mandible. The muscle fibers ran obliquely in the posterolateral direction and it comprised 45% of the total masticatory muscle mass.

The temporalis (Fig. 29a, b and Fig. 31) arose from the lateral border of the temporal fossa. It inserted at the coronoid process, at the mandibular notch, and at the corresponding medial surface of the mandible. The anterior muscle fibers run straight downwards, those in the center anteriorly downwards and those posterior with a marked oblique inclination also downwards. The temporalis showed a triangular form with the apex inferior to the mandibular notch and the base at the lateral surface of the skull. It comprised 28% of the whole masticatory muscle mass.

The lateral pterygoid (Fig. 29b and Fig. 31) originated from the cartilage of the lateral border of the lateral pterygoid process and from the ossified greater wing of the sphenoid bone. Its insertion was visualized at the medial surface of the condylar process, at the neck of the mandible, and also at the anterior border of the articular disc. The fibers run posterolaterally in this parallelogram-like shaped muscle. Despite the three regions of insertion being able to be visualized, a separation into three corresponding heads was morphologically not very obvious. The lateral pterygoid accounted for 12% of the total masticatory muscle mass.

The medial pterygoid (Fig. 29b and Fig. 31) arose from the medial surface of the cartilaginous lateral process of the sphenoid bone and was attached to the medial and inferior border of the angular process of the mandible and at the medial surface of the mandibular ramus. The muscle fibres of this rectangular-like shaped muscle run obliquely, following a posterolateral direction. The medial pterygoid was divided by a fascia into superior and inferior heads and it comprised 15% of the total masticatory muscle mass.

The stylomandibularis (Fig. 30a, b) did not count among the masticatory muscles, but it was found in our region of interest. It originated from the styloid process of the temporal bone and

attached to the anterior part of the medial surface of the angular process. It showed a cylindrical form with no divisions inside.

The body of the parotid gland was located lateral and posterior to the masseter and it had increased in size posteriorly to extend 2136 μm in the anterior-posterior direction. The straight excretory duct extended from the anterior part of the body and reached the oral cavity at the level of the first molar tooth bud.

The lacrimal gland was visualized superior to the masseter and lateral to the masseter, at the same level as the condylar process. The size of the gland's body remained almost the same (448 μm in the anterior-posterior direction) as in the previous stage and the excretory duct ran straight to reach the eyeball.

The maxilla (Fig. 29a) was the main bone of the midface. It was composed of the body and three processes, i.e. frontal, palatine and zygomatic, the last of which was the site of origin of the masseter.

The zygomatic bone (Fig. 29a) was a long and cylindrical structure composed of three parts and situated lateral to the mandible and the maxilla and inferior and anterior to the temporal bone. The whole structure served as the origin for the masseter.

The temporal bone (Fig. 32a, c) was situated at the lateral surface and at the base of the skull, and its squamous and petrous parts were clearly discerned. The first one was the largest and it contained the glenoid fossa, the articular tubercle, and the zygomatic process among other structures. The glenoid fossa formed the temporal component of the temporomandibular joint and it was separated by 403 μm from the condyle. The very slight articular tubercle formed the anterior boundary of the glenoid fossa and showed no significant changes compared to stage E16. At least three muscles originated from this bone: the masseter from the zygomatic arch, the temporalis from the temporal and the stylomandibularis from the styloid process.

The sphenoid (Fig. 31) was located at the base of the skull and was composed of different parts. The greater wing of the sphenoid bone had entirely ossified, while the body and the lateral process remained cartilaginous. The medial process was composed of secondary cartilage at its most inferior part and of bone at the superior part. This process was the site of insertion of the tensor veli palatini whereas the lateral and medial pterygoid arose from the lateral process.

The mandible (Fig. 32a-d) had reached its adult shape and showed a prominent concavity at the posterior border of the mandibular ramus. The secondary cartilage of the condylar process had increased in volume and it extended 768 μm in the anterior-posterior direction. Three layers, namely the fibroblastic/polymorphic tissue layer, the flattened chondrocytes zone, and the zone of hypertrophic chondrocytes, could be observed in the secondary cartilage. At the same time the

ossification of the mandible advanced. The angular process had undergone similar changes as the condylar process. Its secondary cartilage was also larger (744 µm in the anterior-posterior direction) and it also presented these three layers. The coronoid process had increased its anterior-posterior volume and it ran straight vertically. As in the previous stage, Meckel's cartilage (Fig. 33a, b) was found to be a discontinuous structure and a small segment remained at the most anterior portion of the mandible. The posterior segment ran from the middle of the mandible to the region of the middle ear, where it was found indivisible of the malleus. A nerve fibre bundle, namely the inferior alveolar nerve (Fig. 32a-d), was situated at the medial surface of the mandible and it ran superiorly and laterally to Meckel's cartilage. Anteriorly, the nerve gave off the mental branch, which passed through the mental foramen.

Some components of the temporomandibular joint (Fig. 32a-d), which were visible at this developmental stage with our histological methods, were the condylar process of the mandible, including the three layers of its secondary cartilage, the glenoid fossa of the temporal bone, and the articular disc composed of mesenchymal tissue.

The bilaminar zone (Fig. 32a, b and Fig. 35) was situated between the temporomandibular joint and the middle ear. Some of the structures that composed it were the retromandibular vein, arterioles and some other small blood vessels, the auriculotemporal nerve, adipose tissue and the parenchyma of the parotid gland. The bilaminar zone was laterally delimited by straight collagen fibres and by the masseter.

Malleus, incus and stapes (Fig. 34) were composed of cartilaginous tissue forming the incudomalleolar and incudostapedial joints. The manubrium of the malleus was larger than in the previous stages.

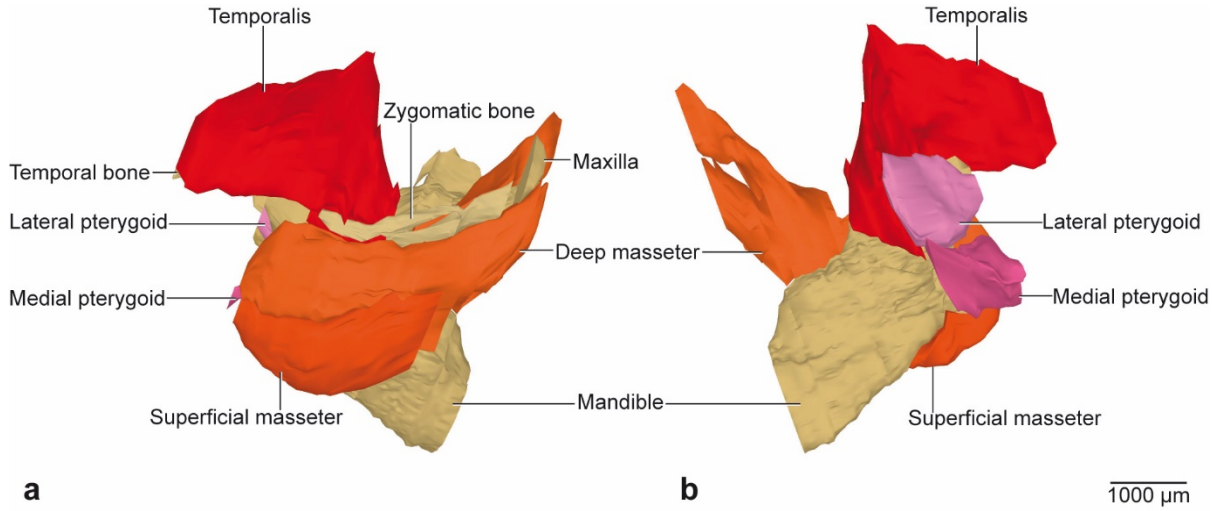

Fig. 29: Stage E17 (51-08). 3D reconstruction of the right half of the mandible and masticatory muscles.

a: Extension and attachments of the masseter and temporalis. Lateral view.

b: Extension and attachments of the lateral and medial pterygoids. Medial view

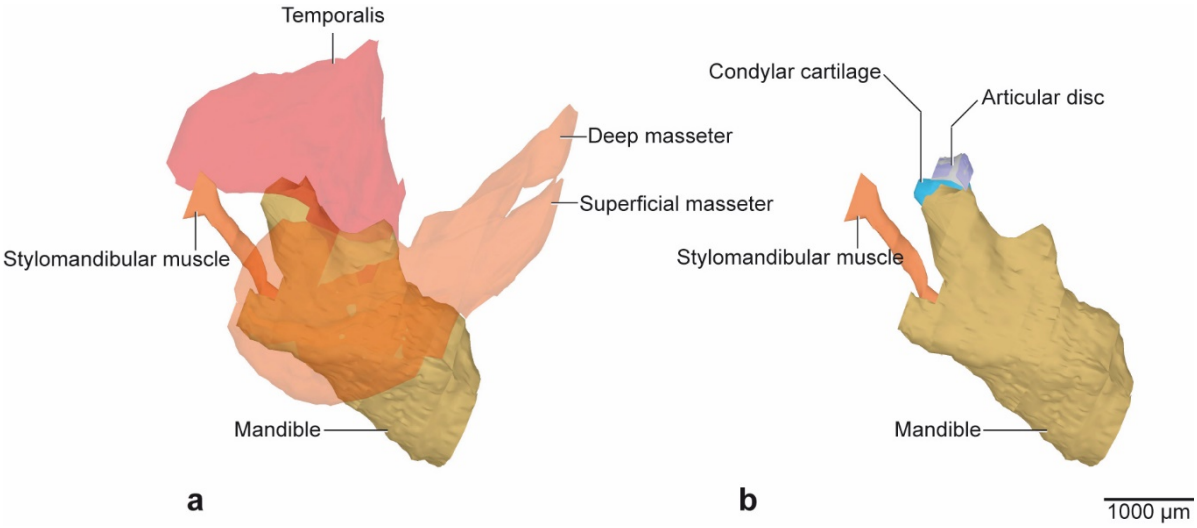

Fig. 30: Stage E17 (51-08). 3D reconstruction of the right half of the mandible and of the masseter, temporal and stylomandibular muscle.

a: Masseter and temporal made transparent to visualize the location of the stylomandibular muscle. Lateral view.

b: There is a large space of approximately 760 µm between the stylomandibular muscle and the articular disc, and therefore, no attachment into it is obvious. Lateral view.

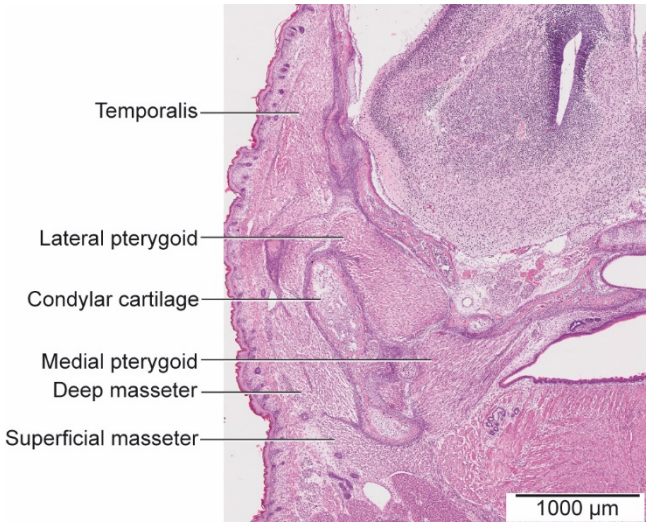

Fig. 31: Stage E17 (51-08): Histological section of the right half of the mandible through the condylar cartilage indicating the anatomical arrangement of the muscles.

Frontal plane, HE staining.

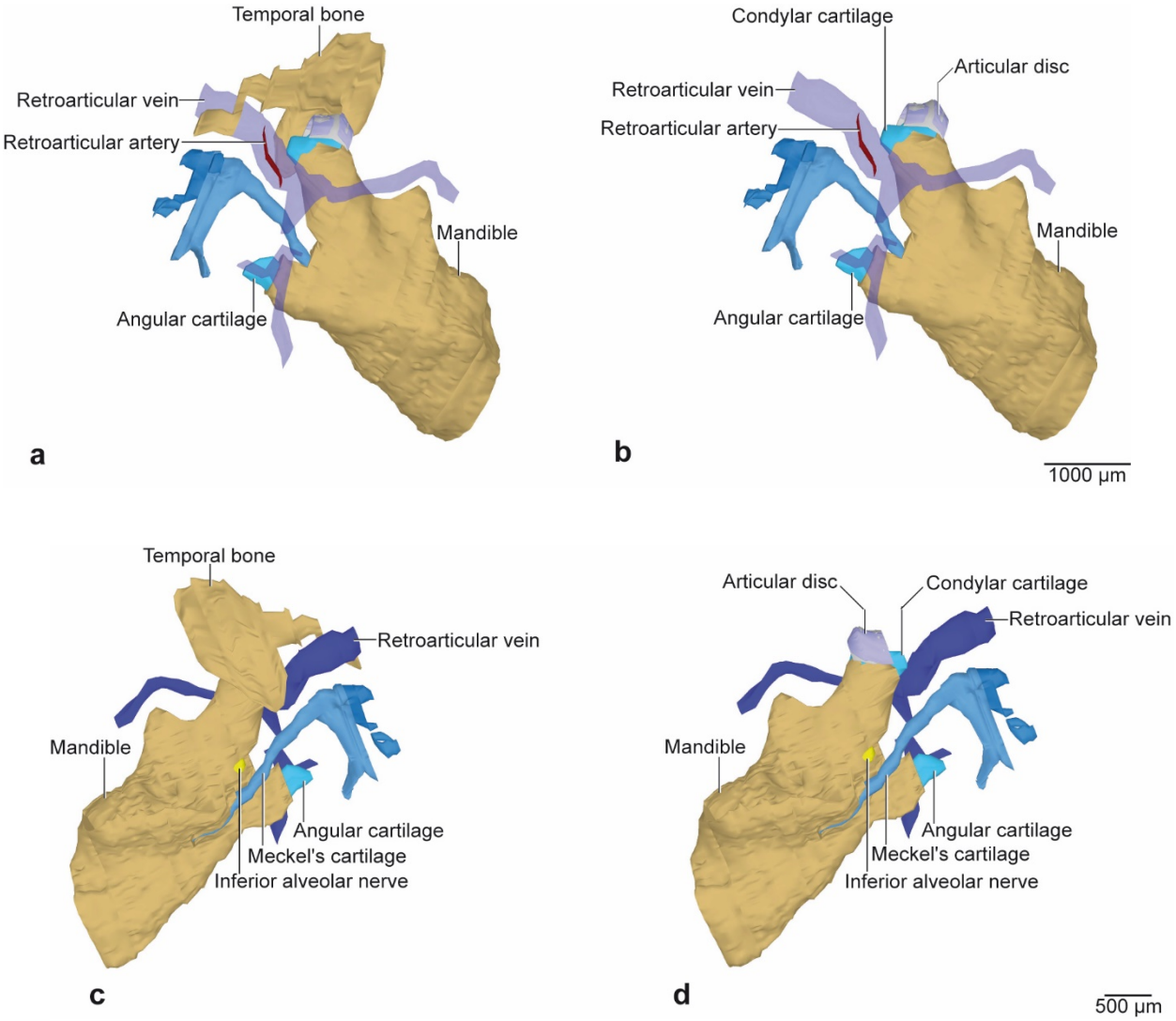

Fig. 32: Stage E17 (51-08). Partial 3D reconstruction of some components of the right temporomandibular joint and the region of the bilaminar zone.

a: Temporomandibular joint region with its temporal bone. Retromandibular vein made transparent to visualize the content and extension of the bilaminar zone. Lateral view.

b: Temporomandibular joint region, temporal bone removed to visualize the articular disc. Retromandibular vein made transparent to visualize the content and extension of the bilaminar zone. Lateral view.

c: Temporomandibular joint region with its temporal bone. Medial view.

d: Temporomandibular joint region, temporal bone removed to visualize the articular disc. Medial view.

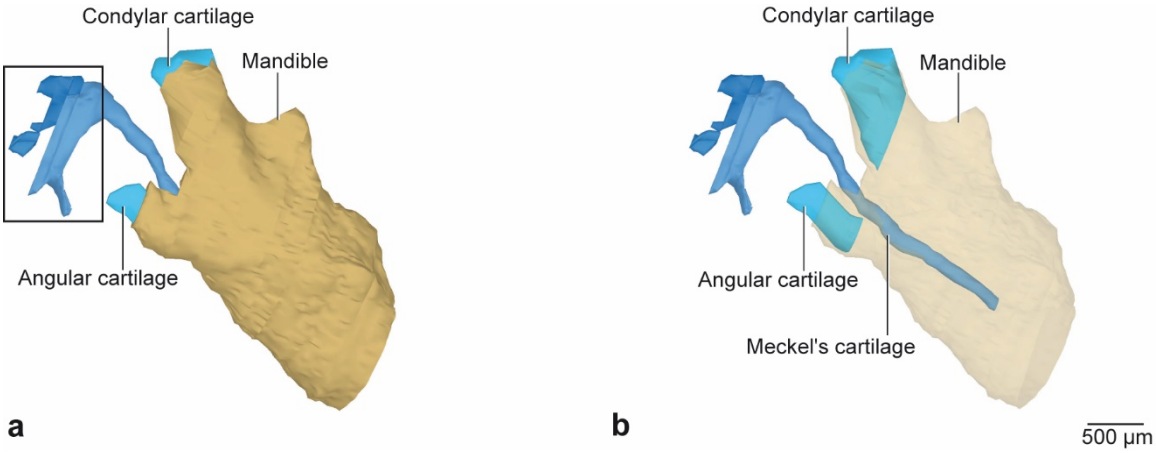

Fig. 33: Stage E17 (51-08). 3D reconstruction of the right half of the mandible, Meckel's cartilage and middle ear ossicles.

a: Lateral view. Box: see Fig. 34.

b: Same view with mandible made transparent. Lateral view.

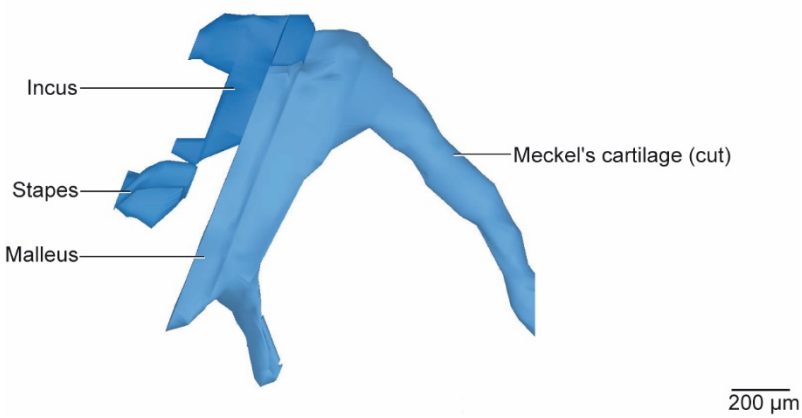

Fig. 34: Stage E17 (51-08). 3D reconstruction of a detailed view of the right middle ear ossicles.

Lateral view

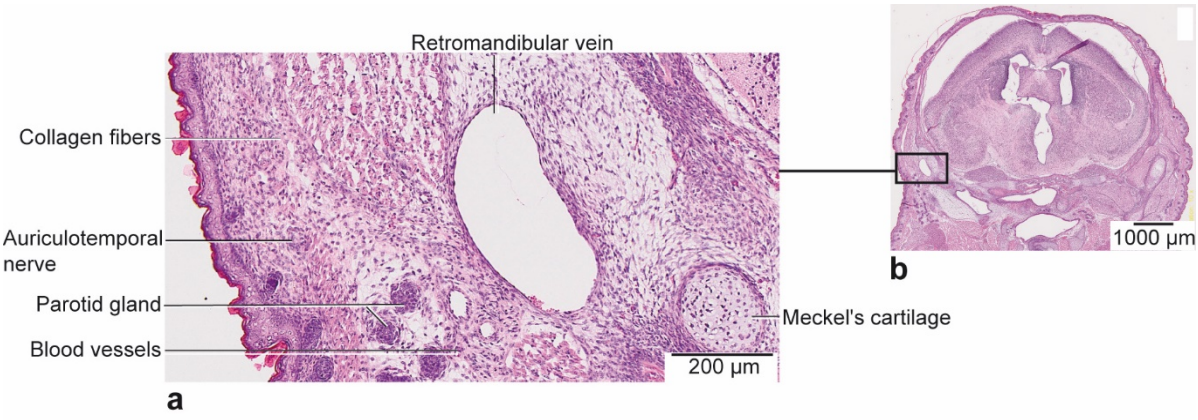

Fig. 35: Stage E17 (51-08). Bilaminar zone.

a: Histological section of the region through the right bilaminar zone. Frontal plane, HE staining.

b: Survey of the whole section.

5.2.7 Stage E18

With regard to the masseter (Fig. 36a, b and Fig. 37), the origin of the superficial layer was found at the anterior two thirds of the lateral border of the zygomatic arch and at the zygomatic process of the maxilla. It inserted at the lateral border of the angular process, at the inferior third of the lateral surface of the ramus and at the masseteric tuberosity of the mandible. The origin of the deep layer was situated at the posterior third of the lateral border of the zygomatic arch and also at the medial surface of this bone. It attached to the superior two thirds of the lateral border of the ramus of the mandible. The microscopic visualization allowed us to determine the oblique orientation of the muscular fibers in the posterolateral direction. The muscle showed a triangular-like form with the apex on the maxilla and the base on the mandible. It comprised 57% of the whole masticatory muscle mass.

The temporalis (Fig. 36a, b and Fig. 37) arose from a large area located on the lateral fossa of the temporal bone. It attached to the coronoid process, to the mandibular notch, and to a corresponding small area of the medial surface of the body of the mandible. The orientation of the muscular fibers varied depending on the part of the muscle: in the anterior third the fibers run vertically downwards, in the center slightly obliquely, and in the posterior third notably obliquely. The shape of the temporalis was also seen as triangular, showing the apex on the mandible and the base on the skull. Any boundary could be observed inside it so, therefore, only one muscle has been described. This accounted for 27% of the masticatory muscle mass.

The lateral pterygoid (Fig. 36b and Fig. 37) originated from the cartilaginous lateral surface of the lateral process of the sphenoid bone. A further origin was also situated at a small cartilaginous area and at a large ossified part of the greater wing of the sphenoid bone. It inserted into the medial surface of both the condylar process and the neck of the mandible. Some fibers of the lateral pterygoid extended to the anterior part of the articular disc. The muscle fibers of the lateral pterygoid were orientated posterolaterally. It had a parallelogram-like shape and represented 5% of the whole masticatory muscle mass.

The medial pterygoid (Fig. 36b and Fig. 37) arose from the cartilaginous medial border of the lateral pterygoid process of the sphenoid bone. It inserted into the medial surface of the angular process and the mandibular ramus, and also into the inferior border of the angular process. The muscle fibers run obliquely from the sphenoid bone to the mandible. A significant fascia divided it into a superior and an inferior head and it gave the muscle the appearance of a rectangle. Both heads accounted for 11% of the total masticatory muscle mass.

The major salivary parotid gland, located lateral and posterior to the masseter and anterior to the external acoustic meatus, was composed of an excretory duct and a body. The straight duct

opened into the oral cavity opposite to the primordium of the maxillary first molar and the body was surrounded by a capsule. The anterior-posterior size of the body was 1220 μm.

The exocrine lacrimal gland was situated superior to the masseter and at the lateral side condylar process. Its body showed an almond shape and extended 500 μm in the anterior-posterior direction, and its duct reached the eyeball.

The maxilla (Fig. 36a) was located at the midface and showed a voluminous body and three processes, in particular the frontal, palatine and zygomatic, from which the masseter originated.

The zygomatic bone (Fig. 36a) was located lateral to the mandible and the maxilla and anterior and inferior to the temporal bone. It was composed of three cylindrical-like shaped parts and the origin of the masseter was found along the zygomatic arch.

The temporal bone (Fig. 38a, c) was composed of several parts: the squamous contained the glenoid fossa (separated by 349 μm from the condyle), the flattened articular tubercle, and the zygomatic process, which was the most anterior projection of the squamous part. The temporal fossa was also situated in the squamous part and was the site of origin of the temporalis.

The sphenoid bone (Fig. 37) was comprised of different tissues: primary cartilage at the lateral pterygoid process and at the body and bone, and a small area of secondary cartilage at the medial process. The greater wing showed bone at its superior two thirds and cartilage at its inferior third. Both pterygoid muscles originated from the lateral pterygoid process, and the tensor veli palatini from the medial process.

Regarding the mandible (Fig. 38a-d), the extension of the secondary cartilage in both the condylar and angular processes was 600 μm in the anterior-posterior direction, smaller than in the previous prenatal stages. The three layers that composed the secondary cartilage, namely the fibroblastic/polymorphic tissue layer, the flattened chondrocytes zone, and the zone of hypertrophic chondrocytes, could be clearly visualized. The coronoid process was surrounded by mesenchymal tissue and did not show any discernible change compared to stage E17. Meckel's cartilage (Fig. 39a, b) also remained very similar to the previous stage and could be divided into two segments: the anterior one from the symphysis of the mandible, and the posterior segment, which ran from an area posterior to the mental foramen and reached the malleus. The inferior alveolar nerve (Fig. 38a-d) passed along the medial aspect of the mandible and crossed into the lateral direction through the mental foramen, which showed a more round shape than in the previous stages.

Regarding the temporomandibular joint (Fig. 38a-d), the secondary cartilage of the condylar process had diminished compared to the previous stage, as well as the distance between it and the articular disc. The glenoid fossa was closer to the condylar process and the articular disc was

composed of mesenchymal tissue and fibroblasts. Between these last two components, the superior joint cavity was observed for the first time.

In the bilaminar zone (Fig. 38a, b and Fig. 41), some loose mesenchymal tissue could be found but the major area was occupied by the retromandibular vein. There were some other blood vessels, such as arterioles and venules, and also vascular spaces. The bundles of straight collagen tissue were more obvious than in the previous stages, and they ran vertically at the lateral border of the bilaminar zone. Numerous arterioles, the auriculotemporal nerve, adipose tissue and the parenchyma of the parotid gland could be also detected in the bilaminar zone.

As in the previous stage, the malleus, incus and stapes (Fig. 40) were cartilaginous and formed the incudomalleolar and incudostapedial joints.

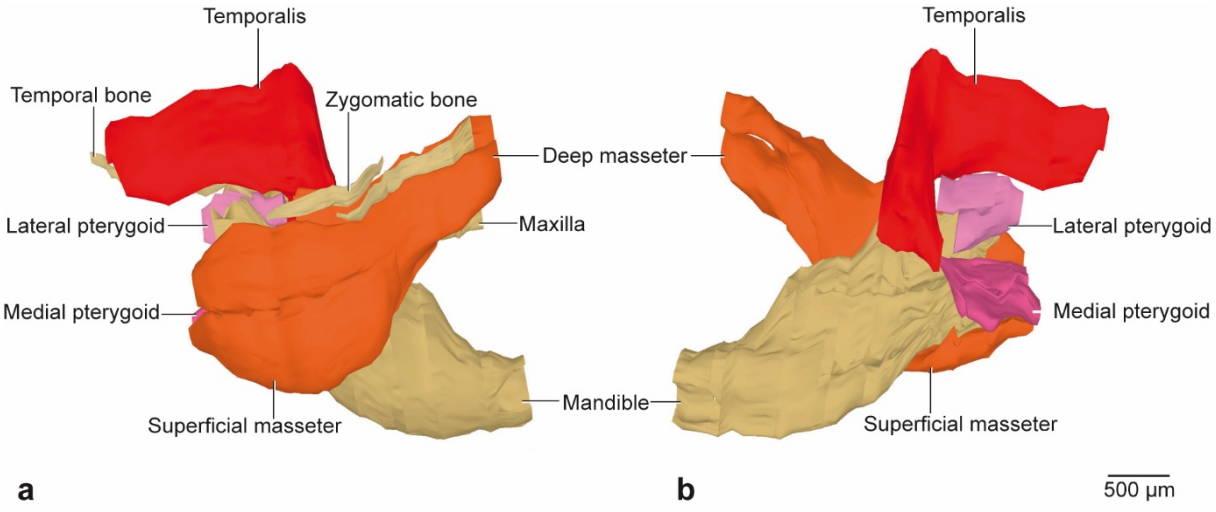

Fig. 36: Stage E18 (102-11) 3D reconstruction of the right half of the mandible and masticatory muscles.

a: Extension and attachments of the masseter and temporalis. Lateral view.

b: Extension and attachments of the lateral and medial pterygoids. Medial view.

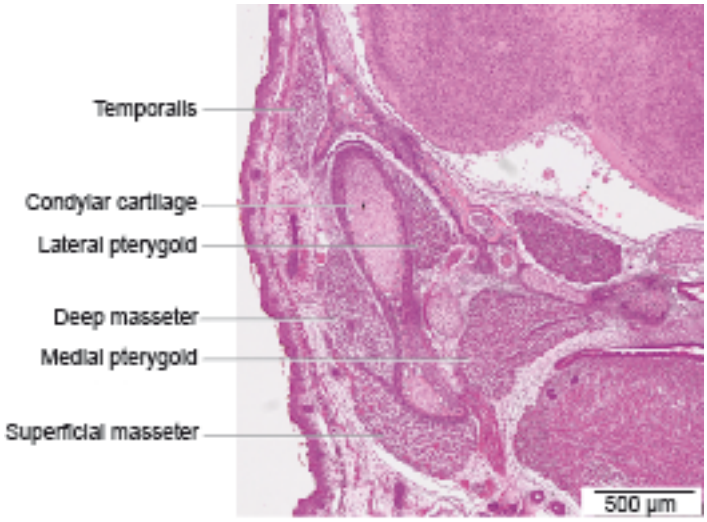

Fig. 37: Stage E18 (102-11). Histological section of the right half of the mandible through the condylar cartilage indicating the anatomical arrangement of the masticatory muscles.

Frontal plane, HE staining.

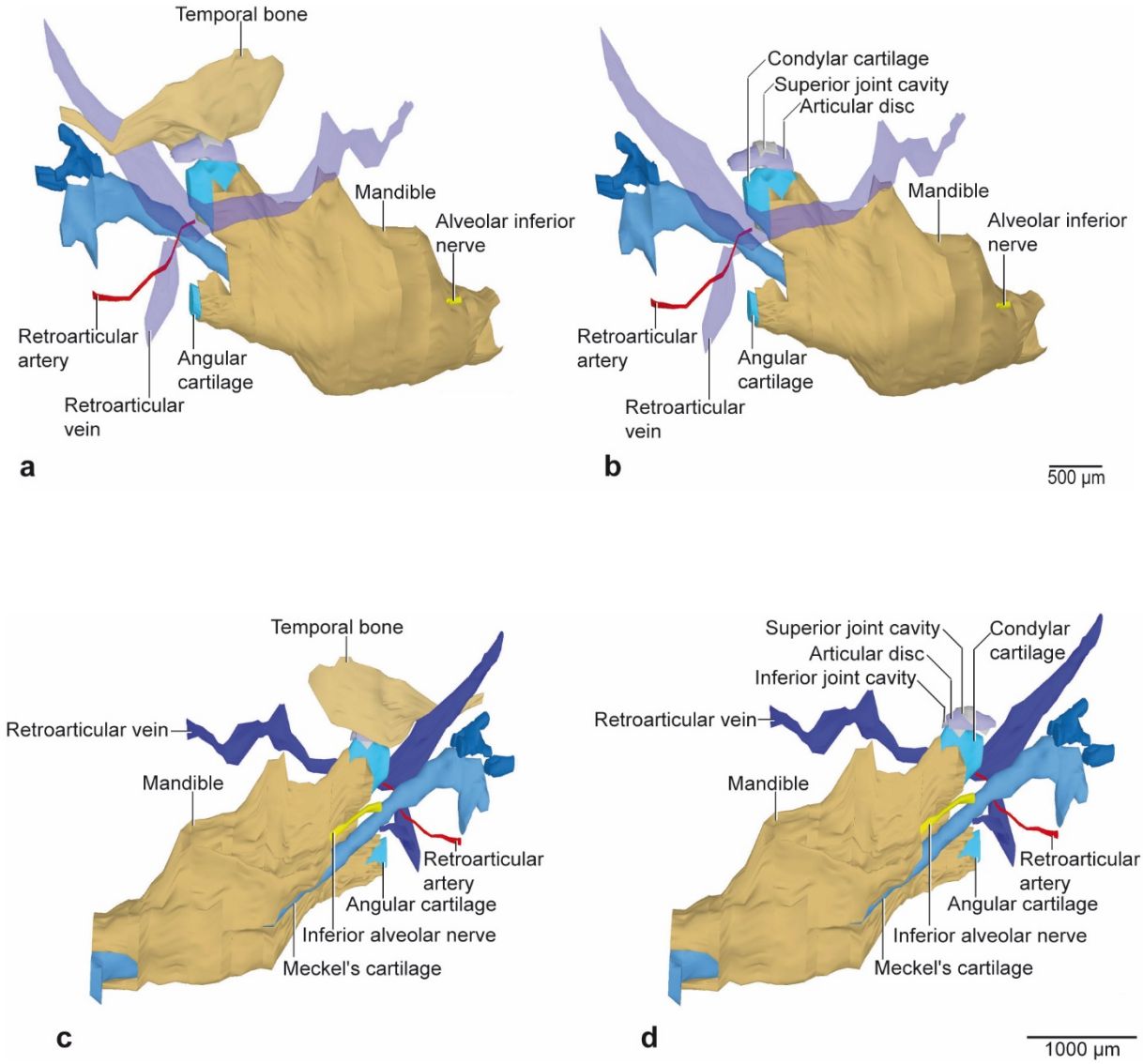

Fig. 38: Stage E18 (102-11). Partial 3D reconstruction of some components of the right temporomandibular joint and the region of the bilaminar zone.

a: Temporomandibular joint region with its temporal bone. Retromandibular vein made transparent to visualize the content and extension of the bilaminar zone. Lateral view.

b: Temporomandibular joint region, temporal bone removed to visualize the superior joint cavity and the articular disc. Retromandibular vein made transparent to visualize the content and extension of the bilaminar zone. Lateral view.

c: Temporomandibular joint region with its temporal bone. Medial view.

d: Temporomandibular joint region, temporal bone removed to visualize the superior joint cavity and the articular disc. Medial view.

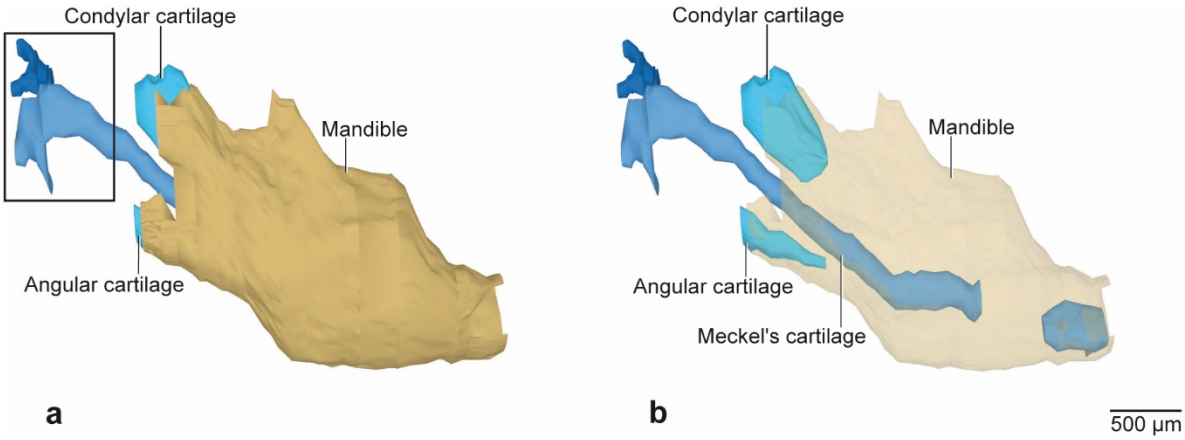

Fig. 39: Stage E18 (102-11). 3D reconstruction of the right half of the mandible, Meckel's cartilage and middle ear ossicles.

a: Lateral view. Box: see Fig. 40.

b: Same view with mandible made transparent. Lateral view.

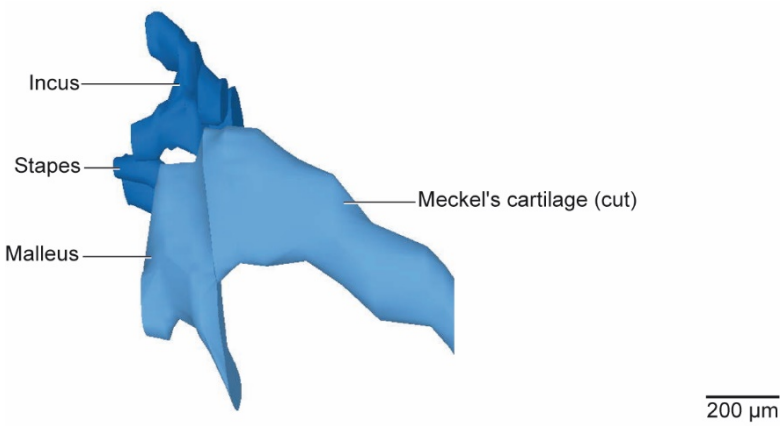

Fig. 40: Stage E18 (102-11). 3D reconstruction of a detailed view of the right middle ear ossicles.

Lateral view.

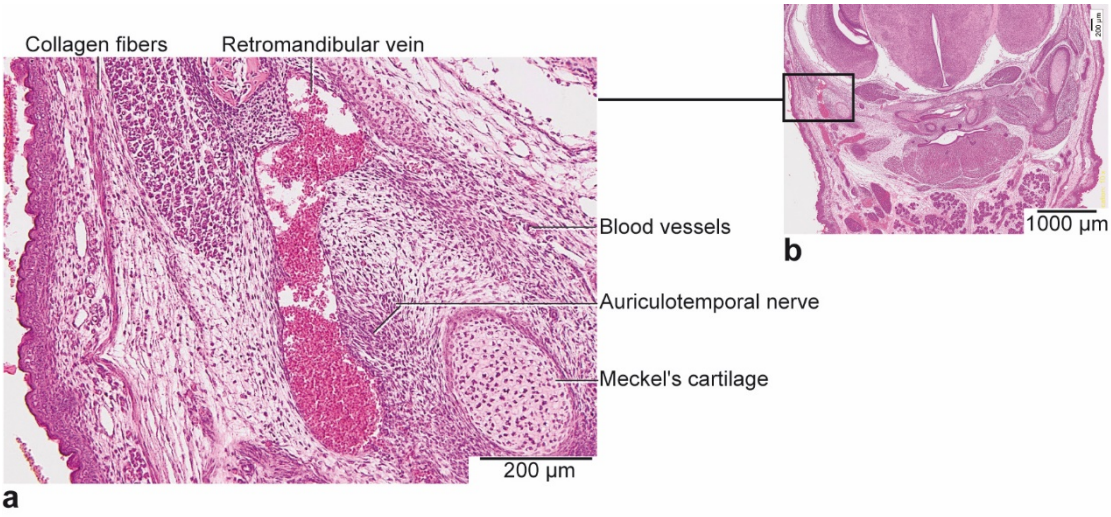

Fig. 41: Stage E18 (51-08). Bilaminar zone.

a: Histological section of the region through the right bilaminar zone. Frontal plane, HE staining.

b: Survey of the whole section.

5.2.8 Stage E20

Concerning the masseter (Fig. 42a, b and Fig. 43), the superficial belly originated from the anterior two thirds of the inferior lateral edge of the zygomatic arch and from the zygomatic process of the maxilla. It attached to the lateral surface of the angular process, to the inferior third of the lateral border of the mandible, and to the masseteric tuberosity. The deep belly of the masseter had its origin at the posterior third of the inferior lateral edge and at the medial surface of the zygomatic arch. Its insertion was found at the superior two thirds of the lateral surface of the mandible. The direction of the muscle fibers of both bellies was oblique in the posterolateral direction. The muscle showed a triangular shape with the apex in the anterior part of the maxilla and the base in the posterior part of the mandible. It accounted for 60% of the masticatory muscle mass.

The temporalis (Fig. 42a, b and Fig. 43) originated at the lateral surface of the temporal fossa and it inserted at the coronoid process, at the anterior part of the mandibular notch, and at the medial surface of the mandible at this level. The anterior muscle fibers of the temporalis run vertical, the central fibers with a slight oblique inclination, and the posterior fibers with a marked anterior inclination. As in the previous stages, the form of the temporalis could be described as triangular with the apex in the anterior part of the maxilla and the base in the posterior part of the mandible. This non-compartmentalized muscle accounted for 25% of the total masticatory muscle mass.

The lateral pterygoid (Fig. 42b and Fig. 43) arose from the cartilaginous lateral surface of the lateral pterygoid process and from the ossified greater wing of the sphenoid bone. It attached to the entire medial surface of the condylar process and to the superior part of the neck of the mandible. A further attachment was found at the anterior part of the articular disc. The histological methodology allowed us to observe the posterolateral direction of the muscle fibers, but morphologically it was not possible to clearly visualize the three heads of the lateral pterygoid muscle despite the three regions of insertion. The form of this muscle created a parallelogram. At this stage, the lateral pterygoid comprised 7% of the whole masticatory muscle mass.

The medial pterygoid (Fig. 42b and Fig. 43) had its origin at the cartilage of the medial surface of the lateral pterygoid process of the sphenoid bone. Its fibers run obliquely in a posterolateral direction to attach at the medial and inferior surfaces of the angular process as well as at the medial surface of the mandibular ramus. This rectangular-like shaped muscle contained a remarkable fascia that divided it into a superior and an inferior belly. Both together accounted for 8% of the total masticatory muscle mass.

The parotid gland was found at either sides of the face, situated lateral to the masseter. Its superior pole was confined to the condylar process and its inferior pole to the angular process. The anteroposterior length of the body had doubled its size compared to the previous stage and it reached approximately 2104 μm. The excretory duct followed an anterior direction and opened into the oral cavity at the level of the first maxillary molar bud.

The maxilla (Fig. 42a) was the main bone of the midface. It comprised the body and three processes (frontal, zygomatic and palatine), which were larger than in the previous stage. This structure was the site of origin of the masseter.

The zygomatic bone (Fig. 42a) was found lateral to the mandible and maxilla, and anterior and inferior to the temporal bone. It projected posteriorly, articulating with the zygomatic process of the temporal bone to form the zygomatic arch from which the masseter originated. The arch was composed of two cylindrical-like shaped parts.

The temporal bone (Fig. 44a, c) was located at the sides and base of the skull. The squamous region, situated superiorly, was flat and plate-like and contained the glenoid fossa, the articular tubercle, and the zygomatic process. The glenoid fossa represented the temporal component of the temporomandibular joint and was separated by 335 μm from the condyle. The temporal fossa was the site of origin of the temporalis.

The sphenoid bone (Fig. 43), situated at the base of the skull, showed diverse kinds of tissue differentiation: the lateral pterygoid process, from which both pterygoids arose, was cartilaginous. In contrast, the endochondral ossification on the medial pterygoid process had progressed and secondary cartilage was limited to its inferior third. The binding site of this process to the cartilaginous body was clearly visible. The greater wing was completely ossified and the tensor veli palatini was larger than in the previous stage.

Regarding the mandible (Fig. 44a-d), in the condylar as well as in the angular processes, the extension of the secondary cartilage in the superior-inferior direction was considerably reduced compared to the previous stages. However, the extension in the anterior-posterior direction remained almost stable, accounting for 544 μm for the condylar cartilage and 472 μm for the angular cartilage. The coronoid process was found to not be straight, as in the previous stages, but with a slight posterior curvature showing a hook-like appearance. The degeneration of the intramandibular portion of Meckel's cartilage (Fig. 45a, b) had continued at the anterior region of the mandible and the posterior region remained attached to the malleus. After branching from the mandibular nerve, the inferior alveolar nerve (Fig. 44a-d) entered the mandibular canal and followed an anterior direction superiorly and laterally to Meckel's cartilage. It passed through the mental foramen to give off the mental nerve.

The aspect of the temporomandibular joint (Fig. 44a-d) was similar to the previous stage with the exception of the slight smaller secondary condylar cartilage and the formation of the inferior joint cavity between the condyle and the articular disc. This last structure was composed mainly of mesenchymal tissue and the distance between it and the condylar process had decreased. Compared to the stage E18, the superior joint cavity was larger.

In the bilaminar zone (Fig. 44a, b and Fig. 47) loose mesenchyme could be found in much less proportion. Arterioles and venules, as well as vascular spaces were more abundant. The retromandibular vein was more voluminous and some structures were discernible around it, such as numerous bundles of straight collagen fibers, the auriculotemporal nerve and the masseter. Some fat tissue and parenchyma of the parotid gland were also observed in the bilaminar zone.

As in the previous stages, all components of the middle ear ossicles, i.e. malleus, incus and stapes, (Fig. 46) were cartilaginous and the incudomalleolar and incudostapedial joints were detected.

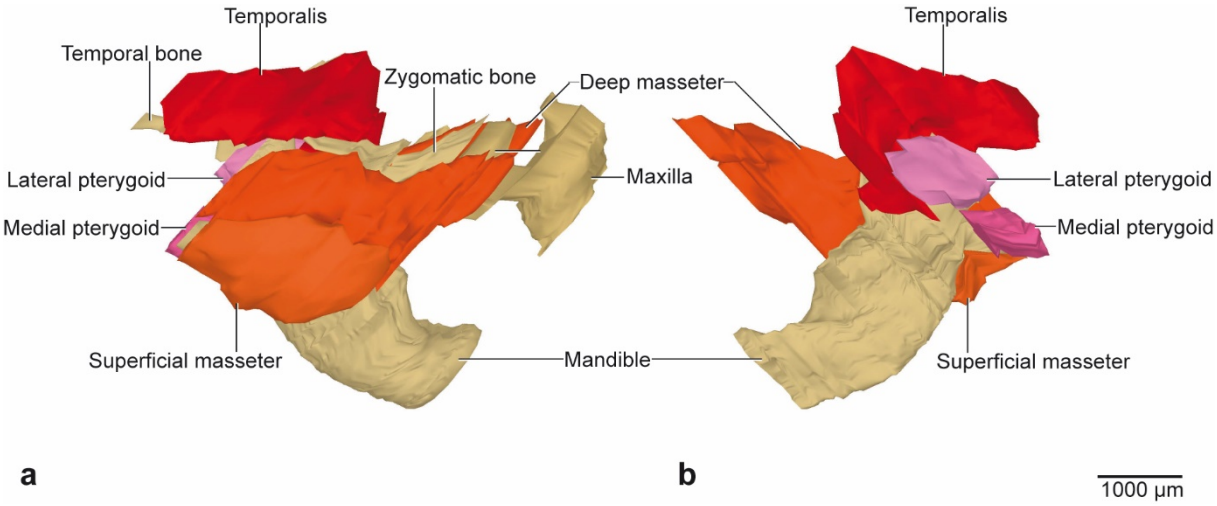

Fig. 42: Stage E20 (115-08). 3D reconstruction of the right half of the mandible and masticatory muscles.

a: Extension and attachment of the masseter and temporalis. Lateral view.

b: Extension and attachment of the lateral and medial pterygoid muscles. Medial view.

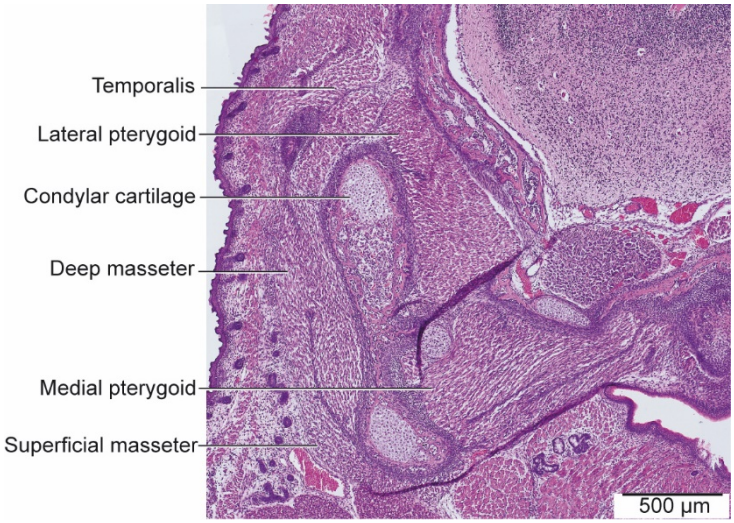

Fig. 43: Stage E20 (115-08). Histological section of the right half of the mandible through the condylar cartilage indicating the anatomical arrangement of the masticatory muscles.

Frontal plane, HE staining.

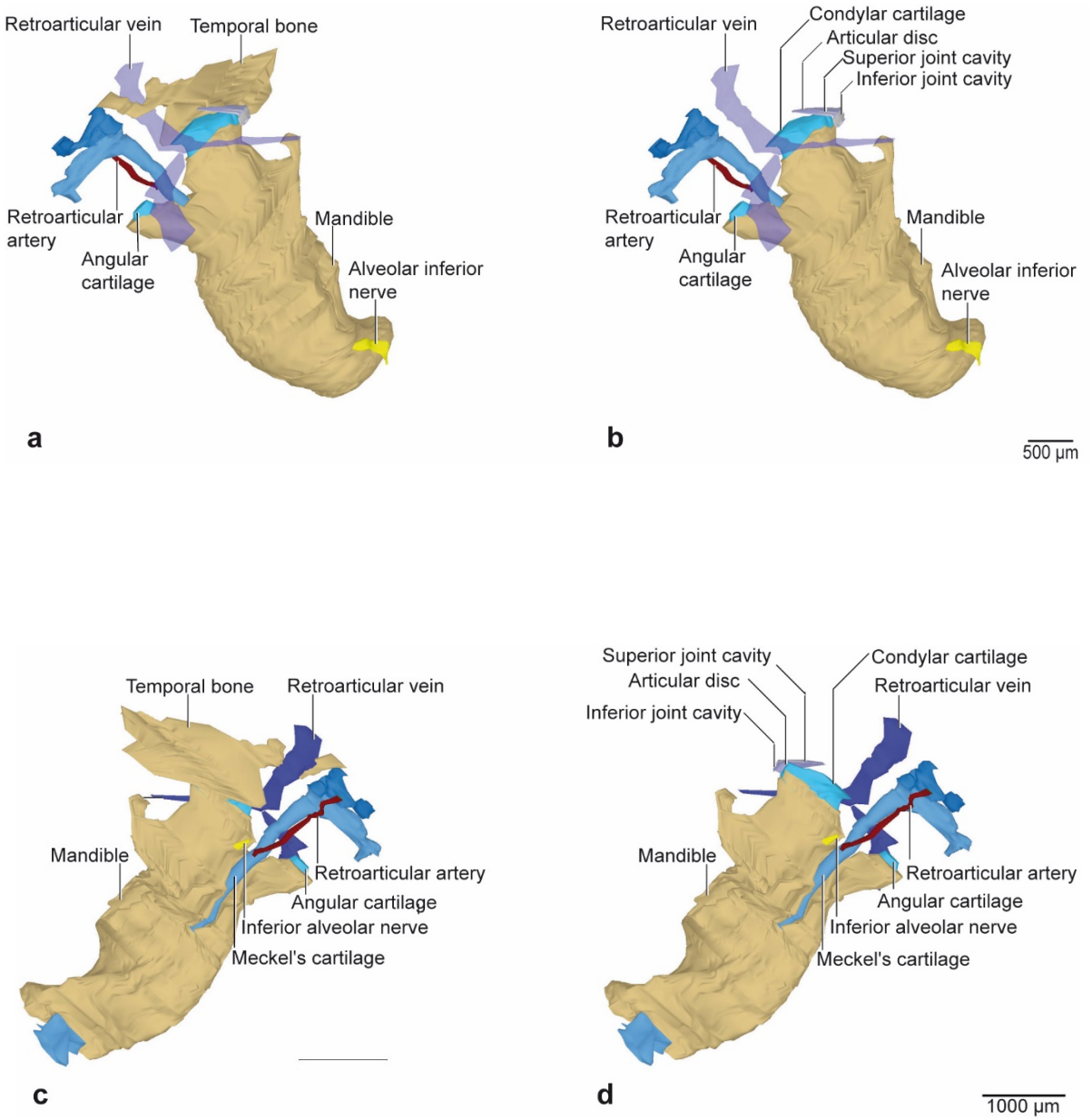

Fig. 44: Stage E20 (115-08). Partial 3D reconstruction of some components of the right temporomandibular joint and the region of the bilaminar zone.

a: Temporomandibular joint region with its temporal bone. Retromandibular vein made transparent to visualize the content and extension of the bilaminar zone. Lateral view.

b: Temporomandibular joint region, temporal bone removed to visualize the joint cavities and the articular disc. Retromandibular vein made transparent to visualize the content and extension of the bilaminar zone. Lateral view.

c: Temporomandibular joint region with its temporal bone. Medial view.

d: Temporomandibular joint region, temporal bone removed to visualize the joint cavities and the articular disc. Medial view.

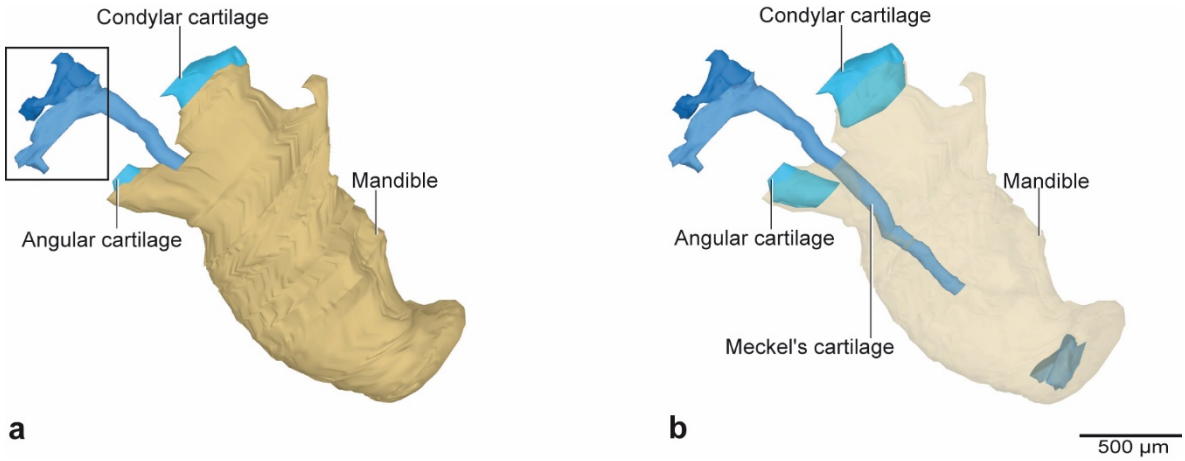

Fig. 45: Stage E20 (115-08). 3D reconstruction of the right half of the mandible, Meckel's cartilage and middle ear ossicles.

a: Lateral view. Box: see Fig. 46.

b: Same view with mandible made transparent. Lateral view.

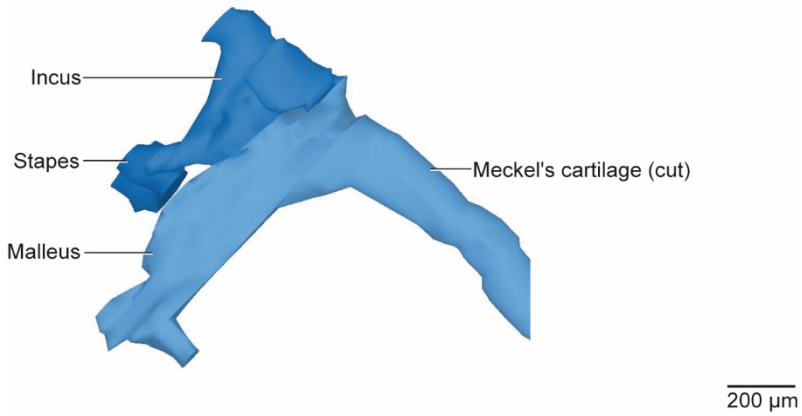

Fig. 46: Stage E20 (115-08). 3D reconstruction of a detailed view of the right middle ear ossicles.

Lateral view.

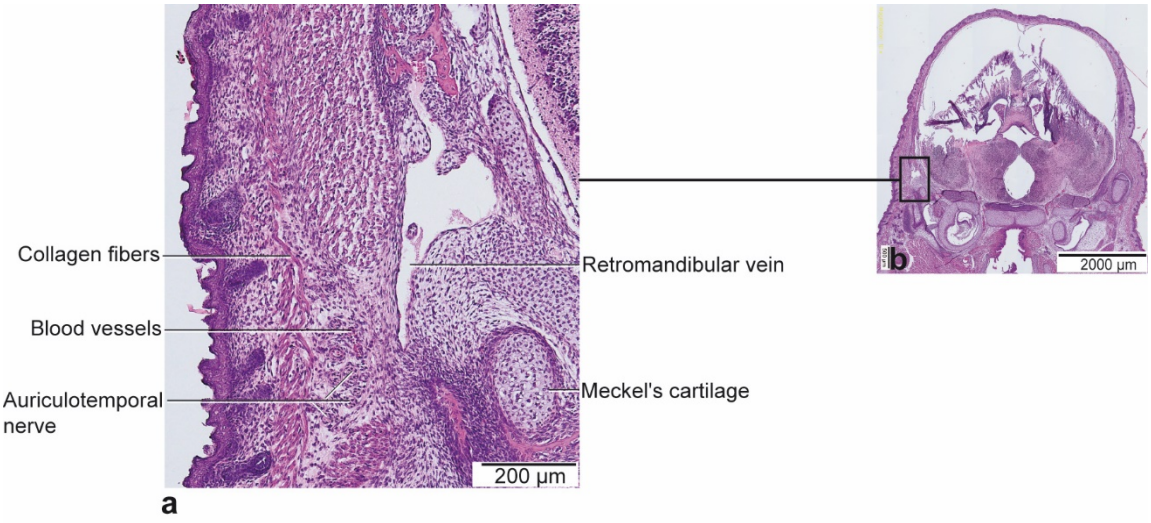

Fig. 47: Stage E20 (115-08). Bilaminar zone.

a: Histological section of the region through the right bilaminar zone. Frontal plane, HE staining.

b: Survey of the whole section.

5.2.9 Stage P0

With regard to the masseter of the newborn (Fig. 48a, b and Fig. 50a), the superficial belly originated from the lateral surface of the anterior two thirds of the zygomatic arch and from the zygomatic process of the maxilla. It attached to the lateral and inferior border of the angular process and to the inferior third of the lateral surface of the ramus of the mandible. A further insertion was observed at the masseteric tuberosity. The deep belly had its origin at the lateral surface of the posterior third of the zygomatic arch and at the entire medial border of it. This belly inserted into the superior two thirds of the lateral border of the ramus of the mandible. The muscle fibers run posterolaterally. The masseter showed a triangular shape, with the apex at the anterior part of the maxilla and the base at the posterior part of the mandible. It was clearly divided into a superficial and deep belly, and both together comprised 57% of the masticatory muscle mass.

The temporalis (Fig. 48a, b and Fig. 50a) arose from the lateral fossa of the temporal bone and it attached to the coronoid process, to the mandibular notch, and to the corresponding medial surface. The anterior fibers of the temporalis followed a straight vertical direction, the central fibers ran slightly obliquely, and the posterior fibers ran markedly obliquely in anterior direction. This triangular-like shaped muscle had its apex in the coronoid process and the base in the lateral surface of the skull. It did not show any division inside and accounted for 18% of the total masticatory muscle mass.

The lateral pterygoid (Fig. 48b and Fig. 50a) originated from the ossified greater wing and from the partially ossified lateral surface of the lateral pterygoid process of the sphenoid. It attached to the anterior-medial border of the articular disc and to the medial surface of the condylar process and neck of the mandible. The muscle fibers ran posterolaterally and it showed a parallelogram-like shape. The lateral pterygoid comprised 13% of the whole masticatory muscle mass.

The medial pterygoid (Fig. 48b and Fig. 50a) had its origin from the ossified medial surface of the lateral pterygoid process. It inserted at the medial and inferior surface of the angular process as well as from the medial surface of the mandibular ramus. The fibers of this rectangular-like shaped muscle followed an oblique direction, and a superior and an inferior head could be distinguished. The medial pterygoid accounted for 12% of the total masticatory muscle mass in this developmental stage.

The stylomandibularis (Fig. 49a, b and Fig. 50b) was seen again at this stage in anatomically close relationship with the masticatory muscles, but it did not belong to this group. It had its origin at the styloid process of the temporal bone and it extended anteriorly to insert into the

anterior-medial part of the angular process of the mandible. This cylindrical-like shaped muscle did not show any division.

The parotid gland of the newborn mouse had increased its size compared to the previous stage and the body had reached 2450 μm of extension. The duct followed an anterior-superior direction and it opened into the mouth at the level of the superior first molar.

The lacrimal gland was situated superior to the parotid gland and it was larger than in the previous stage, accounting for 1200 μm in the anterior-posterior direction. It comprised a body and a duct that had reached the eyeball.

The maxilla of the newborn (Fig. 48a) was located at the midface and it showed a body and three processes (frontal, zygomatic and palatine). This voluminous structure was the site of origin of the superficial masseter.

The zygomatic bone (Fig. 48a) was located lateral to the mandible and maxilla, and anterior to the temporal bone to which it articulated through the zygomatic process. It showed a cylindrical-like shape and it served as origin for both the superficial and the deep masseter.

The temporal bone of the newborn mouse (Fig. 51a, c) was situated at the lateral surface and at the base of the skull. The squamous part represented the largest area of the bone and its glenoid fossa was one of the components of the temporomandibular joint. The distance between it and the condyle remained almost the same at 340 μm. The temporal fossa, which was formed by the temporal bone among others, was the site of origin of the temporalis.

The ossification of the sphenoid, a large bone located at the base of the skull, had advanced and was even observed at the lateral process. Meanwhile, the greater wing was completely ossified and the ossification of the body had started. A small part of the lateral pterygoid process also showed primary cartilage, whereas the same region of the medial process was formed by secondary cartilage. The sphenoid was the attachment site of the tensor veli palatini and the origin site of the pterygoids.

Concerning the mandible (Fig. 51a-d), the condylar and angular processes showed a reduction in the extension of its secondary cartilages accounting for 520 μm and 440 μm, respectively, in the anterior-posterior direction. Within these cartilages four layers, instead of three as in the previous stages, were recognized, namely the fibrous cell layer, the polymorphic progenitor layer, the flattened chondrocytes zone and the zone of hypertrophic chondrocytes. The coronoid process was larger than in the prenatal stages and the posterior curvature was far more pronounced. Meckel's cartilage (Fig. 52a, b) remained almost the same, with an anterior segment separated from the posterior portion that was continuous with the malleus. The mandible surrounded the inferior alveolar nerve (Fig. 51a-d) that ran lateral to Meckel's cartilage. It left

the mandibular canal through the mental foramen, which was situated between the anterior border of the mandibular molar and the posterior surface of the anterior segment of Meckel's cartilage. This foramen showed an ovoid form.

The temporomandibular joint of the newborn mouse (Fig. 51a-d) did not show any significant change compared to the previous stage. It was formed by the condylar process with its secondary cartilage, the glenoid fossa of the temporal bone, the articular disc, which had the same convex shape as the condylar process, and the superior and inferior joint cavities, among other structures.

In the bilaminar zone (Fig. 51a, b and Fig. 54), the mesenchymal tissue around the retromandibular vein had decreased, unlike the number of blood vessels and vascular spaces, which had increased. Straight collagen fibers running in a vertical direction could be visualized at the lateral border of this region. Some other structures were arterioles, the auriculotemporal nerve, adipose tissue, parenchymal tissue of the parotid gland and numerous muscle fibers of the masseter

For the first time, the ossification of the malleus could be visualized, which had started at the most anterior part of this structure. However, the incus and stapes remained cartilaginous (Fig. 53).

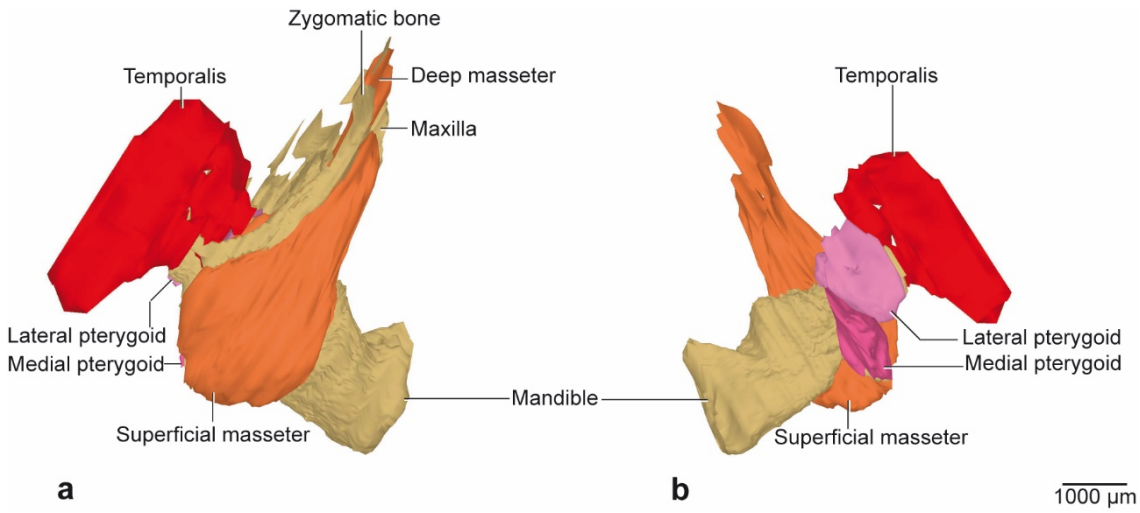

Fig. 48: Stage P0 (65-08). 3D reconstruction of the right half of the mandible and masticatory muscles.

a: Extension and attachments of the masseter and temporalis. Lateral view.

b: Extension and attachments of the lateral and medial pterygoids. Medial view

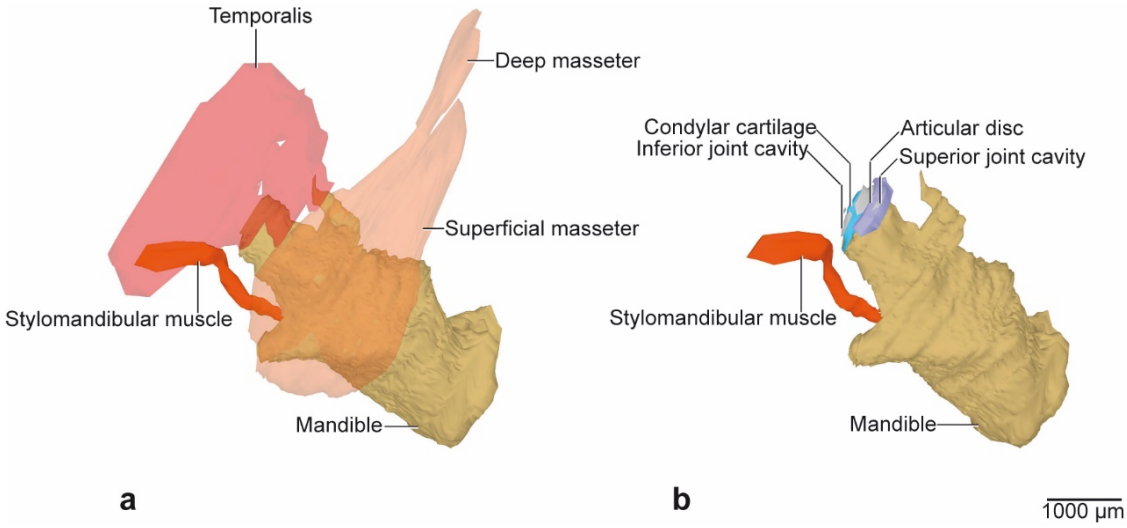

Fig. 49: Stage P0 (65-08). 3D reconstruction of the right half of the mandible, and of the masseter, temporal and stylomandibular muscle.

a: Masseter and temporal made transparent to visualize the location of the stylomandibular muscle. Lateral view

b: There is a large space of approximately 538 µm between the stylomandibular muscle and the articular disc, so therefore no attachment into it is obvious. Lateral view.

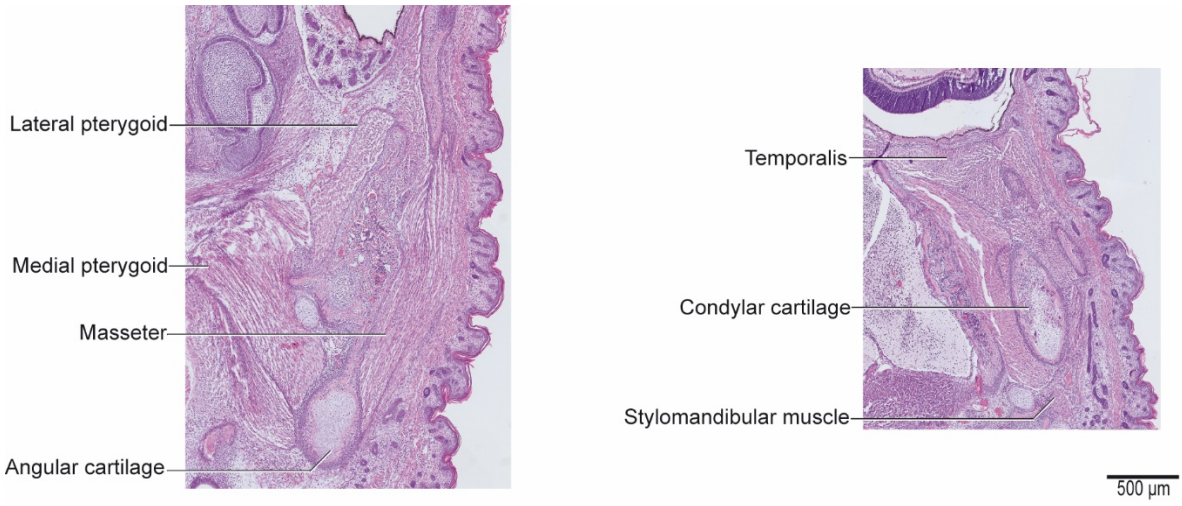

Fig. 50: Stage P0 (65-08): Histological section of the right half of the mandible through the condylar cartilage showing the fibre orientation of the muscles.

a: Horizontal plane, HE staining.

b: 80 µm cranial from Fig. 50a. Horizontal plane, HE staining.

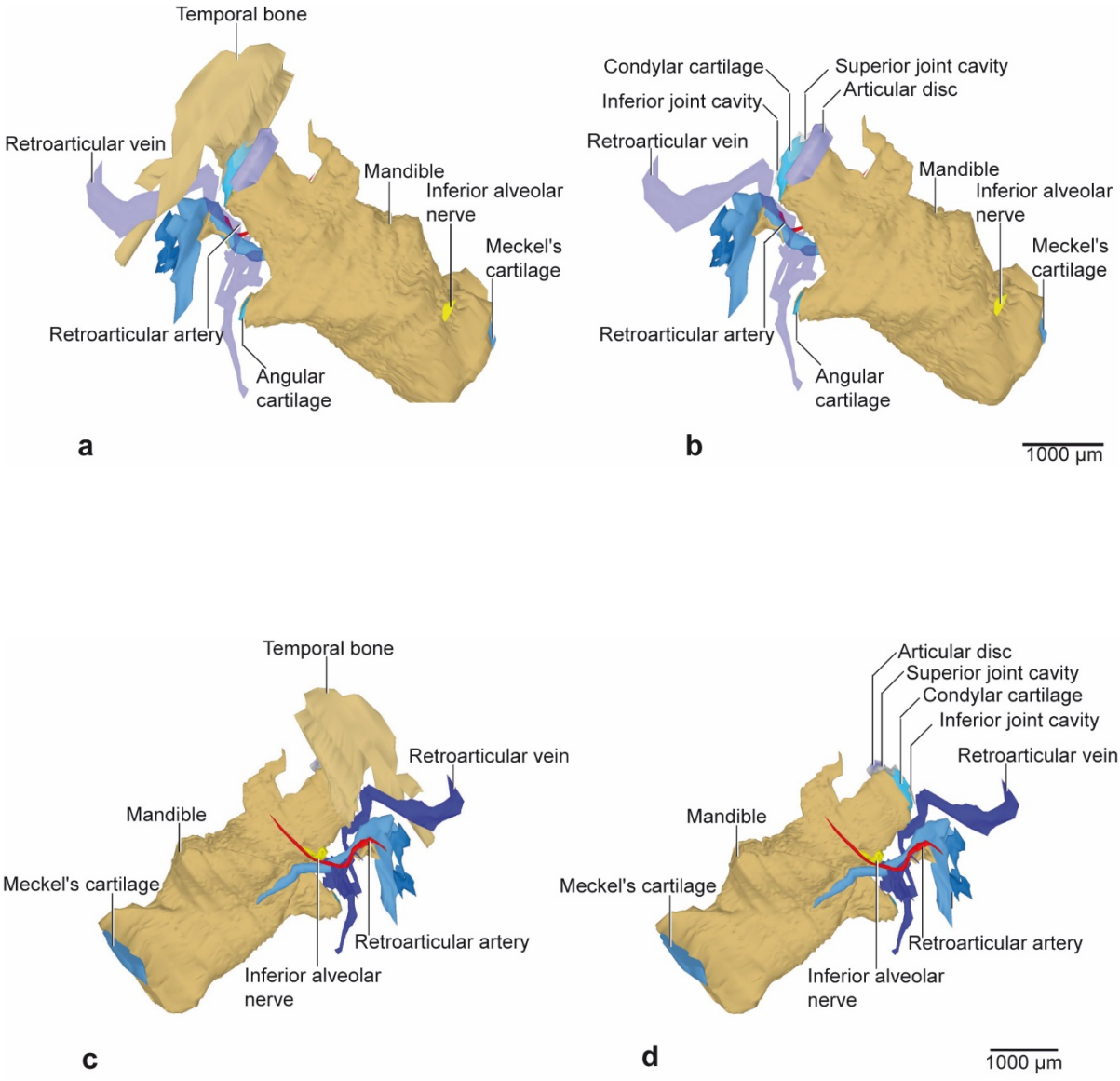

Fig. 51: Stage P0 (65-08). Partial 3D reconstruction of some components of the right temporomandibular joint and of the region of the bilaminar zone.

a: Temporomandibular joint region with its temporal bone. Retromandibular vein made transparent to visualize the content and extension of the bilaminar zone. Lateral view.

b: Temporomandibular joint region, temporal bone removed to visualize the joint cavities and the articular disc. Retromandibular vein made transparent to visualize the content and extension of the bilaminar zone. Lateral view.

c: Temporomandibular joint region with its temporal bone. Medial view.

d: Temporomandibular joint region, temporal bone removed to visualize the joint cavities and articular disc. Medial view.

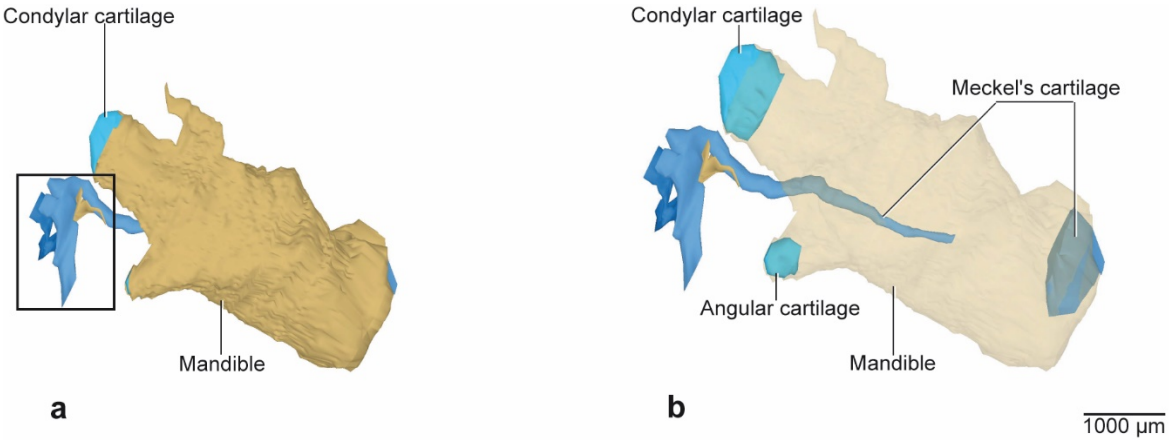

Fig. 52: Stage P0 (65-08). 3D reconstruction of the right half of the mandible and middle ear ossicles.

a: Lateral view. Box: see Fig. 53.

b: Same view with mandible made transparent. Lateral view.

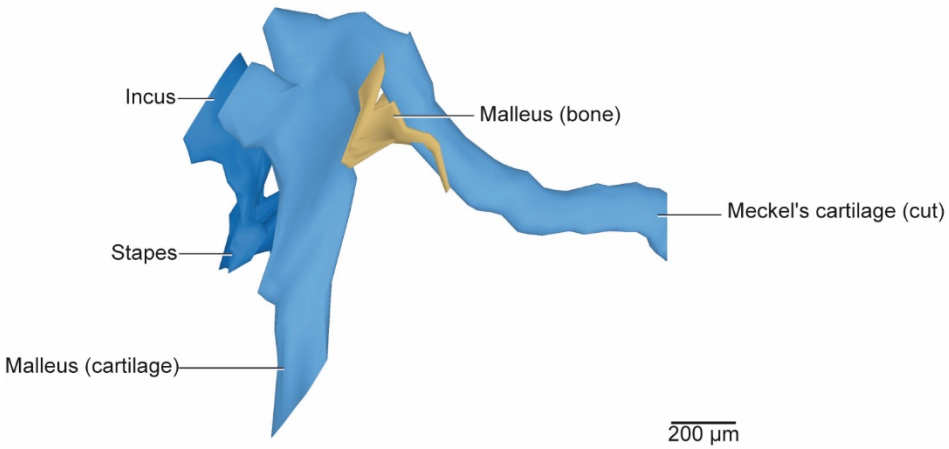

Fig. 53: Stage P0 (65-08) 3D reconstruction of a detailed view of the right middle ear ossicles.

Appearance of the first ossification center of the malleus.

Lateral view.

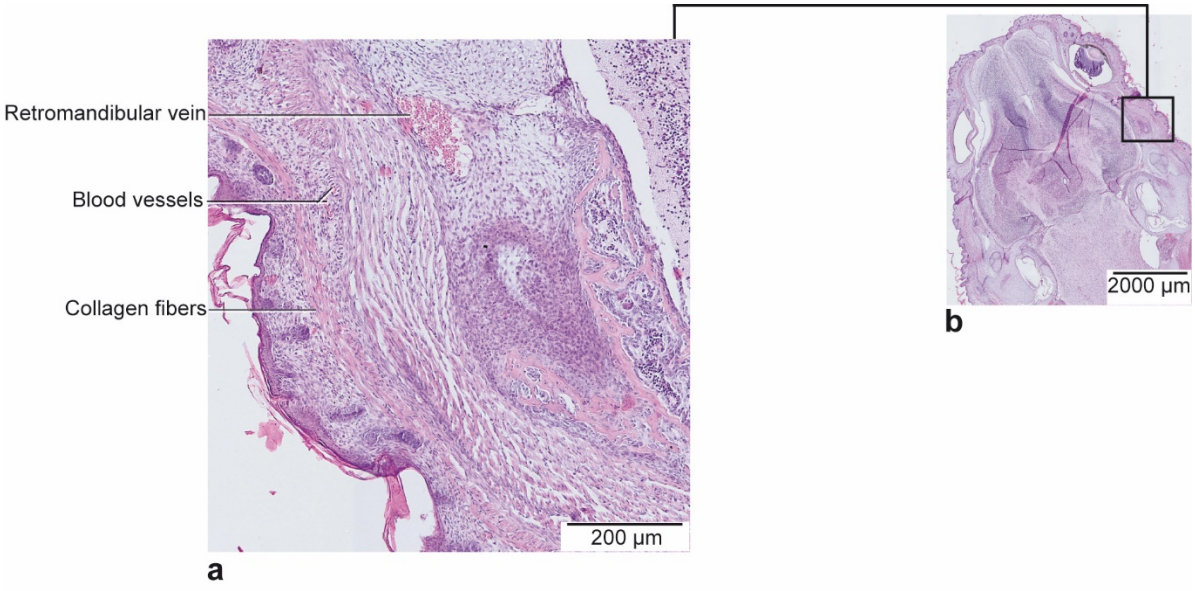

Fig. 54: Stage P0 (65-08). Bilaminar zone.

a: Histological section of the region of the right bilaminar zone. Horizontal plane, HE staining.

b: Survey of the whole section.

5.2.10 Stage P2

The masseter (Fig. 55a, b and Fig. 57) originated at the anterior two thirds of the inferior lateral border of the zygomatic arch, and at the zygomatic process of the maxilla for the superficial belly, and at the posterior third of the inferior lateral border, and at the medial border of the zygomatic arch for the deep belly. The insertion was found at the inferior third of the ramus of the mandible, at the lateral surface of the angular process, and at the masseteric tuberosity for the superficial belly, and at the superior two thirds of the ramus of the mandible for the deep belly. The direction that the muscle fibers followed could be described as oblique in a posterolateral orientation. The boundary between the two bellies was distinguished unambiguously, and both together gave the appearance of a triangular-like shaped muscle with its apex at the maxilla and its base at the mandible. The masseter comprised 53% of the total masticatory muscle mass.

The temporalis (Fig. 55a, b and Fig. 57) ran from the temporal fossa to the coronoid process, mandibular notch, and medial surface of the mandible at this level. Only the anterior fibers followed a straight vertical direction. In the center the fibers ran slightly obliquely, while in the posterior region their inclination was more pronounced. The shape of the temporalis was also triangular, with the base at the lateral surface of the skull and the apex at the mandible. We were unable to find any boundary inside the muscle, which accounted for 26% of the whole masticatory muscle mass.

The lateral pterygoid (Fig. 55b, Fig. 56a, b and Fig. 57) showed its origin at the cartilaginous and ossified lateral surface of the lateral pterygoid process and at the ossified greater wing of the sphenoid bone. It was inserted at the medial surface of the condylar process, at the neck of the mandible and at the anterior surface of the articular disc. The histological visualization allowed us to distinguish the posterolateral direction of the muscle fibers and the lack of clearly morphological divisions into heads, despite the three regions of insertion. The lateral pterygoid showed a parallelogram-like shape and it accounted for 9% of the overall masticatory muscle mass.

The medial pterygoid (Fig. 55b, Fig. 56a, b and Fig. 57) originated from the partly cartilaginous and partly ossified medial surface of the lateral pterygoid process of the sphenoid bone. Its attachment was situated at the medial surface of the angular process and at the ramus of the mandible. The muscle fibers ran obliquely from the cranial base to the inferior border of the mandible. A well-visualized fascia divided this rectangular-like shaped muscle into a large superior and a small inferior heads. Both comprised 12% of the masticatory muscle mass.

The parotid gland was located lateral to the masseter and included a duct and a body. The duct arose from the anterior-superior border of the body and ran straight in an anterior direction to

open into the mouth opposite to the first maxillary molar. The body was surrounded by a capsule of dense connective tissue and accounted for 1450 μm in the anterior-posterior direction.

The lacrimal gland was composed of a body and a duct. The first one was located superior to the parotid gland, inferior to the temporalis and lateral to the masseter, and its size was 950μm. The duct left the anterior surface of the gland to run in an anterior-superior direction into the eye.

The maxilla (Fig. 55a) was located at the midface and consisted of a body and three processes, i.e. frontal, palatine and zygomatic, and the origin of the masseter was situated at the last of these.

The zygomatic bone (Fig. 55a) was located lateral to the mandible and the maxilla. This structure became slightly wider from posterior to anterior and consisted of two parts that, together with the zygomatic process of the temporal bone, formed the zygomatic arch, which served as the origin for the masseter. Unlike in the previous stages, this structure showed an inferior curvature at its middle portion.

The temporal bone (Fig. 58a, c) showed that the squamous part was the largest and it contained the glenoid fossa, the articular tubercle, and the zygomatic process among other structures. The concavity of the glenoid fossa had developed so far that it had acquired its adult shape, and it also covered the lateral surface of the articular disc. The separation between the fossa and the condyle accounted for approximately 363 μm. Other parts of the temporal bone had barely changed their morphology compared to the previous stage.

With regard to the sphenoid (Fig. 56a, b and Fig. 57), its body was ossified, along with a part of the lateral pterygoid process and the entire medial pterygoid process, except for its most inferior part where secondary cartilage could be found. The tensor veli palatini was situated medial to the medial pterygoid process, which was more voluminous than in the previous stages. The lateral and medial pterygoids arose from the lateral process.

Concerning the mandible (Fig. 58a-d), in contrast to the secondary cartilage of the condylar process, that of the angular process was clearly reduced in size, and comprised 300 μm in the anterior-posterior direction. The cartilage of both processes showed four distinct zones: a fibrous layer, a polymorphic progenitor cell layer, a zone of flattened chondrocytes, and a zone of hypertrophic chondrocytes. The ossification of the anterior segment of the intramandibular portion of Meckel's cartilage had continued, and additionally, at this developmental stage, a small segment at the level of the mandibular second molar had ossified (Fig. 59a, b). The inferior alveolar nerve (Fig. 58a-d) passed along the mandible. It gave off the mental nerve, which exited the bone via the mental foramen situated anterior to the first mandibular molar.

The temporomandibular joint (Fig. 58a-d) comprised secondary condylar cartilage, a convex glenoid fossa, and an articular disc, among other structures. The posterior extension of the disc was larger than by stage P0 and it was mainly composed of mesenchyme. Both joint cavities had increased in size. Moreover, the inferior joint cavity had extended so far that it showed the same length as the condylar cartilage.

In the bilaminar zone (Fig. 58a, b and Fig. 61), the proportion of mesenchymal tissue was insignificant compared to the previous stages, and the major part of this region was occupied by the retromandibular vein. Some small vascular vessels and vascular spaces could also be visualized. The collagen fibers run straight downwards at the lateral border of the bilaminar zone. Some branches of the retroarticular artery and auriculotemporal nerve, as well as adipose tissue and parenchyma of the parotid gland, could be distinguished in this region. The masseter was also observed in the inferior part of this zone.

With regard to the middle ear (Fig. 60), the endochondral ossification of the malleus had extended to its posterior and superior regions, and for the first time, ossified tissue was also found in the incus. No remarkable changes could be observed in the stapes, which remained cartilaginous.

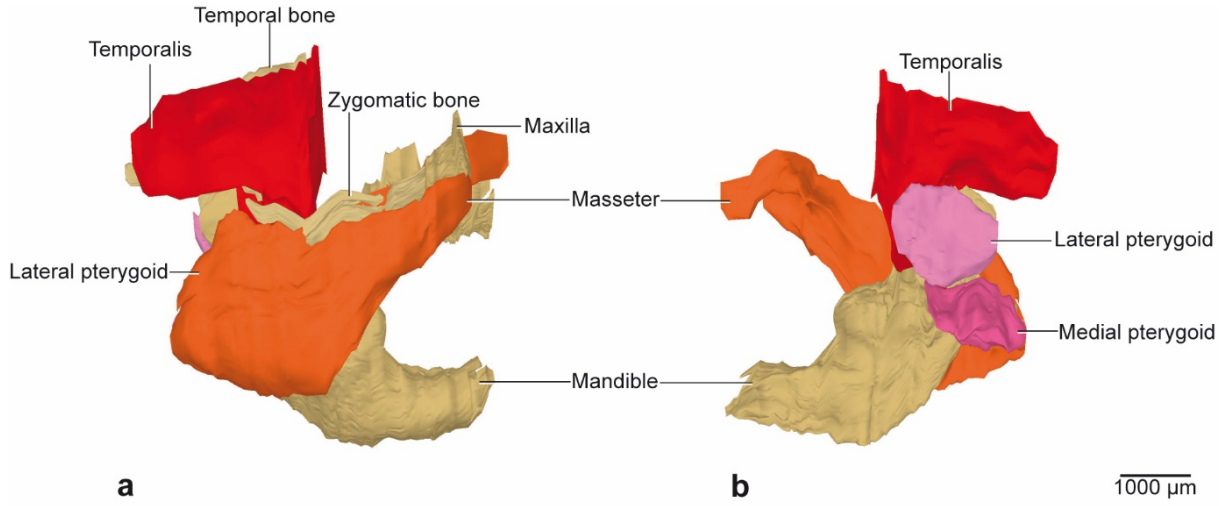

Fig. 55: Stage P2 (70-08). 3D reconstruction of the right half of the mandible and masticatory muscles.

a: Extension and attachments of the masseter and temporalis. Lateral view.

b: Extension and attachments of the lateral and medial pterygoid muscles. Medial view

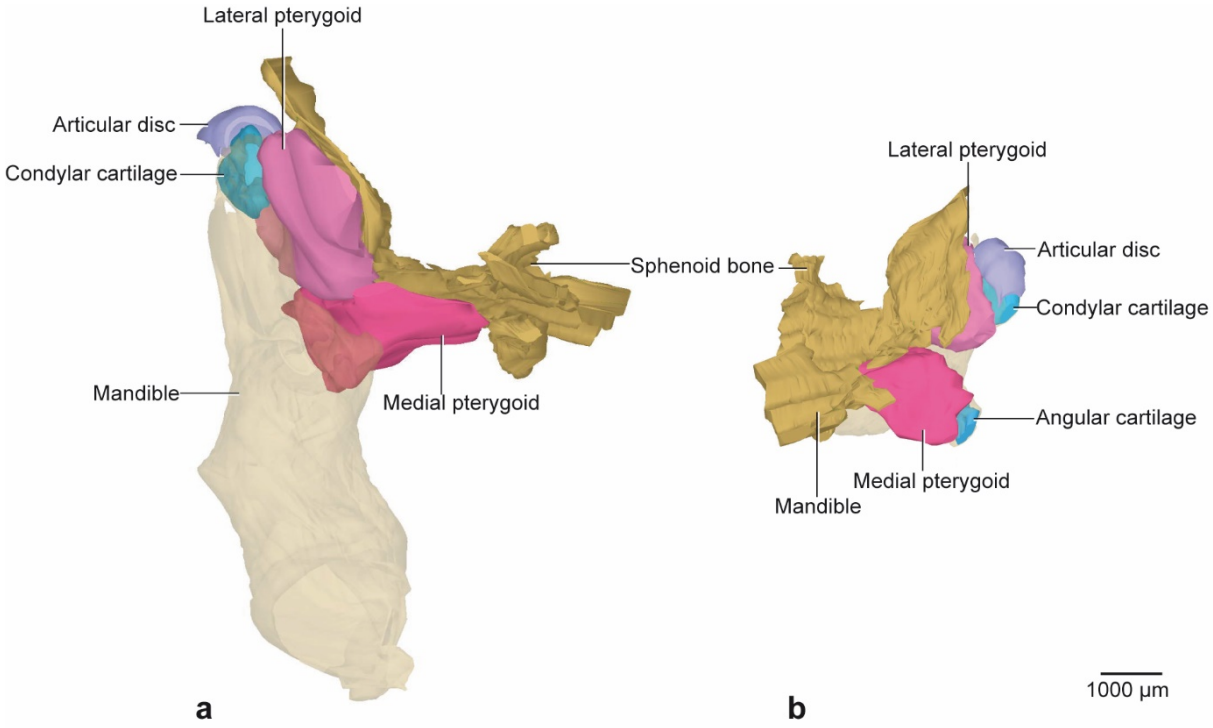

Fig. 56: Stage P2 (70-08). 3D reconstruction of the right half of the mandible (made transparent), sphenoid bone and pterygoid muscles.

a: Origin of the lateral pterygoid at the greater wing and lateral surface of the lateral pterygoid process of the sphenoid bone. Origin of the medial pterygoid at the medial surface of the lateral pterygoid process of the sphenoid bone. Frontal view.

b: Special relationship between the lateral pterygoid and the articular disc, condylar cartilage and condylar process (insertion of the muscle fibres in Fig. 57). Proximity of the medial pterygoid to the angle and ramus of the mandible. Dorsomedial view.

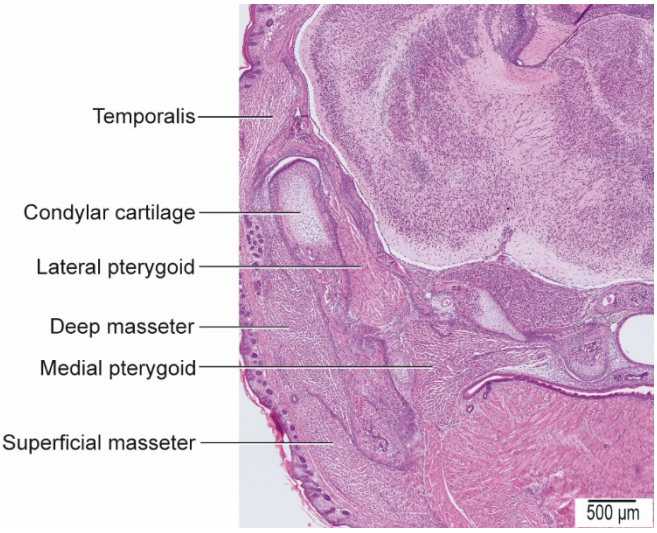

Fig. 57: Stage P2 (70-08). Histological section of the right half of the mandible through the condylar cartilage indicating the anatomical arrangement of the masticatory muscles.

Frontal plane, HE staining.

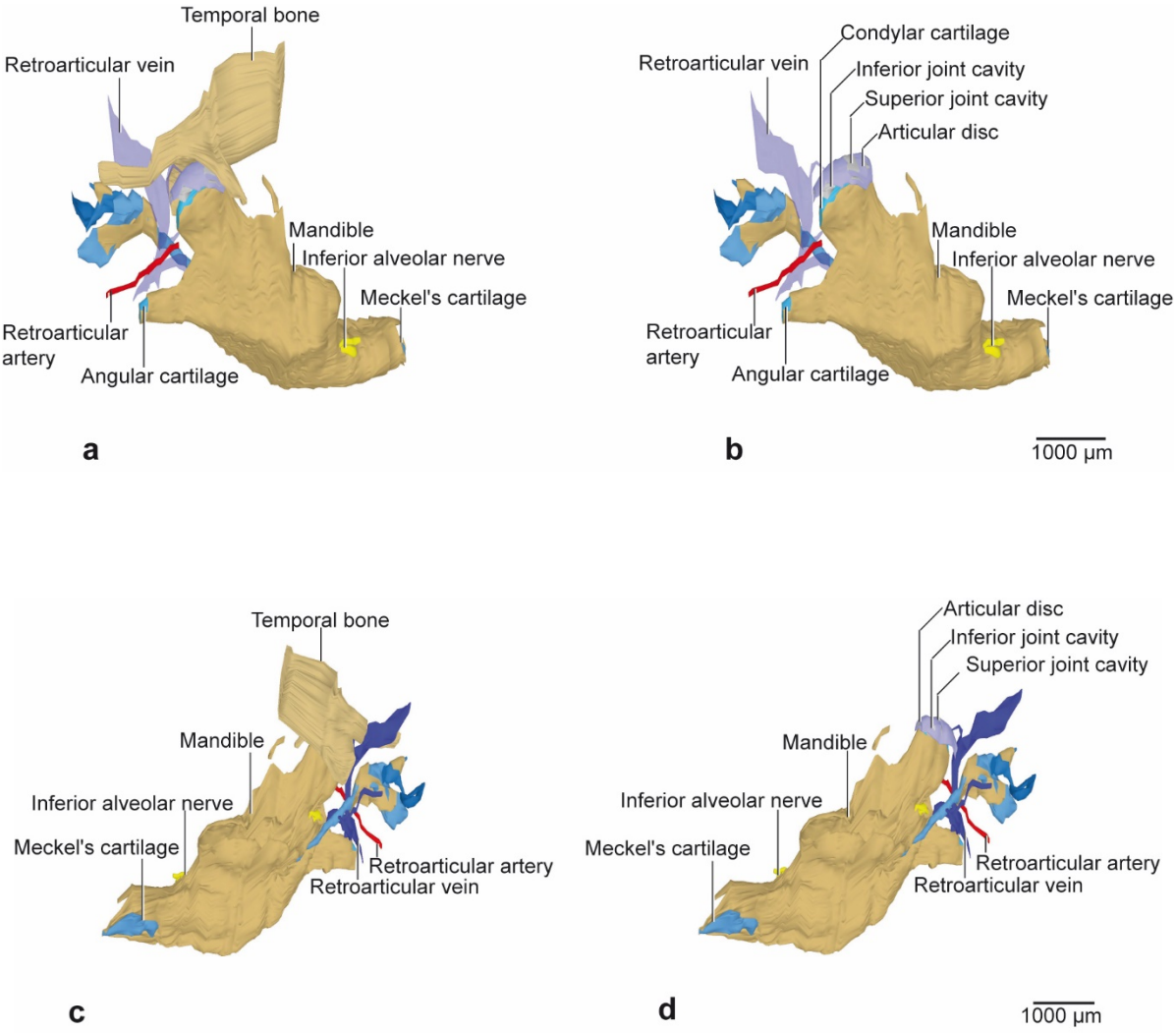

Fig. 58: Stage P2 (70-08). Partial 3D reconstruction of some components of the right temporomandibular joint and the region of the bilaminar zone.

a: Temporomandibular joint with its temporal bone. Retromandibular vein made transparent to visualize the content and extension of the bilaminar zone. Lateral view.

b: Temporomandibular joint, temporal bone removed to visualize the joint cavities and the articular disc. Retromandibular vein made transparent to visualize the content and extension of the bilaminar zone. The inferior joint cavity is clearly larger than in the previous stages. The articular disc is posteriorly larger than in the previous stages. Lateral view.

c: Temporomandibular joint with its temporal bone. Medial view.

d: Temporomandibular joint, temporal bone removed to visualize the joint cavities and the articular disc. Medial view.

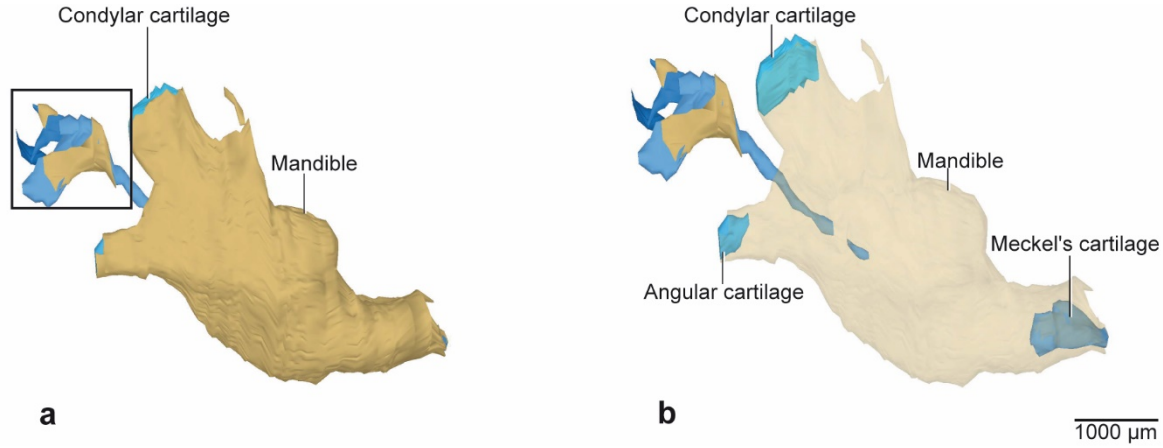

Fig. 59: Stage P2 (70-08). 3D reconstruction of the right half of the mandible, Meckel's cartilage and middle ear ossicles.

a: Lateral view. Box: see Fig. 60.

b: Same view with mandible made transparent. Compared to the previous stage, a small segment of the posterior intramandibular portion of Meckel's cartilage has ossified at the level of the mandibular second molar. Lateral view.

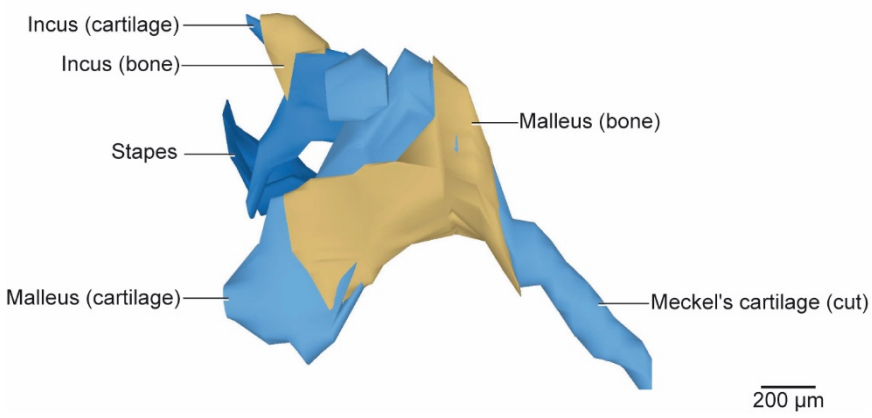

Fig. 60: Stage P2 (70-08). 3D reconstruction of a detailed view of the right middle ear ossicles.

First appearance of an ossified portion at the incus. The malleus bone is clearly larger at its posterior part than in the previous stages. Lateral view.

Fig. 61: P2 (70-08). Bilaminar zone.

a: Histological section of the right bilaminar zone. Frontal plane, HE staining.

b: Survey of the whole section.

5.2.11 Stage P4

With regard to the masseter (Fig. 62a, b and Fig. 65), the superficial belly originated from the anterior two thirds of the inferior-lateral surface of the zygomatic arch and from the zygomatic process of the maxilla, and it attached at the lateral surface of the angular process and at the inferior third of the ramus of the mandible. Furthermore, it inserted at the masseteric tuberosity. The deep belly had its origin at the posterior third of the inferior-lateral border and at the medial surface of the zygomatic arch. It inserted at the superior two thirds of the lateral border of the ramus of the mandible. The muscle fibers run posterolaterally and the whole muscle showed a triangular shape with two bellies, the superficial and the deep. Its base was situated in the posterior part of the mandible and its apex in the anterior part of the maxilla. Both heads accounted for 57% of the total muscle mass.

The temporalis (Fig. 62a, b, Fig. 64a, b and Fig. 65) originated from a large area on the lateral surface of the temporal fossa and extended posteriorly to the temporomandibular joint, with no attachment to any part of the disc, and anteriorly to the coronoid process, where it inserted. Furthermore, it attached to the mandibular notch and to the corresponding medial surface of the mandible. The anterior fibers of the temporalis run straight downwards, the central fibers with a slight oblique inclination downwards, and the posterior fibers anteriorly downwards. It showed a triangular form with the base in the temporal fossa and the apex in the coronoid process. It accounted for 20% of the masticatory muscle mass.

The lateral pterygoid (Fig. 62b, Fig. 63a, b and Fig. 65) had its origin at the ossified greater wing, and at the lateral border of the lateral pterygoid process of the sphenoid bone. It attached to the medial border of the condylar process, to the superior part of the neck of the mandible, and to the anterior-medial border of the articular disc. The microscopic visualization allowed us to distinguish the posterolateral direction of the muscle fibers. The lateral pterygoid showed a parallelogram form. Despite the three regions of insertion being observed clearly, a separation into three heads was morphologically not obvious. The lateral pterygoid accounted for 11% of the overall muscle mass.

The medial pterygoid (Fig. 62b, Fig. 63a, b and Fig. 65) originated from the medial border of the lateral pterygoid process, and the muscle fibers run obliquely in a posterolateral direction to reach the medial surface of the angular process at the same high as the masseter. Furthermore, it attached to the medial surface of the ramus of the mandible and extended anteriorly beyond the coronoid process. A prominent septum divided the superior and inferior heads of the medial pterygoid. This rectangular-like shaped muscle accounted for 12% of the total masticatory muscle mass.

The parotid gland was situated posteriorlateral to the ramus of the mandible, except for a part of the gland that extended between the coronoid and angular processes, and anteriorlateral to the external acoustic meatus. Some small parts of the gland could be also found in the bilaminar zone. The body of the parotid extended 1650 μm in the anterior-posterior direction and was surrounded by a capsule. The duct emerged from the anterior surface of the gland, and ran superficially to the masseter in a straight and slightly superior direction to open into the mouth at the level of the first maxillary molar.

The body of the lacrimal gland was located superior to the parotid gland and lateral to the condylar process and showed no relation to the bilaminar zone. It showed an extension of 1000 μm in the anterior-posterior direction. The duct emerged from the anterior border of the gland and followed an anterior-superior direction to finally reach the eyeball.

The maxilla (Fig. 62a), situated at the midface, was formed by a body and by the frontal, palatine and zygomatic processes. This last one was the site of origin of the masseter.

The zygomatic bone (Fig. 62a) could be observed lateral to the mandible and maxilla, and anterior and inferior to the temporal bone. Its posterior end articulated with the zygomatic process of the temporal bone to give rise to the zygomatic arch, the site of origin of the masseter. The inferior curvature of this structure was more pronounced than in the previous stage.

The temporal bone (Fig. 66a, c) was located at the sides and base of the skull and appeared more voluminous than at stage P2. The squamous part was the largest and showed a plate-like shape. The glenoid fossa, articular tubercle, and zygomatic process formed, among other structures, this part of the temporal bone. The glenoid fossa was separated by 392 μm from the condyle and the temporal fossa was the site of origin of the temporalis.

The sphenoid bone (Fig. 63a, b and Fig. 65) was a prominent structure located at the base of the skull. It could be divided into four parts: the central body, the greater and lesser wings on either side of the bone, and a paired of pterygoid processes also on either side. The entire bone had ossified except for the inferior third of the medial process, where secondary cartilage had formed, and a small region of the lateral process with primary cartilage. Both processes were found in close relationship with the surrounded musculature: the lateral process with the pterygoid muscles and the medial process with the tensor veli palatini.

Concerning the mandible (Fig. 66a-d), the condylar and angular secondary cartilages had diminished, but they still remained slightly at the top of the condylar process. Both were divided into four distinct portions: a fibrous layer, a polymorphic progenitor cell layer, a zone of flattened chondrocytes, and a zone of hypertrophic chondrocytes. Almost the entire intramandibular portion of Meckel's cartilage had ossified and only a small segment, situated

between the midline and the vicinity of the mental foramen, remained cartilaginous. The posterior part of the extramandibular portion appeared for the first time separated from the malleus (Fig. 67a, b). The mandible surrounded the inferior alveolar nerve (Fig. 66a-d) until it reached the mental foramen located at the anterior border of the first mandibular molar.

Regarding the temporomandibular joint (Fig. 66a-d), the articular disc was composed of cells and fibrous connective tissue with no vessels inside. It had the same length as the condylar cartilage, and was divided into a thin anterior part, an intermediate part and a thick posterior part. Both the superior and inferior joint cavities had clearly increased in posterior and lateral extension compared to stage P2.

The bilaminar zone (Fig. 66a, b and Fig. 69) was filled almost completely by the retromandibular vein. Some other venules and arterioles were found at this developmental stage. Many collagen fibers run vertically and laterally to the retromandibular vein. Branches of the auriculotemporal nerve, connective tissue of the parotid gland, adipocytes, and some fibers of the masseter, were also detected in this zone.

With regard to the middle ear (Fig. 68), the ossification of the malleus had progressed at its inferior and anterior parts. The incus had almost completely ossified and only two portions at its posterior border remained cartilaginous. The roundish shaped stapes continued to be composed exclusively of cartilage.

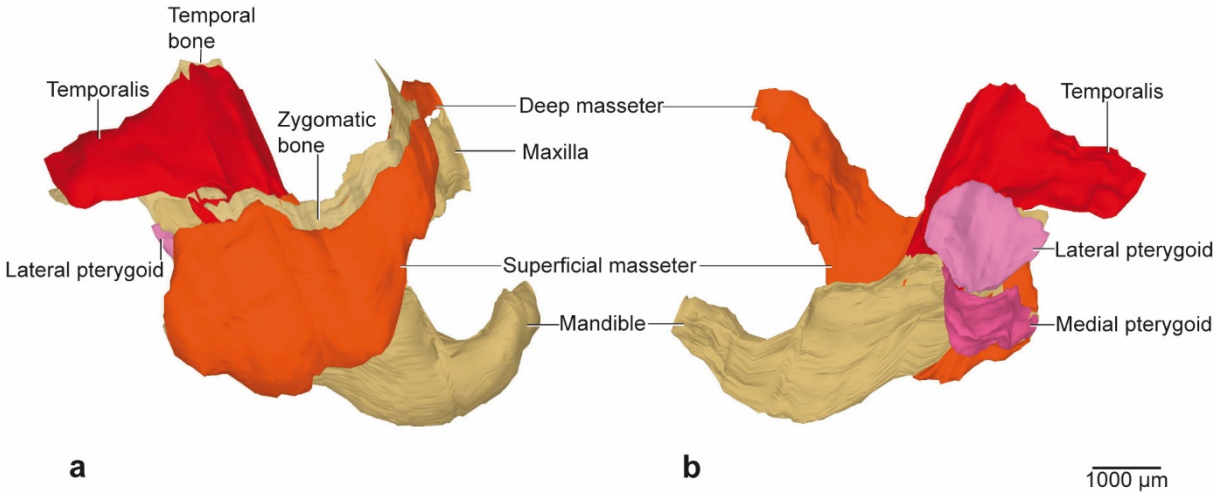

Fig. 62: Stage P4 (73-08). 3D reconstruction of the right half of the mandible and masticatory muscles.

a: Extension and attachments of the masseter and temporalis. Lateral view.

b: Extension and attachments of the lateral and medial pterygoids. Medial view.

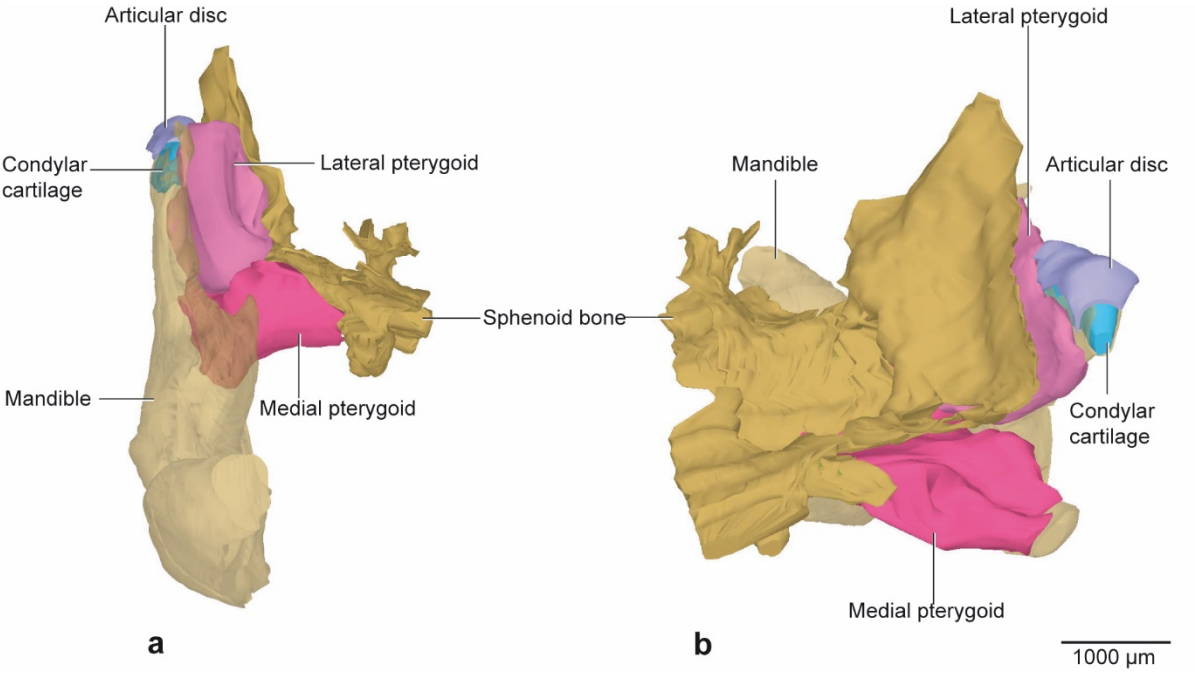

Fig 63: Stage P4 (73-08). 3D reconstruction of the right half of the mandible, sphenoid bone and pterygoid muscles.

a: Origin of the lateral pterygoid at the greater wing and lateral surface of the lateral pterygoid process of the sphenoid bone. Origin of the medial pterygoid at the medial surface of the lateral pterygoid process of the sphenoid bone. Frontal view.

b: Special relationship between the lateral pterygoid and the articular disc, condylar cartilage and condylar process (Insertion of muscle fibres in Fig. 63). Proximity of the medial pterygoid to the angle and ramus of the mandible. Dorsomedial view.

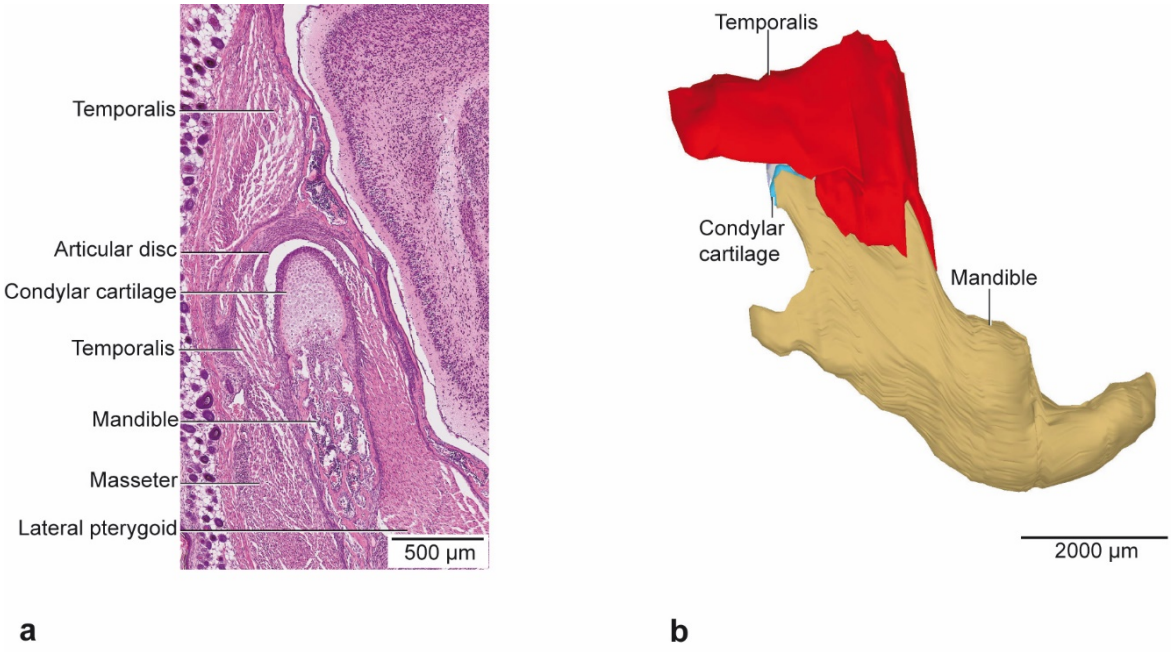

Fig 64: Stage P4 (73-08). Histological section and 3D reconstruction of the temporalis.

a: Histological section of the right half of the temporomandibular joint shows the extension of the temporalis posterior to the temporomandibular joint. Frontal plane, HE staining.

b: 3D reconstruction of the right half of the mandible and temporalis shows the relationship between the muscle and the articular disc. Lateral view.

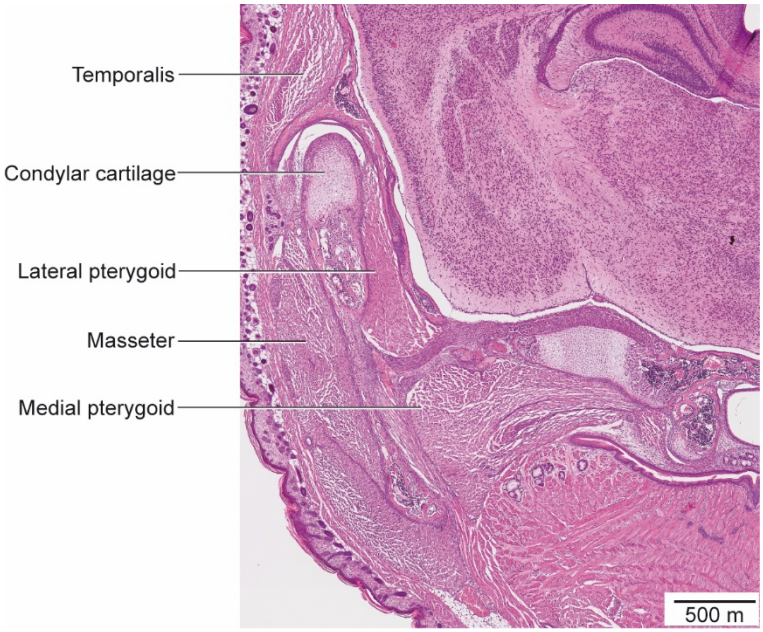

Fig. 65: Stage P4 (73-08). Histological section of the right half of the mandible through the condylar cartilage indicating the anatomical arrangement of the masticatory muscles.

Frontal plane, HE staining.

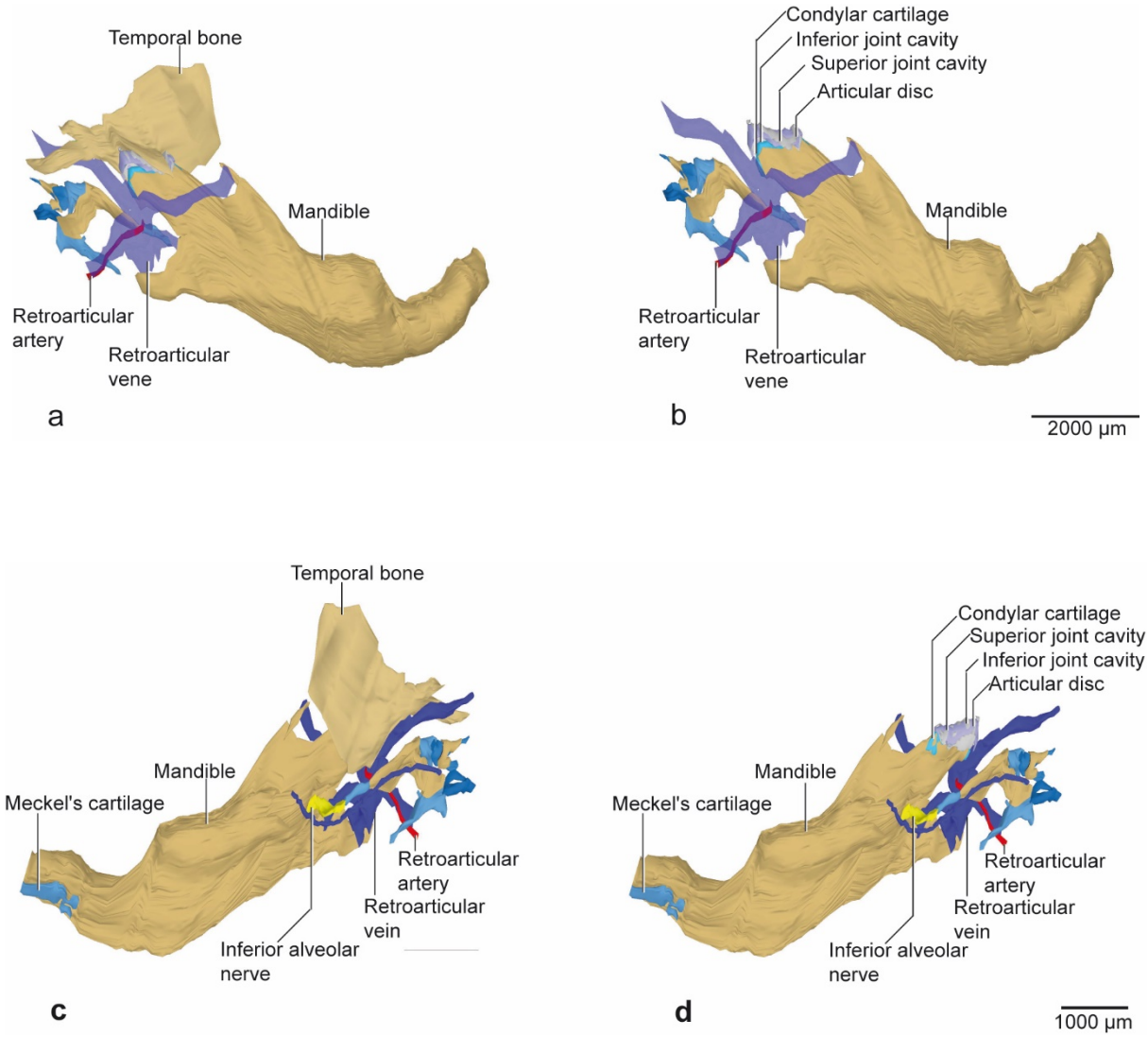

Fig. 66: Stage P4 (73-08). Partial 3D reconstruction of some components of the right temporomandibular joint and the region of the bilaminar zone.

a: Temporomandibular joint region with its temporal bone. Retromandibular vein made transparent to visualize the content and extension of the bilaminar zone. Lateral view.

b: Temporomandibular joint region, temporal bone removed to visualize the joint cavities and the articular disc. Retromandibular vein transparent to visualize the content and extension of the bilaminar zone. Lateral view.

c: Temporomandibular joint region with its temporal bone. Medial view.

d: Temporomandibular joint region, temporal bone removed to visualize the joint cavities and the articular disc. Medial view.

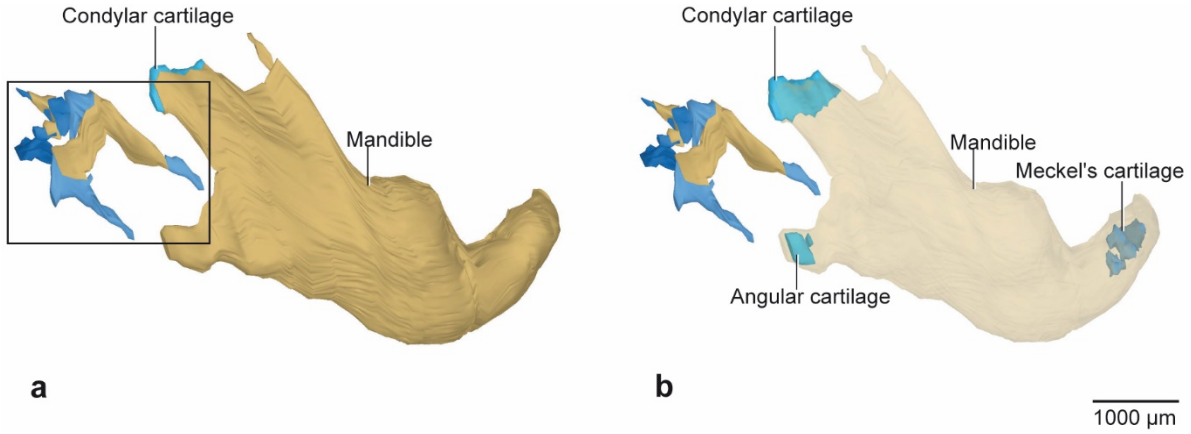

Fig. 67: Stage P4 (73-08). 3D reconstruction of the right half of the temporomandibular joint, Meckel's cartilage and middle ear ossicles.

a: Lateral view. Box: see Fig. 68.

b: Same view with mandible made transparent. Almost the entire intramandibular portion of Meckel's cartilage has ossified, and only a small segment at the most anterior part of the mandible remains cartilaginous. For the first time, the posterior part of the extramandibular portion appears separated from the malleus. Lateral view.

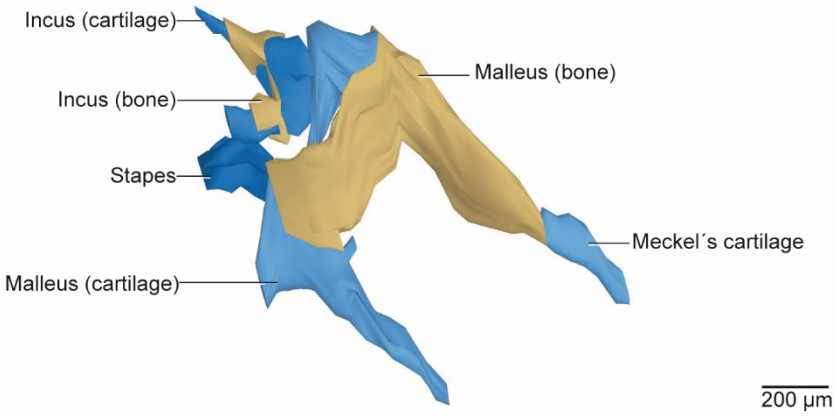

Fig. 68: Stage P4 (73-08). 3D reconstruction of a detailed view of the right middle ear ossicles.

The ossified part of the incus and malleus is larger than in the previous stages. Lateral view.

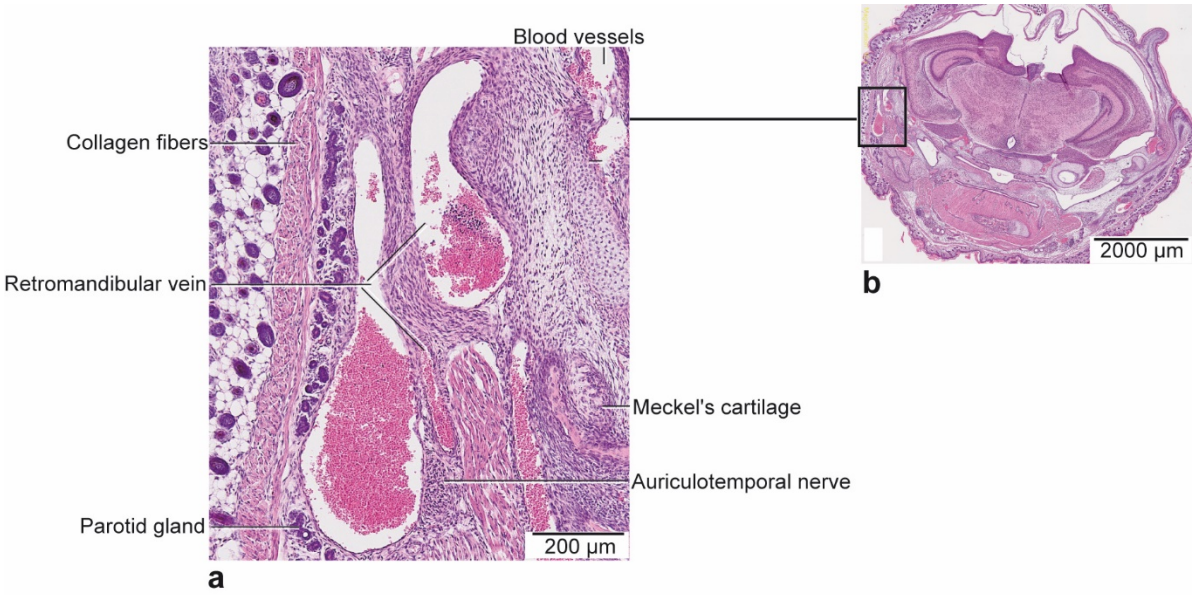

Fig. 69: Stage P4 (73-08). Bilaminar zone.

a: Histological section through the region of the right bilaminar zone. Frontal plane, HE staining.

b: Survey of the whole section.

5.3 Morphometry

5.3.1 Specimens brought to the same scale

Stage E13.5

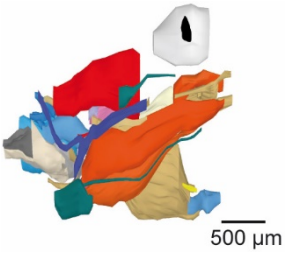

Stage E14.5

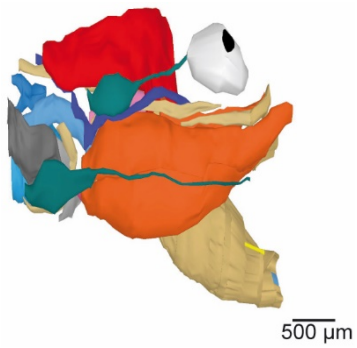

Stage E15

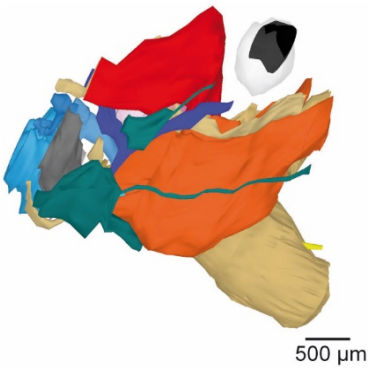

Stage E16

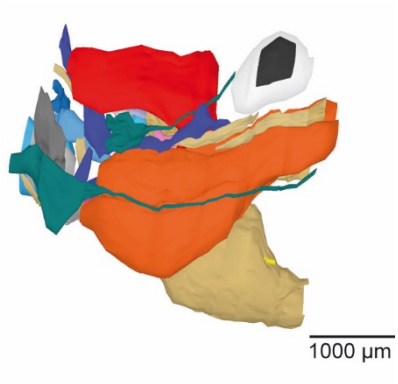

Stage E18

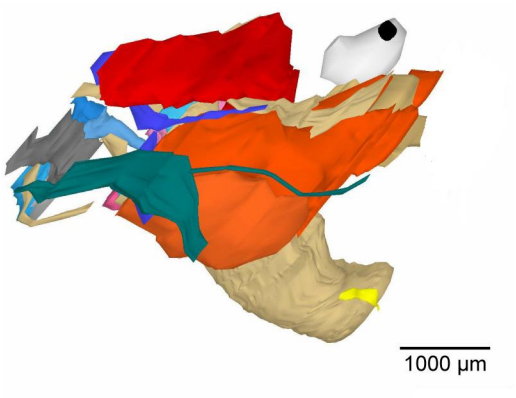

Stage E20

Stage P0

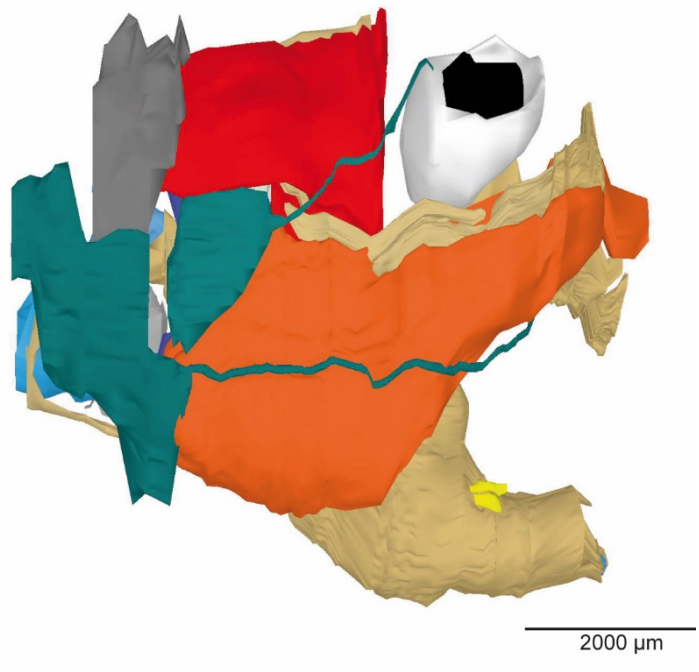

Stage P2

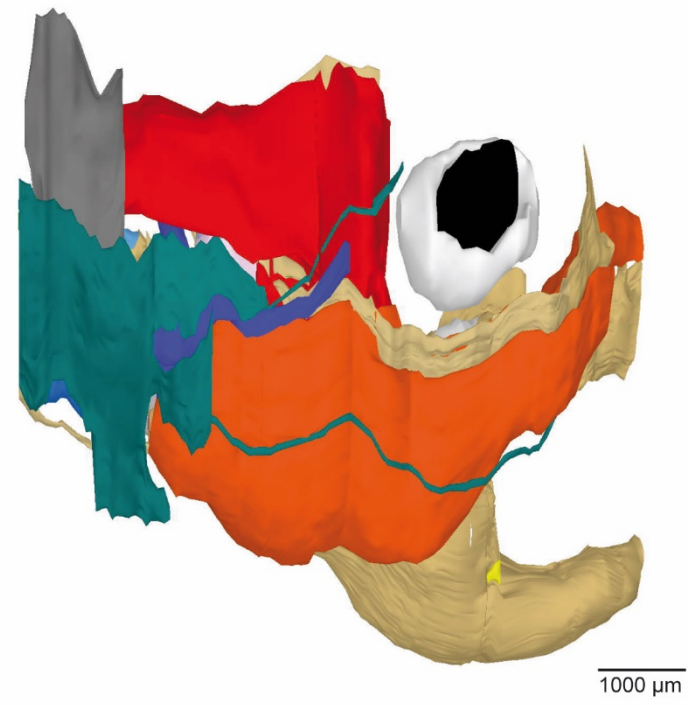

Stage P4

Fig. 70: 3D reconstructions of all the specimens, from stages E13.5 to P4, brought to the same scale.
The structures depicted in this figure have been labelled in detail in the section “results”. Furthermore, the colour code corresponds to Table 2.

5.3.2 Volume of the masticatory muscles

Table 3: Volume (in µm³) of the masticatory muscles of the mouse from stages E14.5 to P4.

Stage	Masseter	Temporalis	Lateral pterygoid	Medial pterygoid
E14.5	216,169,253	95,673,857	22,463,461	46,108,401
E15	528,993,028	246,112,759	68,853,645	102,740,846
E16	625,509,465	288,661,025	103,364,077	130,990,473
E18	864,680,196	410,889,544	63,179,320	164,071,964
E20	1,734,654,193	714,444,394	200,132,852	234,100,548
P0	1,917,728,759	592,939,382	447,910,557	380,124,366
P2	2,059,540,839	1,008,113,778	373,046,817	461,358,130
P4	2,845,103,230	1,020,166,784	540,140,529	629,197,719

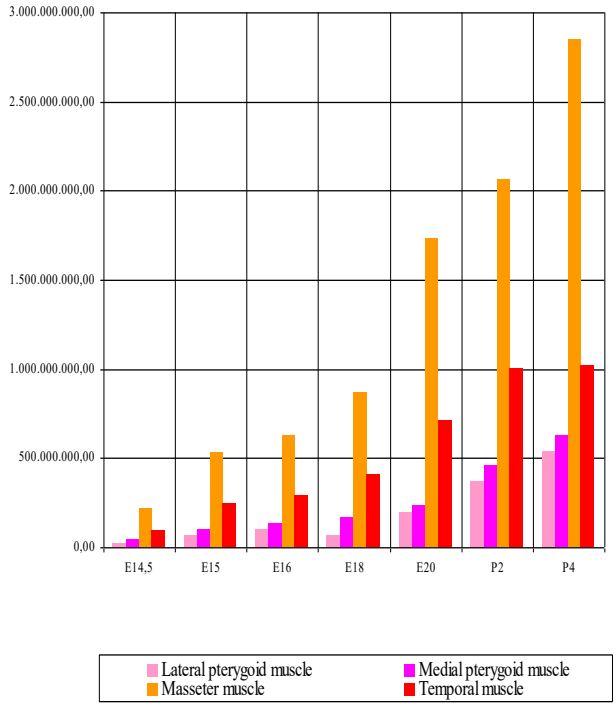

Graphic 1: Volume (in µm³) of the masticatory muscles of the mouse from stages E14.5 to P4 based on the data of Table 3.

5.3.3 Measurements of the distances anterior and posterior to the joint

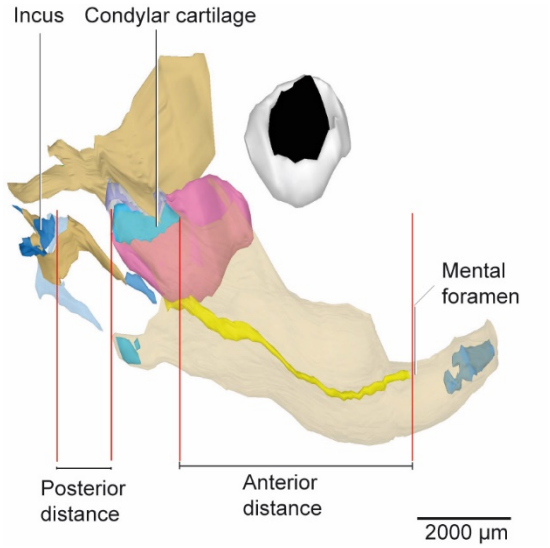

Fig. 71: Stage P4 (73-08). Partial 3D reconstruction of some components of the right temporomandibular joint.

The red lines indicate the points of reference used to measure the distances anterior and posterior to the temporomandibular joint. These landmarks were determined along a reference line (deleted in the picture) running from the orbitale (the most inferior point on the margin of the orbit) to the most superior point of the incus. The anterior distance was defined between the anterior surface of the condylar cartilage or condylar process (in the case of stage E14.5) and the mental foramen of the mandible. The posterior distance had its boundaries at the posterior surface of the condylar cartilage and at the anterior surface of the incus.

Table 4: Measurements of the anterior and posterior distances to the temporomandibular joint.

Comparison of the length of the area anterior and posterior to the temporomandibular joint using some cephalometric landmarks.

Stage	Anterior distance	Posterior distance
E14.5	695 µm	426 µm
E15	1433 µm	600 µm
E16	1565 µm	534 µm
E18	1804 µm	608µm
E20	1766 µm	466 µm
P2	2900 µm	500 µm
P4	4208 µm	913 µm

6 DISCUSSION

6.1 Discussion of the materials

For practical and ethical reasons the mouse (*Mus musculus* C57Bl/6J) was the chosen animal for the present study. The aim of this section is to validate the use of rodents as a model organism with respect to the topic of our investigation.

Humans, mice and other mammals had a common ancestor approximately 80 million years ago, and one of the main consequences is that nowadays they share 80% of their genes. As a result of this biological similarity, mice and humans have analogous diseases and conditions (Bernuy, 2013). Some other characteristics that make rodents one of the major organisms for modelling are the low cost, the short gestation time (19-21 days, depending on the strain), the short generation time (10 weeks from being born to giving birth), the prolific reproduction (5-10 pups per litter), and the fast lifespan. Apart from that, the major advantage of the mouse compared to other mammals is that it is a well-established experimental model. There are also two important factors, aside from the ethical and pragmatic reasons mentioned above, that made us choose rodents instead of humans for our study: one is the lack of human material at the very early postnatal stages, and the other is that the mouse, together with the rat, is the primary animal model of craniofacial system investigation. However, there are also some differences between human and mouse that should not be omitted, for example, the lower genetic variation between mice, the lack of deciduous teeth, the specialized diets, and the high fertility (Hallgrímsson & Lieberman, 2008). In particular, two specific problems were found in this investigation in choosing the mouse as the animal model: on the one hand, dating the exact age of the rodents, and on the other, that only one mouse per stage was 3D reconstructed and analyzed. The first problem occurred because the pregnancy of the dams was checked only once per day, so we have counted with an error margin of 24 hours. The solution for the second difficulty would have been a higher number of mice, but this was dismissed for ethical reasons, and because the focus of this study is on a longitudinal view of the morphogenesis over many stages. A horizontal consideration of the individual stages remains open for future studies (Nowak, 2016). Moreover, the amount of work required for the reconstruction of each specimen does not allow us to analyze more than a single mouse at a given stage.

6.2 Discussion of the methods

6.2.1 Histology

The prerequisites for the 3D reconstructions with AnalySIS® 5.0 software (OSIS, Münster, Germany) were the histological serial sections. This method is typically associated with artefacts, and although the sections with evident errors were dismissed, possible dimensional deviations should be considered when evaluating the results. Some of these artefacts could include shrinkage during fixation and dehydration, distortion during embedding, and compression and deformation during sectioning. There are some alternatives to creating 3D reconstructions, but they are not short of errors. Scanning electron microscopy is one of them, but performing micropreparations is a difficult task, and afterwards the material is destroyed forever. Another alternative is using whole-mount preparations, but they fail to show all structures. Equally, micro-computed tomography is limited to calcified tissue structures, while micro-magnetic resonance microscopy still needs to be applied in later developmental stages (Radlanski & Renz, 2010). It should be emphasized that during this investigation, analyses with polarized light microscopy were performed with the goal of a better visualization of the bilaminar zone. However, the results did not show any relevant information compared to those obtained with light microscopy.

6.2.2 3D Reconstruction

Nowadays, the craniofacial system is being researched using modern 3D imaging techniques, which include ultrasound, magnetic resonance, computer tomography, and computer-aided 3D reconstructions obtained from histological serial sections. This last one dates back to the beginning of the last century when Born built the first wax plate models (Born, 1883). At the end of 1945, Blechschmidt began a systematic collection of 3D reconstructed human embryo models, which are displayed in glass showcases in the Center for Anatomy, University Medical Center of Göttingen (Georg-August-University of Göttingen, Germany) (Born, 1883; Low, 1909; Fawcett, 1910; Blechschmidt, 1954, 1963; Gaunt & Gaunt, 1978). Computer-aided 3D reconstructions, like solid models, provide a greater advantage as they allow for electronic dissection. They also allow us to select what we want to visualize by omitting or selecting specific anatomical structures, making them transparent or taking them away. In addition, the structures can be exposed layer by layer and a stack animation can be created (Radlanski & Renz, 2010). Apart from that, the degree of detail of 3D reconstructions in early developmental stages is impossible to obtain with non-invasive techniques, such as magnetic resonance (de Bakker et al., 2016),

computed tomography or ultrasound. Another reason to perform 3D reconstructions is that histological sections usually deteriorate over time and those stained with HE fade. Therefore, digitization is one of the methods of choice to conserve histological material that can be easily accessed worldwide. Although the methodology used in this study destroyed the specimens by sectioning, they became almost fully restorable once the 3D reconstructions were performed, and subsequently, virtual dissections can be accomplished repeatedly without any destruction or further damage (Radlanski & Renz, 2010).

6.2.3 Morphometry

The temporomandibular joint and some selected surrounding structures of the specimens - aging from embryonic day 14, 15, 16, 18 and 20, and postnatal day 0, 2 and 4 - were mathematically analyzed in this study. Although the embryos at stages 13.25, 13.5 and 17 were morphologically described, and the last two of them were also 3D reconstructed, it was necessary to exclude them from the morphometric analysis for the following reasons. At stage E13.25 we were not able to visualize any component of the temporomandibular joint or any masticatory muscle. At stage E13.5 the only masticatory muscle that could be identified was the masseter, and in a very immature form. Finally, the mouse at stage E17 did not match in size and maturation with the other specimens, which was attributed either to an incorrect staging, or to a faster prenatal development. Saller (1932) showed that there are many factors that could affect the growth of the mice, such as the litter size, the birth weight and the sex, but none of these was considered in the present study. For the remaining specimens, the volume of the four masticatory muscles was determined by using the corresponding function of the software. In addition, the anterior and posterior regions of the temporomandibular joint were measured using cephalometric landmarks. When using this last method, there are some considerations that should be noted (Bernuy, 2013). First, the landmarks should be equivalent at different developmental stages and across different specimens. Second, it can be difficult to choose landmarks when structures are developing, due to the constant remodeling that they undergo. Third, the measurements performed do not take “form” in consideration and therefore, they do not show any information, such as curvatures. The cephalometric landmark “Or" (orbitale) has been used, as well as some analogous landmarks at specific places on the incus, the mental foramen and the condylar cartilage. All of them avoid the previously mentioned problems, as they could be visualized early in the development, and their position and proportions barely changed along the stages. Since both the volume and landmark-based measurements were performed on 3D reconstructions, and manual alignment was used for that, the image projections should be taken as approximations. In any case, these

relative values allowed for comparison between different stages of development. Some other measurements were performed in the histological serial sections, and in this case it is important to acknowledge the errors resulting from the fixation of tissues and that were already discussed in section 6.2.1. Measurements using unfixed specimens would have been ideal, but was not possible due to the fragility of the tissues.

6.3 Discussion of the results

6.3.1 Preliminary remarks

In this section, the morphological results will be first discussed and compared with the available literature. Next, the peculiarities of the lateral pterygoid muscle and its relevance in the study of the temporomandibular joint will be described. Following this, the role of mechanical forces in muscle differentiation, and the interaction between muscle and bone during development, will be also discussed.

It is important to point out that the process of development cannot be observed in histological serial sections and only anatomical "snapshots" are available instead. Therefore, the descriptions in our 3D reconstructions are only an approximation of the continuous developmental process (Radlanski et al., 2016).

Furthermore, when describing the process of development, the changes of curvature that the embryo undergoes during the prenatal stages need to be considered: from a high curvature (particularly of the head) at the early stages to a straighter embryo during the last days before birth (Fig. 72).

Stage E13.5 **Stage E15.5** **Stage E17.5**

Fig. 72: Visualization of stages E13.5, E15.5 and E17.5 of the mouse embryos to show changes of curvature during development.

Images obtained from Koplocki (2011).

6.3.2 Discussion of the morphogenesis

6.3.2.1 Masticatory muscles

The masticatory muscles are anatomically complex in all mammals. Despite there being a deep and rich literature about the masticatory system of rodents, such as rats, chinchilla, squirrels, guinea pigs and mice (Howell, 1926; Wood & White, 1950; Das, 1955; Schumacher, 1961; Hiiemae & Houston, 1971; Cox & Jeffery, 2011), very little has been published specifically regarding the musculature of the mouse *Mus musculus* (Patel, 1978; Baverstock et al., 2013). What is more, to the best of our knowledge, in no case has the prenatal morphogenesis of the whole group been described before. In this section, some qualitative characteristics (e.g. origins, attachments and number of muscular heads) and quantitative data (e.g. muscular masses and percentages of total mass) will be reported. In addition, comparisons with the available literature will be made, current controversies will be addressed, and the differences between mouse and human musculature will be highlighted.

Regarding the first appearance of the masticatory musculature, back in 1971 Rayne and Crawford affirmed that in rats the four muscles originated at the same time. By contrast, the temporalis is the first to be detected in humans, followed by the pterygoids and the masseter, all of them having originated from the so-called temporal muscle primordium (Oğütcen-Toller & Keskin, 2000). In this investigation, we were first able to identify the primordium of the masseter at stage E13.5, followed by the other three muscles at stage E14.5, all of them arising well separated from each other.

The masseter comprised between 45% and 57% of the total masticatory muscle mass in the present study, while in the adult *Mus musculus* it amounted for 60.5% (Baverstock et al., 2013), versus a range of 54.9% to 76.8% in other five species of mice (Ginot et al., 2018). Therefore, the masseter is by far the largest masticatory muscle and it exerts the largest forces (Schumacher, 1961; Abe et al., 2008; Baverstock et al., 2013). As a result, the related skull components of the masseter, such as the zygomatic arch and the angular process, are well developed in the mouse compared to other species (Patel, 1978). Yamane (2005) reported the differentiation of myoblasts that later give rise to the masseter at stage E13, and the maturation of myofibers at stage E15, which continued after weaning, when the feeding behaviour changed at around four weeks after birth from lactation to mastication. Anatomically, the partition of this muscle is related to the appearance of internal tendons. In this way, Sato et al. (2014) detected as early as at stage E12.5 the expression of Tenomodulin (a molecular marker of tendons) in the middle region of the mesenchyme. However, there is a complete lack of consensus on how many layers

the masseter is divided into, and whether all of these layers should be referred as the masseter or as different muscles (Cox & Jeffery, 2011). Most authors divided it into superficial, deep and zygomaticomandibularis (Turnbull 1970; Cox & Jeffery 2011; Baverstock et al., 2013). The superficial masseter is subdivided by fascia which follow the same anterior direction in the mouse, but in humans it lacks any division and it runs vertically (Herring, 2007). The deep masseter is the largest masticatory muscle in the mouse (Schumacher, 1961; Baverstock et al., 2013) and has been divided into two regions, anterior and posterior (Cox, 2011), or even into three, anterior, infraorbital and posterior (Patel, 1978). However, recent studies (Baverstock et al., 2013) have reported it as a single muscle, which is in accordance with the results of this investigation. The separation between the superficial and deep bellies was observed at stage E14.5, both layers running side by side, yet with clear fiber orientation, and overlapping each other in the following stages until the superficial masseter almost covered the deep masseter in the newborn. Regarding the zygomaticomandibularis, some authors recognize it as a separate muscle from the deep masseter in rodents (Cox & Jeffery 2011; Druzinsky et al., 2011; Baverstock et al., 2013) and even in humans (Hwang et al., 2005; Matsugana et al., 2009), although only as a degraded or rudimentary muscle in this latter species (Hwang et al., 2005). Contrarily, our findings and those of Byrd (1981) and Satoh (1997) did not recognize the zygomaticomandibularis as a separate muscle. Since the present investigation described the origin of the deep masseter along the entire medial surface of the zygomatic arch and also an anterior extension, it is obvious that the zygomaticomandibularis has been included as part of the deep masseter.

The temporalis represented between 18% and 27% of the total muscle mass in the prenatal and young newborn. Towards adulthood, it accounted for 22.4% in the house mouse (Baverstock et al., 2013), and between 18.7% and 22.3% in other mouse species (Ginot et al., 2018). It is, therefore, the second largest masticatory muscle in rodents (Schumacher 1961; Baverstock et al., 2013) and the largest in humans, but it shows the fastest contraction forces in both species (Abe et al., 2008). Some authors recognized the separation of the temporalis into two muscles, lateral and medial, also referred to as anterior and posterior (Cox & Jeffery, 2011; Baberstock et al., 2013). Unlike them, in the present study only one muscle has been reported, probably due to the methodology used, since the above-mentioned studies employed micro-CT images, which made the visualization of the septa between both parts possible.

The pterygoids have similar morphology in all rodents, as opposed to the great variety showed by the masseter and the temporalis. The lateral pterygoid comprised between 5% and 13% of the total masticatory muscle mass in our study, while it represented 4.7% in the adult *Mus musculus*

(Baverstock et al., 2013), and ranged from 7.4% to 16.3% in other mouse species (Ginot et al., 2018). Therefore, it is the smallest masticatory muscle in mice, contrary to humans where it is enormous (Herring & Liu 2001; Herring, 2003). It exerts weak forces (Suzuki & Iwata, 2016) and, as a result, the lateral pterygoid plays an essential role in the stabilization of the condyle against the glenoid fossa (Satoh, 1997). Another anatomical peculiarity of the lateral pterygoid is that it is the only masticatory muscle with horizontally arranged fibers (Stöckle et al., 2019). The present investigation gives a more accurate description about the origins and insertions of the lateral pterygoid when compared to Patel (1978) and Baverstock et al. (2013), since they described its attachment only at the medial surface of the condyle, whereas we also observed it at the neck of the mandible and at the articular disc. Due to the importance of the lateral pterygoid for the purpose of the present study, a detailed assessment will be discussed in section 6.3.3.

The medial pterygoid amounted for 8% to 12% of the total masticatory muscle mass in our investigation, versus 11.56% in the adult *Mus musculus* (Baverstock et al., 2013), and a range of 6.8% to 14.6% in five other mouse species (Ginot et al., 2018). Compared to humans, the distance between the pterygoid fossa and the angle of the mandible is larger in mice, resulting in longer muscle fibers (Schumacher, 1961). Hiiemae & Houston (1971) stated that the medial pterygoid helps to stabilize the angular process against the tendency of the masseter to evert it. Again, the present study has made a more precise description of this muscle compared to the studies of Patel (1978) and Baverstock et al. (2013), by reporting two heads instead of only one.

Taking our results together, it is obvious that there are different anatomical findings in the literature regarding the number of bellies. These disagreements have arisen mostly due to the methodology used (macrodissections or contrast-enhanced micro-CT images versus histological sections), and also because of disparities in the interpretation of the results as well as differences between species.

Some morphological discrepancies between humans and mice have been also stated, and they are derived, among other reasons, from different eating habits between species: in omnivores (including the mouse) which perform anterior-posterior movements of the mandible, the masseter and the medial pterygoid are more emphasized compared to carnivores, in which the temporalis is more dominant (Herring, 2007). However, the masticatory muscles of the mouse are sufficiently similar in morphology and development to their counterparts in humans to validate the use of *Mus musculus* for future studies.

6.3.2.2 Parotid and lacrimal gland

The salivary glands are formed in embryonic development by the process of branching morphogenesis, which includes complex epithelium-mesenchyme interactions for maximization of the epithelium and minimization of empty volumen within the tissue.

Domon and Kurabayashi (1987) affirmed that the morphogenesis of the parotid gland began late in prenatal life, and that at the time of birth the gland is still very immature. In our investigation, the duct of the gland was first discerned at stage E13.5, and only one day later, the body. In the following days, the number of secretory units and ducts increased as well as the size of the body. The study of Domon and Kurabayashi (1987) also highlighted that the ductal branching pattern depended on the strain of the mouse.

The lacrimal gland in mice comprised two lobes (the large exorbital lobe and the small intraocular lobe), in contrast to humans, which have only one (Mattiske et al., 2006). The literature describes the first anlage of the lacrimal gland between stage E12.5 (Pan et al., 2010) and stage E13.5 (Garg & Zhang, 2017) as a thickening of the conjunctival epithelium that invades the underlying mesenchyme. The present study reported this event at stage E14.5 and referred to it as the exorbital lobe. At this stage, the gland was already composed of a body and a duct. Next, the epithelium elongates and branches (Garg & Zhang, 2017).

6.3.2.3 Maxilla

The midfacial region comprises the maxilla, zygomatic bone, nose, superior lip, and primary palate. These structures are derived from seven processes, in particular the frontonasal process, the paired lateral and medial nasal processes, and the paired maxillary processes. They all arise from the cranial neural crest cells in combination with ectoderm and mesoderm, and during early development, these processes grow and merge. Notably for us, the maxillary processes start growing medially at stage E12, and they merge in the midline at stage E13 forming one continuous structure, the maxilla, which composes the main bone of the middle third of the face (Suzuki, 2016) (Fig. 73). Nagata et al. (1991) made an accurate description of the development of this bone, which starts at E12 with the formation of the first intramembranous center of the premaxilla, located lateral to the developing incisor tooth. This structure is also known as incisive bone, intermaxillary bone or Goethe's bone, and it forms the intermaxillary segment of the maxilla that contains the incisives. Subsequently, Nagata et al. (1991) reported the first ossification center of the maxilla lateral to the inferior orbital nerve and adjacent to the molar tooth bud. At stage E14 he identified three processes in the maxilla that were detected by us at

stage E14.5, these being the zygomatic, frontal and palatine, which increased significantly in size during the following days.

It is in our interest to mention that the growth of the premaxillary-maxillary or incisive suture plays an important role in craniofacial morphology during postnatal life. Although there is no data about when exactly this suture closes, the study by Vora et al. (2016) throws some light on this question by reporting a single bone with an ossified suture at stage P42.

Fig. 73: Prominences that give rise to the main structures of the face in mice.

Frontal view.

Depiction obtained from Suzuki (2016).

6.3.2.4 Zygomatic bone

The zygomatic bone is usually called the zygoma, cheekbone or malar in mammals, and jugal bone or jugal in reptiles, amphibians, and birds (Dechow & Wang, 2016). It differentiates from the cranial neural crest cells that populate the first pharyngeal arch. Anatomically, the zygomatic bone is described as paired craniofacial bones that articulate to the maxilla, temporal bone, sphenoid, and frontal bone. This investigation identified it at stage E14.5 as a small structure that grew greatly and ossified during fetal development. The body of the zygoma had two processes, namely the frontal and temporal, and the latter articulates with the zygomatic process of the temporal bone to form the zygomatic arch. This arch has significant functional importance since it serves as origin for the masseter and for several facial muscles (Dechow & Wang, 2016) and, as a result, the zygomatic bone experiences the largest stresses in the skull (Cox & Jeffery, 2011). In the present investigation, the zygomatic arch was first observed at stage E16, and before that the masseter was attached to the zygomatic bone. Another function of the zygoma is to connect the facial skeleton with the cranial bone (Dechow & Wang, 2016).

In this section, it is also important to emphasize that the majority of the publications on the zygomatic bone have focused on clinical studies related to a wide of variety topics, such as fracture repair or surgical management of craniofacial tumors (Dechow & Wang, 2016). Numerous studies have also analyzed the biomechanics of this bone (Rafferty et al., 2000) and many others have described its evolution (Dechow & Wang, 2017). These last investigations

have concluded that the variations of the zygomatic bone among mammals are related to functional specializations (Márquez et al. 2017) and therefore, they reflect the adaptation of the midface during evolution (Dechow & Wang, 2016).

6.3.2.5 Temporal bone

The paired temporal bones are situated at the sides and base of the skull and they consist of four parts, i.e. squamous, petrous, mastoid, and tympanic, that ossify independently, either by endochondral or by intramembranous ossification.

The squamous part, located in the most superior part of the bone, belongs to the cranial vault and undergoes intramembranous ossification. This part has great interest for us since it comprises the glenoid fossa that forms the temporal component of the temporomandibular joint. The primordium of this fossa was identified at stage E13 by Tsuchikawa et al. (2010), at stage E14 by Ohshima et al. (2011), and at stage E14.5 by Gu et al. (2014) and Liang et al. (2016). Frommer (1964) described the first observation of the glenoid fossa at stage E16 as a small center of ossification that experienced rapid bone formation from stage E17 onwards. These results are in accordance with our observations, since we first visualized the glenoid fossa as a purely flattened intramembranous bone surrounded by mesenchyme at stage E14.5, that acquires a slight convexity of the superior border at stage E16. The squamous part also contains the zygomatic process which, together with the temporal process of the zygomatic bone, forms the zygomatic arch.

The petrous part is located between the sphenoid and the occipital bone, houses the auditory apparatus, and ossifies endochondrally like the mastoid part.

The tympanic part is relatively small and is situated inferior to the squamous part, anterior to the mastoid part and superior to the styloid process. It is air-filled and contains structures that conduct sound energy to the cochlea, such as the tympanic membrane, and the middle ear ossicles, muscles, and ligaments.

6.3.2.6 Sphenoid

The sphenoid is an unpaired and large bone situated at the base of the skull and surrounded by the frontal, temporal, and occipital bones. It consists of a central body (with the sella turcica housing the pituitary gland and the sphenoidal sinuses), with the greater and lesser wings on either side of the body, and the pterygoid processes descending directly from the connection between the greater wing and the body. It also presents a hook-like projection, the pterygoid hamulus (Yamamoto et al., 2017). The sphenoid shows many foramina and fissures, through

which nerves and blood vessels of the head and neck pass. Other functions of this bone are to be part of the base and sides of the skull, and of the floor and walls of the orbits. It is also the site of origin of two masticatory muscles, the lateral and medial pterygoids that arise from the lateral pterygoid process, and also of the tensor veli palatini, that originates at the medial pterygoid process.

The sphenoid presents many ossification centers, and can be divided during development into a presphenoidal part (anterior to the tuberculum sellae) and a postsphenoidal part (Fawcett 1910; Yamamoto et al., 2017). There are two very recent publications (Yamamoto et al., 2017; Hirouchi et al., 2018) that have explored the sequential development of the sphenoid bone, which shows that the intricate formation of this structure is still a topic of interest. Chronologically, we first observed at stage E13.5 the body composed of cartilaginous tissue. Next, at stage E14.5, we found all parts of the sphenoid cartilaginous, except for the medial pterygoid process, where osteoid-like tissue was discernible in the superior region, and secondary cartilage in the middle region (Fig. 74). Based on the degree of cell differentiation and changes in the surrounding matrix, the cell population of this secondary cartilage could be divided into a fibroblastic/polymorphic layer, a flatted chondrocyte layer, and a hypertrophic cell layer (Hirouchi et al., 2018). Some investigators (Baume, 1962; Duterloo & Jansen 1970; Vinkka-Puhakka & Thesleff, 1993) maintained the historical view that secondary cartilage originates from a separate and preprogrammed blastema, while others (Symons, 1952; Shibata et al. 1996, 2013) affirmed that it arises from cells of the adjacent bone. The study by Yamamoto et al. (2017), confirmed this last theory, since the cells of the mesenchymal mass of the medial pterygoid process were connected with the periosteum of the lateral pterygoid process cartilage. We also could observe that at stage E15 the number of secondary cartilage cells had increased, whereas at stage E16 it has started to decrease. Conversely, the endochondral ossification in the inferior part of the medial pterygoid process and the intramembranous ossification in the superior part had progressed. Our results are in accordance with those of Yamamoto et al. (2017): the endochondral ossification in the medial pterygoid advanced rapidly between stages E15 and E18, and the attachment of the tensor veli palatini to the medial pterygoid was clearly seen at stage E16. Since jaw movements start at stage E15.5 (Jahan et al. 2010), the mechanical stress due to the contraction of this muscle is responsible for the rapid endochondral bone formation according to Yamamoto et al. (2017). It is worthy to point out that a clearly binding zone between the medial process and the body was revealed in our 3D reconstructions at stage E20, while Yamamoto et al. (2017) reported this occurrence two days before. The time-course developmental process of other parts of the sphenoid is in accordance with the results of

Yamamoto et al. (2017). Special attention should be given to the fact that, while the medial pterygoid process is formed by a combination of endochondral and intramembranous ossification as mentioned before, the lateral process, the wings, and the body underwent exclusively endochondral ossification (Yamamoto et al. 2017; Hirouchi et al. 2018).

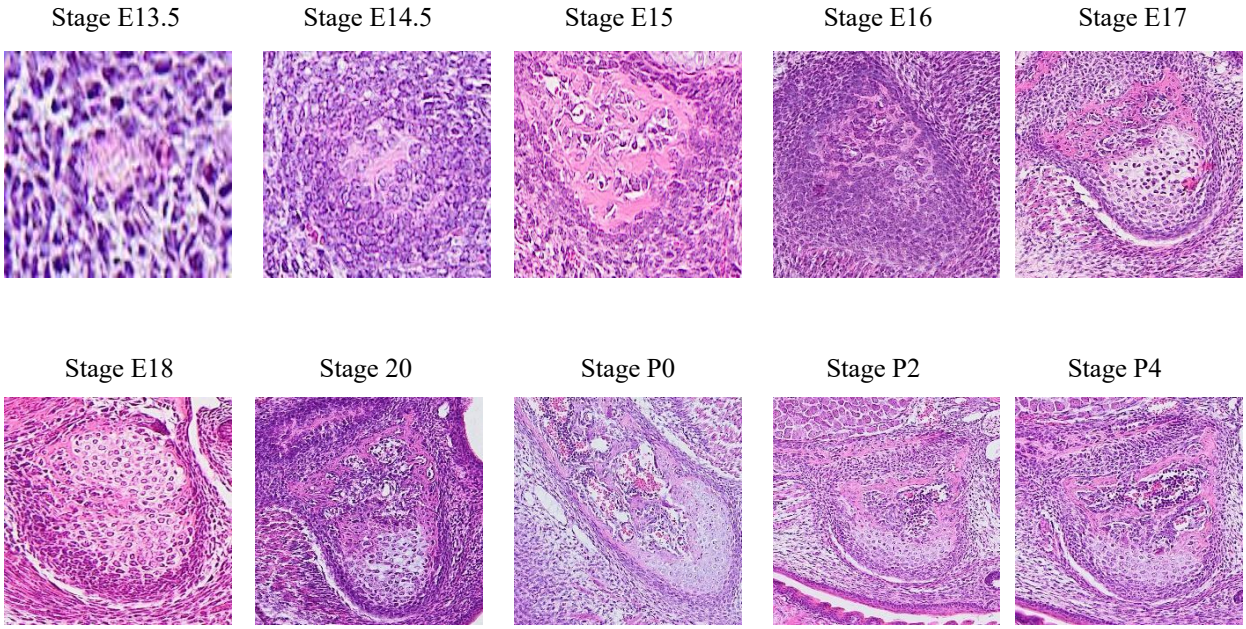

Fig. 74: Histological sections of the medial pterygoid process of the sphenoid of the mouse from stage E13.5 to stage P4.

Frontal plane, HE staining.

6.3.2.7 Mandible

The mandible is a complex structure that develops from neural crest cells within the first pharyngeal arch. It is formed by intramembranous ossification, but its secondary cartilages strongly influence the further development and growth (Ramaesh & Bard, 2003). When describing the timing of appearance of the mandible it should be mentioned that this bone, together with the clavicle, shows the earliest ossification in the mouse (Frommer 1964). The first anlage of its body and ramus was detected by Tsuchikawa et al. (2010) at stages E12.25 and E13, respectively. In the present investigation, the first ossification center of the mandible was identified at stage E13.5 as a “plate” of condensed mesenchyme with small regions of osteoid tissue located in the vicinity of the first molar tooth bud and lateral to Meckel’s cartilage. This result is in accordance with Ramaesh & Bard (2003). We further observed that the shape of the mandible changed strongly during the following days: while at stage E14, the body and the ramus showed almost the same length; at stage E15 the body significantly increased in length compared to the ramus. Meanwhile, the bone between the three processes, i.e. condylar, angular

and coronoid, did not grow as fast as the processes did, and consequently the two notches became gradually deeper. At stage E17, we identified all components of the mature mandible, which confirms the results of Swiderski & Zelditch (2013), but is in contrast to the study of Frommer (1964), who could not recognize the typical neck of the mandible at stage E20. After birth, growth and shape remodelling took place in every anatomical region. As pointed out by Swiderski & Zelditch (2013), these changes occurred first in the ramus to accommodate the teeth, but when eruption is completed, changes decreased in the ramus and increased in the processes, in order to match the muscle growth. The present investigation has focused on the quantitative and qualitative changes in size and shape of the mandible associated to the masticatory muscles. However, the interface between teeth and bone is beyond the scope of this thesis.

Having explained the main characteristics of the mandibular bone itself, we will focus on the mandibular processes and its related secondary cartilages. Subsequently, we will discuss the development of Meckel's cartilage, and finally, the development of the inferior alveolar nerve.

The condylar cartilage derives from mesenchymal progenitor cells and has unique characteristics as it undergoes endochondral ossification and remodels in response to mechanical loading (Robinson et al., 2015). It has been classified as secondary cartilage due to some differences with the primary cartilage, such as the time of appearance, cell arrangement, pattern of blood vessels, and expression of different types of collagen (Shibata et al., 2013). As mentioned briefly before, when discussing the development of the sphenoid bone, there are two theories that explain the formation of secondary cartilage. One is the "periosteum theory" (Symons, 1952; Shibata et al., 1996, 2013), which assumes that this cartilage arises from the periosteum of membrane bone after (secondary to) bone formation. The other one is the "blastema theory" (Baume, 1962; Duterloo & Jansen, 1970; Vinkka-Puhakka, 1993), which claims that the secondary cartilage derives from a separate, pre-programmed blastema. Tsuchikawa et al. (2010) made an accurate description of the development of the condylar cartilage of the mouse at very early stages. He detected the condyle at stage E12.75 as a mesenchymal cell condensation, which was continuous with the ramus of the mandible at stage E13. At stage E14.5, he observed hypertrophic chondrocytes, and at stage E15, he first recognized endochondral ossification. Shibata et al. (1996) and Robinson et al. (2015) performed similar studies observing the condylar anlage at E13 and cartilage formation at stage E15. The studies of Gu et al. (2008, 2014) detected the condylar blastema and the differentiation of chondrocytes 12 hours later, i.e. at stage E13.5 and at stage E15.5, respectively, in accordance with the recent publication of Liang et al. (2016). Conversely, Ohshima et al. (2011) and Frommer (1964) reported the anlage of the condyle at

stage E15. In the present investigation, we first recognized the condylar process at stage E14.5, situated lateral to Meckel's cartilage and inferior to the trigeminal ganglion. The newly formed condylar cartilage was detected at stage E15 continuous with the ossifying mandible, which confirmed the "periosteum theory". During this period, three zones became distinct within the secondary cartilage according to cellular morphology: the fibroblastic/polymorphic tissue layer, the flattened chondrocytes zone, and the zone of hypertrophic chondrocytes. Hirouchi et al. (2018) affirmed that since jaw movements have been reported to start at stage E15.5 (Jahan et al., 2010), this mechanical stress influences the differentiation of progenitor cells into chondrocytes. Next, at stage E16 we could observe the endochondral ossification of the secondary cartilage, which barely changed in size from stage E18 onwards (see Table 5). During the postnatal stages, four zones instead of three were recognized within the cartilage: the fibrous cell layer, the polymorphic progenitor layer, the flattened chondrocytes zone, and the zone of hypertrophic chondrocytes. Finally, it should be highlighted that the "adaptative" growth of the condylar cartilage occurs largely in response to that of the midface, mainly to the cartilages of the cranial base and the nasal cavity. Therefore, synchronicity between the growth of the mandible and the midface is possible (Petrovic et al. 1986).

The developmental process and characteristics of the angular cartilage are similar to those of the condylar cartilage. The study of Shibata et al. (2006) described the sequence of development of the angular cartilage with a 0.5-1.5 day delay relative to the condylar cartilage: he first recognized the anlage of the angular process at stage E14.5, in accordance to Tengan (1990), the secondary angular cartilage at stage E15, and the endochondral bone formation at stage E17.5. In contrast, the present investigation showed a parallel development of the condylar and angular cartilages, detecting the anlage of the last one also at stage E14.5, the secondary cartilage at stage E15, and the endochondral ossification at stage E16. From stage E18 onwards, the anterior-posterior volume of the angular cartilage decreased (see Table 5). This reduction was also detected by Shibata et al. (2006), and he explained that the size of this cartilage decreased with advancing age, unlike the condylar cartilage that maintained its volume at stage P21. He attributed this characteristic to the articulating function of the condylar cartilage, and affirmed that since the angular cartilage does not work as an articular cartilage, the loss of adequate mechanical force seems to lead to its disappearance.

Table 5: Anterior-posterior size of the condylar and angular secondary cartilages from stage E15 to stage P4. Measurement data were obtained from our histological sections.

Stages	Secondary condylar cartilage	Secondary angular cartilage
E15	464 µm	400 µm
E16	584 µm	648 µm
E17	788 µm	744 µm
E18	600 µm	600 µm
E20	544 µm	472 µm
P0	520 µm	440 µm
P2	620 µm	300 µm
P4	650 µm	250 µm

As with the condylar and angular processes, the coronoid process could also be identified at stage E14.5, but its size was significantly smaller. Specific genes control its appearance and its further development depends on external factors, such as the temporalis attachment (Washburn 1947; Anthwal et al., 2015). The bend shape of the coronoid process of the mouse from stage E20 onwards should also be emphasized, since it differs from that of the human, which appears mainly as straight. This characteristic has been also reported in rats and has been attributed to the posterior pulling force of the temporalis (Kim et al., 2018). Regarding the secondary cartilage, some studies have referred to it in the mouse coronoid process (Rot-Nikcevic et al., 2014; Swiderski & Zelditch 2013). However, we and other authors (Shibata et al. 2003; Zhang et al. 2013; Anthwal et al., 2015) were unable to observe it during pre- or postnatal stages. The lack of secondary cartilage is also found in the guinea pig and opossum, but it is present in other species, such as the rat and human, and this is particularly interesting due to the close phylogenetic relationship between mice and rats. It has been hypothesized that the presence of secondary cartilage may depend upon paracrine signals that seem to be downregulated in the mouse. Mechanical factors of the muscle and the surrounding tissues may also contribute to the lack of secondary cartilage in the coronoid process (Anthwal et al., 2015).

To finish with the discussion of the processes, it is worth mentioning the study by Swiderski & Zelditch (2013), which focused on the postnatal growth of the mandible, and concluded that when eruption is completed around stage P15, gnawing and chewing begin, and therefore, muscle growth is very active. Consequently, changes occur in the three processes.

The formation of Meckel's cartilage begins when ectomesenchymal cells from the neural crest migrate to the mandibular processes and differentiate into chondrocytes to form a pair of rod-like segments at each side of the developing mandible (Bhaskar et al., 1953; Nanci, 2017; Ishizeki et al., 1999). This structure acts as supporting tissue and it provides a morphogenetic template for

the development of the mandibular bone (Kishi et al., 2012). Meckel's cartilage is present transiently during development and it almost disappears just after birth in rodents. Its fate differs according to three regions. At the anterior or distal ends, both sides fuse and undergo endochondral ossification to form the mandibular symphysis. At the posterior or proximal end Meckel's cartilage forms the malleus (with the exception of the anterior process) and the incus. The posterior part of the intermediate or middle portion (running from the mandibular ramus to the malleus) eventually transforms into ligaments, such as the anterior malleolar and the sphenomandibular ligament (Kokot, 2020, in preparation), due to a transdifferentiation of chondrocytes of the perichondrium into fibroblasts (Harada & Ishizeki, 1998; Shibata et al., 2019). Finally, the anterior part of the intermediate portion disappears via endochondral ossification (Bhaskar et al., 1953; Shibata et al., 2019). Yokohama-Tamaki (2011) recognized the blastema of Meckel's cartilage at stage E11.5. In the present investigation, we could observe it first at stage E13.5, as two bars composed of prechondroblasts that joined at the most anterior part. Frommer and Margolies (1971) reported that at stage E14 Meckel's cartilage was composed of chondrocytes and chondroblasts and Yang et al. (2012) claimed that one day later the perichondrium was developed. The first indication of endochondral bone formation within Meckel's cartilage was the hypertrophy, death and disappearance of chondrocytes (Yang et al., 2012) and the replacement by new bone (Ishizeki et al., 1999). However, there is no consensus between authors regarding the developmental stage when this occurs: the present study detected the first sight of degeneration at stage E16, whereas Ishizeki et al. (1999) and Yang et al. (2012) reported it at stage E17, and Frommer and Margolies (1971) at stage E18. Despite this dissidence, we all agree that the initiation site was located anterior to the first molar tooth bud and inferior to the mental foramen. This close spatial relationship between the site of endochondral ossification of Meckel's cartilage, the location of the first ossification center of the mandible, and the locus of initial cartilage formation in Meckel's bars suggested a double induction process: the earliest chondrogenesis of Meckel's cartilage around stage E13 induced the formation of adjacent bone in the mandible, which in turn induced the endochondral ossification of the cartilage (Frommer & Margolies, 1971). According to our observations, at stage P0 almost the entire posterior intramandibular portion of Meckel's cartilage was replaced by bone. Cartilaginous tissue could only be detected at the anterior intramandibular portion and at the mylohyoid groove between the condylar and angular secondary cartilages (Ishizeki et al., 1999). Next, at stage P4 we observed a complete separation of Meckel's cartilage from the malleus. Concerning this topic, Anthwal and Thompson (2016) claimed that the breakdown started at stage P1 and was completed at stage P3. Their findings suggested that it occurred at

this time probably due to the mechanical stress causing by the feeding movements. Since the breakdown of Meckel's cartilage in the anterior region occurred 6-7 days before (around stage E15.5), the study above concluded that different mechanisms controlled the degeneration in the anterior and posterior regions (Anthwal & Thompson, 2016). Despite the development of Meckel's cartilage having been studied greatly since the last century, the manner and degree in which the cartilage participates in the formation of adjacent anatomical structures is still a topic of interest. Some investigations have been published recently about the influence of the cartilage in the formation of the gonial bone (Shibata et al., 2019) and in the development of the mylohyoid muscle (Kishi et al., 2012).

Other neural crest cells migrate into the mandibular and maxillary arches to condense under specific areas of the ectoderm and to differentiate into nerves and ganglia (Chiego, 1995). The inferior alveolar nerve is a sensory branch of the mandibular nerve that gives off the mylohyoid and mental nerves and continues anteriorly as the mandibular incisive nerve. It supplies sensation to the inferior teeth, the chin and the inferior lip. In the mandible, the inferior alveolar nerve is encircled by the mandibular canal, accompanied by lymphatic, venous, and arterial vessels (Chappard et al., 2018). Davies (1988) reported the first visualization of the trigeminal ganglion at stage E9, and the earliest fibers of the inferior alveolar nerve at stage E9.5, which reached the mandibular process at stage E10.5 and the maxillary process at stage E11. He detected that at stage E13 the nerve emerged from the ganglion. His findings are similar to those of Tsuchikawa et al. (2010), who identified the trigeminal ganglion and inferior alveolar nerve at stage E12, and to ours, since we already discerned the trigeminal ganglion and trigeminal nerve in our youngest specimen at stage E13.25. We also detected that at stage E13.5 the ganglion has duplicated its size, and the nerve was situated lateral to Meckel's cartilage and medial to the first ossification center of the mandible. At stage E14.5, the mental nerve passed through the mental foramen and the mandibular canal was not completely developed.

There is evidence that nerve formation influences the development of neighboring structures due to common signaling molecule pathways. One example is the fundamental role that nerves play in the development of the teeth, as a result of signal molecules transmitted between odontoblasts and nerve terminals (Chiego, 1995). Another example is the intimate relation between the migration of the palatal myogenic cells and the extending mandibular nerve (Zhang et al., 1999). Last, the interactions between the axons of the nerves and the formation of a more hierarchical network of blood vessels in the craniofacial region has been also reported (Sugimoto et al., 2015).

6.3.2.8 Temporomandibular joint

The sequence of the temporomandibular joint formation has been divided in three periods. First, the “initiation or appearance stage”, when the condyle and glenoid anlagen first form. This event has been reported at stage E14.5 in our investigation. The process continues with the “growth or cavitation stage”, which comprises the differentiation of the condylar cartilage and the formation of the joint cavities. We have defined it as between stages E15 and E20. Finally, the “maturation or completion stage”, when all the temporomandibular joint structures are formed and only topographic reshaping and growth still take place, occurs from stage E20 onwards.

We have already discussed the development of the bony articular elements that formed the temporomandibular joint. Therefore, in this section we will focus on the articular disc and joint cavities.

With regard to the articular disc, development initiates with the formation of a separate flattened mesenchymal condensation between the developing condyle and temporal bone. Later, the articular disc primordium acquires a characteristic compacted organization, and is flanked by the superior and inferior joint cavities. It eventually develops into a fibrocartilage structure (Frommer 1964) containing approximately 80% water and 20% fibers, mainly collagen (Koyama et al., 2014). It is still an unanswered question as to where its progenitor cells come from. Baume & Holz (1970) claimed that the anterior portion of the disc derived from the condylar blastema and the posterior portion from the glenoid blastema. Symons (1952) and Moffet (1957) affirmed that the lateral pterygoid tendon contributes to the formation of the medial part of the disc, while the lateral part was derived from an independent blastema. However, Sperber (2001) affirmed that the temporomandibular joint was formed by three separate mesenchymal condensations, in particular the condylar, temporal, and disc, that grew toward each other during development. Chronologically, Liang et al. (2016) described at stage E15.5 the appearance of the articular disc condensation, which became more compact and defined over the following days, and by stage E17.5 its lateral fibers combined with the tendon fibers of the masseter, and its medial fibers with the tendon fibers of the lateral pterygoid. Ohshima et al. (2011) reported the first visualization of the articular disc at stage E16, and Gu et al. (2014) at stage E16.5. Conversely, Frommer (1964) described it first at stage E18. During the late postnatal stages, i.e. from P28 to P35, Nakanishi & Iwai-Liao (1990) observed that the central area of the disc contains more dense bundles of collagen fibers, while the periphery was supplied with capillaries, which were continuous with the lateral pterygoid and the fibrous capsule. Our findings described the articular disc at stage E14.5 as a separate mesenchymal condensation between the condyle and the glenoid fossa, which supports the theory of Sperber (2001). It showed a rounded shape inferiorly

assuming the form of the condyle, and a flat shape superiorly like the glenoid fossa, and from stage E15 it became biconcave. Regarding this subject, Strauss et al. (1960) concluded that the morphology of the disc was mainly genetically determined. In the present investigation, at stage E14.5 the mesenchymal condensation was reached by some myoblasts of the lateral pterygoid, and one day later, the insertion of the muscle was clearly discernible. Another controversial topic has been the presence or absence of blood vessels in the articular disc: our results provided sufficient evidence to support the studies of Frommer (1964) and Van Der Linden (1987), who claimed a lack of blood vessels, contrary to Mah (2004), who observed them in the inferior band of the disc.

Ohshima et al. (2011) proposed two hypotheses regarding the formation of the joint cavities of the temporomandibular joint: the fissure hypothesis, when mechanical stimulation expands a fissure so the joint cavity is formed, and the apoptosis hypothesis concerning programmed cell death. He employed the TUNEL method and gave sufficient evidence to support the involvement of the last mechanism in the mouse joint cavity formation. However, the influence of movement in joint cavitation has been demonstrated (Murray & Drachman, 1969) and the opposite, namely immobilization, has shown the absence of joint cavities (Sperber, 1989). Also lubricin, the major component of the synovial fluid, has been suggested to play a key role in the very first steps of this process (Koyama et al., 2014). Joint cavitation is not synchronic, since the time of appearance varies depending on the species. In humans the inferior joint cavity forms first, followed by the superior joint cavity (around the 9th and 11th week of development, respectively) (Mérida Velasco et al., 1999), whereas in rats (Yamaki, 2005; Suzuki, 2005) and in mice (Ohshima et al., 2011; Gu et al., 2014; Liang et al., 2016), the superior precedes the inferior one. According to Frommer (1964), before cavitation starts, the number of vascular infiltrations increases in the area. The initiation of the cavitation between the glenoid fossa and the articular disc to form the superior joint cavity has been described by Nakanishi & Iwai-Liao (1990) at stage E15, and by Uemura-Sumi (1985) and Ohshima et al. (2011) at stage E16 and its completion two days later. Gu et al. (2014) and Liang et al. (2106) reported its first appearance at stage E16.5, and Frommer (1964) at stage E19. In the present research, the appearance of small spaces between the articular disc and glenoid fossa indicated the initial formation of the superior joint cavity at stage E18. The formation of the inferior joint cavity began as a narrow space between the condyle and the future articular disc. Nakanishi & Iwai-Liao (1990) reported this event between stages E17 and E20, and Gu et al. (2014) and Liang et al. (2016) at stage E17.5. Ohshima et al. (2011) described the beginning of the inferior joint cavity formation at stage E18,

and its completion one day later. Uemura-Sumi (1985) and Frommer (1964) identified the first formation of the cavity at stage E19, and the completion at stage P2. We reported it at stage E20. Tsuchikawa et al. (2010) concluded that all the major components of the joint were present as early as stage E16. However, Gu et al. (2014) identified them at stage E17.5, Liang et al. (2016) at stage E18.5, and Ohshima et al. (2011) at stage E19. Frommer (1964) described the complete formation of the joint at stage E20, although he could not identify the fibrous capsule at this time. He assumed that this structure was not as well developed in the mouse as it was in humans. We concluded that the total formation of the joint was also around stage E20 (Fig. 75). This finding supports the conclusion of Ohshima et al. (2011), who postulated that the temporomandibular joint of the mouse would be prepared for the jaw movements necessary for breast-feeding by the time of birth.

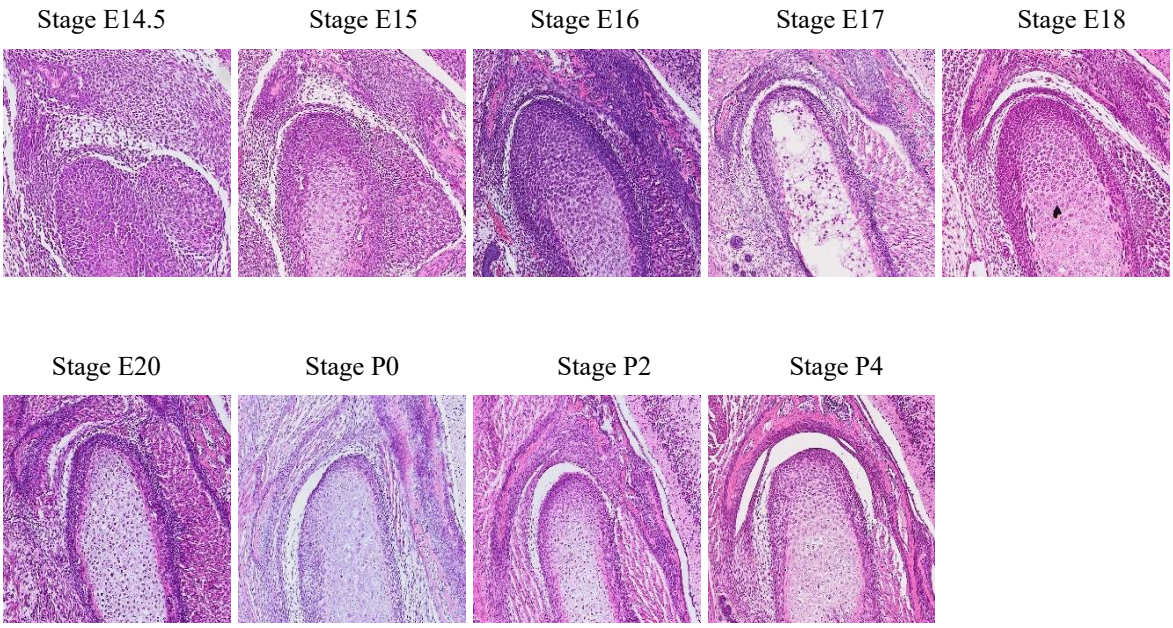

Fig. 75: Histological sections of some components of the temporomandibular joint of the mouse from stage E14.5 to stage P4.

Frontal plane, HE staining

Table 6: Summary of the results of the mouse temporomandibular joint chronology from other authors and comparison with our own results.

	Frommer (1964)	Shibata et al. (1996)	Gu et al. (2014)	Tsuchikawa et al. (2010)	Ohshima et al. (2011)	Liang et al. (2016)	Present study (2020)
Condylar blastema	E15	E13	E13.5	E12.75	E15	E13.5	E14.5
Temporal blastema	E16	E13	E14.5	E13	E14	E14.5	E14.5
Secondary condylar cartilage	No data	E15	E15.5	E14.5	No data	E15.5	E15
Anlage of the articular disc	E18	No data	E16.5	No data	E16	E15.5	E14.5
Superior joint cavity	E19	No data	E16.5	No data	E16	E16.5	E18
Inferior joint cavity	E19	No data	E17.5	No data	E18	E17.5	E20
Completion	E20	No data	E17.5	E16	E19	E18.5	E20

6.3.2.9 Bilaminar zone

The most posterior part of the temporomandibular joint is known as the bilaminar zone. The term "bilaminar" refers to the two layers that composed this zone with a genu vasculosum or intermediate layer in between. The superior layer consists of elastic and collagen fibers, which allow the anterior translation of the disc over the articular eminence. The inferior layer is formed by tight collagen, but few elastic fibers, to maintain the relationship with the condyle. The genu vasculosum contains numerous blood vessels, nerves, and adipose cells (Mérida Velasco et al., 2007). Although our histological methods did not allow the visualization of these two layers, they were evident in magnetic resonance studies (Haiter-Neto et al., 2002) and macroscopic examinations (Mérida Velasco et al., 2007). Contrarily, Kino et al. (1993) reconsidered the bilaminar zone based on histological sections and concluded that these layers did not exist.

The literature about the architecture of this zone is scarce, and publications are mainly focused on its alterations associated with disc displacement in humans as well as animals, mainly rabbits and rats. There does not appear to be any study that explicitly examines this region in the mouse.

The first identification of this bilaminar zone in our investigation was made at stage E14.5 in the vicinity of the parotid gland. It was composed of loose mesenchyme and few collagen fibers. Some vascular spaces, adipose tissue, the retromandibular vein and retroarticular artery, as well as the auriculotemporal nerve, were also detected. These results concerning the innervation agree with the findings in humans of Dixon (1962) and Siéssere et al. (2004). During the following stages the amount of mesenchymal tissue decreased, and the number of blood vessels and vascular spaces as well as the size of the vein increased. At postnatal stages this last structure almost occupied the entire bilaminar zone.

We wish to draw attention to the function of the bilaminar zone because even though it opposes the action of the lateral pterygoid, and therefore, it influences the retrusion of the mandible, it does not play an active role in moving the articular disc backwards, because in terms of traction it cannot compete with the tones of the muscle (Rizzolo & Madeira 2005; Siéssere et al., 2004).

6.3.2.10 Middle ear

The complex mammalian auditory system is divided into three main parts: the outer, middle, and inner ear (Fig. 76). Sound waves reach the outer ear and are transformed into vibrations at the tympanic membrane, and amplified by the middle ear ossicles. Later, they cross the oval window to the inner ear, specifically to the cochlea, where sound waves are converted into electromechanical signs that pass to the brain (Ankamreddy et al., 2019).

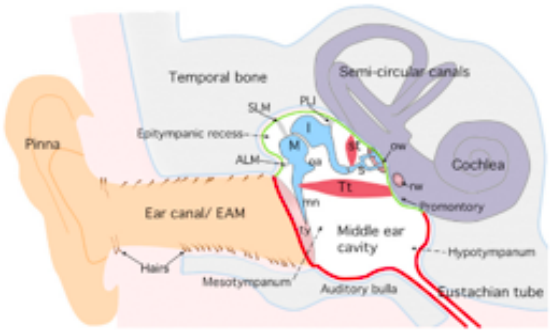

Fig. 76: Schematic representation of the ear, divided into three parts.

The outer ear includes the pinna and ear canal. The middle ear extends from the tympanic membrane to the stapes. The inner ear includes the semicircular canals, the cochlea and the oval window.

ALM: anterior ligament of the malleus, EAM: external auditory meatus, I: incus, M: malleus, mn: manubrium, oa: orbicular apophysis, PLI: posterior ligament of the malleus, rw: round window, s: stapes, SLM: superior ligament of the malleus, st: stapedius, Tb: tensor tympani.

Depiction obtained from Anthwal & Thompson (2016).

The formation of the middle ear ossicles starts when neural crest cells migrate into the pharyngeal arches. The major part of the malleus and the complete incus derive from the first pharyngeal arch, while the second pharyngeal arch is the precursor of the stapes. Malleus, incus and Meckel's cartilage appear as a single condensation, which in the case of the mouse, separates in postnatal stages due to the downregulation of cartilage markers and the upregulation of joint markers (Anthwal & Thompson, 2016; Ankamreddy et al., 2019). However, during prenatal development, cellular arrangements differ between the three components, reflecting the distinct axes of growth (Amin & Tucker, 2006). The three middle ear ossicles are anchored to the skull through the tympanic ring and the gonial bone, and they undergo endochondral ossification (Ankamreddy et al., 2019). Unlike the inner ear, which is almost completed at stage E19, the external and middle ear of the mouse are still very immature at birth. The first and the second branchial arches, from which the middle ear ossicles derive as explained before, could be observed at stage E11 (Nakanishi & Iwai-Liao, 1990), and the primordia of the three middle ear ossicles appeared between stages E12 (Masuda et al., 1986) and E13 (Miyake et al., 1996). Summarizing our results, we concluded that the three ossicles appeared as separate cartilaginous elements at stage E14.5, whereas the malleus comprised the posterior end of Meckel's cartilage. At stage 16 we also detected the incudomalleolar and incudostapedial joints. Next, we identified the first ossification center at P0 in the anterior process of the malleus, at P2 in the incus, and the stapes remained completely cartilaginous even at stage P4. The breakdown of Meckel's cartilage from the malleus takes place between stages P2 and P4, since at P4 we observed these elements as two separated structures (Fig. 77). We reported this event posterior to the mylohyoid groove, in a location where Meckel's cartilage had become thinner since early prenatal stages. Nakanishi & Iwai-Liao (1990) reported a great ossification of this area between stages P4 and P5, and at stage P6 they could only distinguish a thin layer of hyaline cartilage in the articular surfaces of the incudomalleolar and incudostapedial joints. These results are in accordance with those of Nishizaki & Anniko (1997), who reported the ossification of the malleus and incus at stage P5, but not of the stapes, which started at stage P7. At stage P12, the ossicles have almost reached adult size, and the mesenchymal tissue that surrounded the middle ear ossicles has been resorbed to form the tympanic cavity, according to Roberts and Miller (1998) and Anthwal and Thompson (2016).

The origin of the middle ear ossicles is usually cited as an example of evolutionary transformation (Urban et al., 2017), as explained in the introduction. In accordance, we confirm the coexistence of the primary and the secondary joints until stage P2. At stage P4, the

breakdown of Meckel's cartilage from the malleus has already occurred, and therefore only the temporomandibular joint remains (Göbel, 2020, in preparation).

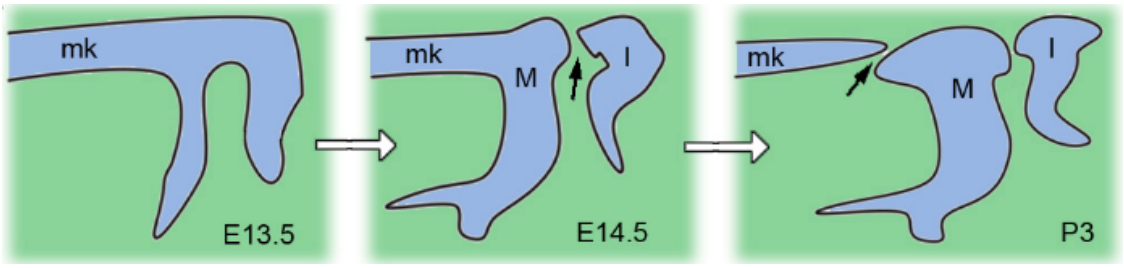

Fig. 77: Schematic representation of the separation of the malleus, incus and Meckel's cartilage at stages E13.5, E14.5 and P3.

Depiction obtained from Anthwal (2016).

Taking together our findings and those in the available literature, we have come across some anatomical and embryological differences between the human and mouse middle ear. Probably the most remarkable one is that while humans have a freely mobile middle ear, where the malleus is linked to the tympanic ring via a ligament, mice have a fixed malleus accompanied by a well-developed incudomalleolar joint (Nishizaki & Anniko, 1997). In addition, the stapedial artery persists through life in mice, but in humans is a vestigial structure (Anthwal & Thompson, 2016), and the external auditory meatus is closed at birth in the mouse, but already open in humans (Anthwal & Thompson, 2016). Moreover, the ossification of the middle ear ossicles in humans takes place in prenatal stages: first in the incus, followed by the malleus and the stapes (Scheuer & Black, 2000); whereas in mice ossification starts after birth first in the malleus, then in the incus and later in the stapes. A further morphological difference is the size of the murine incus in relation to the malleus, which is relatively smaller compared to humans. The size of the cochlea increased twice in mice, and two and a half times in humans, during development (Lee et al., 2009). Despite all these differences, mice are widely accepted as a model organism in middle ear studies (Louryan 1993).

6.3.3 Relevance of the lateral pterygoid in the study of the joint

The lateral pterygoid has been extensively studied from different approaches, owing to reasons that go from morphological singularities to clinical implications in temporomandibular joint disorders (Carranza et al., 2006). This muscle has been examined using anatomical, imaging and functional methods: the first, i.e. anatomical dissection, is a complicated task due to the deep location of the muscle in the infratemporal fossa. From a clinical point of view, computer tomography and magnetic resonance imaging are the most common diagnostic techniques. Finally, functional methods, like electromyographic examination, have also been employed (Stöckel et al., 2019). Resulting as a consequence of the examining method used, the lateral pterygoid has allowed for great variability when describing the number of bellies (Rajeshwari & Pushpa, 2015; Stöckle et al., 2019), their width (Rajeshwari & Pushpa, 2015), and their regions of insertion (Rajeshwari & Pushpa, 2015; Tapia Contreras et al., 2011). After Troiano (1967) detected a third head between the superior and the inferior and named it “the medial head”, many other authors have also described it. We highlight a recent systematic review by Stöckle et al. (2019) for the human lateral pterygoid, where the frequency of a single-headed muscle ranged between 7.7% and 26.7%, two heads between 61.4% and 91.1%, and three heads between 4.0% and 35.0%. The discrepancies regarding attachment mainly concerned the superior head (Tapia Contreras et al., 2011; Rajeshwari & Pushpa, 2015): it clearly arises from the greater wing and the lateral process of the sphenoid, and runs inferiorly and posteriorly to insert into the anteromedial aspect of the articular disc, with disparity in the percentage of the muscle inserted on it, and into the joint capsule and condyle (Tapia Contreras et al., 2011). In the present study, we have described the attachment of the lateral pterygoid at the anteromedial part of the articular disc, at the condylar process and at the neck of the mandible, but the three corresponding heads were morphologically not obvious.

Regarding the function, the lateral pterygoid is anyhow active during a great number of movements (jaw closure and opening, protrusion and retrusion, and ipsilateral and contralateral movements), either as an agonist or an antagonist. For a better comprehension of the different groups of muscles that take part in mastication, we have functionally classified them in Table 8.

Table 7: Main characteristics of the muscles involved in mastication.

Jaw-closing group muscles (masticatory muscles)	Masseter, temporalis, lateral pterygoid, and medial pterygoid Arise from the skull and insert into the mandible
Jaw-opening group muscles	Suprahyoid group: Mylohyoid, digastric, stylohyoid, and geniohyoid Arise from the mandible or the temporal bone and insert into the hyoid bone
	Infrahyoid group: Omohyoid, sternohyoid, thyrohyoid, and sternothyroid Arise from the sternum, scapula or thyroid cartilage and insert into the hyoid bone or the thyroid cartilage
Accessory muscles	Muscles of the floor of the mouth: Digastric, mylohyoid, geniohyoid, genioglossus Some facial muscles: Buccinator and orbicularis oris, among others

The relevance of the lateral pterygoid in adjacent structures during development should be also considered, since this muscle is an essential mediator of growth at the condylar cartilage. It has been demonstrated that the protrusion of the lateral pterygoid by intraoral orthodontic appliance (Mcnamara & Carlson, 1979), or by electrical stimulation (Kantomaa & Rönning, 1982), increases the thickness of the condylar cartilage. Conversely, forced retrusion (Petrovic et al., 1986) or loss of incisal function (Hinton & Carlson, 1986) has the opposite effect. Apart from that, its early insertion into human Meckel's cartilage also has an effect on primary joint movements (Wyganowska-Świątkowska et al., 2012), and therefore, Yamamoto et al. (2014b) affirmed that the lateral pterygoid contributes to jaw motion earlier than other muscles. Unlike in humans, only the mylohyoid could be observed attached at early prenatal stages (in particular at stage E16) to Meckel's cartilage in our specimens. Subsequently, some fibers were transposed from the cartilage to the developing mandible between stages E17 and E20, to finally attach only at the mandible from the newborn onwards.

In the same way that there is no consensus about some anatomical characteristics of the lateral pterygoid, the implication of this muscle in temporomandibular joint disorders has also been controversial for decades. Some authors (Murray et al., 2004; Rajeshwari & Pushpa, 2015) have found a causal relationship between joint dysfunctions and alterations in the lateral pterygoid,

since this has been considered the only true articular muscle (Carpentier et al., 1988). Conversely, other studies (Murray et al., 2004; Dergin et al., 2012) have reported that such scarce amounts of fibers go through the joint capsule and attach to the articular disc that they dismissed any correlation between the lateral pterygoid and clinical problems. In any case, there is a very close relationship during prenatal development between the lateral pterygoid and the articular disc, and some publications (Symons, 1952; Moffett, 1957) even recognize that the disc is derived from the muscle tendon. Moreover, it has been also suggested that the masseter and the temporalis attach to the anterolateral part of the disc in order to counteract the medial traction of the superior head of the lateral pterygoid during closing (Rees, 1954). However, there is no literature about the presence of a muscle in the posterior part of the disc that could prevent anterior displacements by pulling the articular disc back. Although functionally the existence of this "direct antagonist of the lateral pterygoid" could be seen as reasonable, one of the possible reasons of its lack has been explained in this study in terms of space availability.

6.3.4 Dynamics in muscle formation

Molecular analysis has demonstrated that signaling molecules are essential for tissue differentiation, but it cannot explain the morphological aspect involved in creating organic shape. Hence, it is assumed that molecules are mediators rather than creators of form, and that mechanical force of the neighboring tissues, which arise during physical cell and tissue interaction, play an essential role (Radlanski & Renz, 2006). This old approach of developmental mechanics traces back to the embryologists His (1874), Carey (1920a, 1920b, 1935) and Blechschmidt (1948, 1954), when they claimed that forces are essential in histogenesis and morphogenesis. The work of D'Arcy Thompson (1917) also reinforced this point of view, since his main thesis was that biological form was the consequence of physical processes and mechanical forces. The contributions of these authors and some others to the field of morphogenesis is the central point of this section.

His (1874) explained that mechanical forces exerted by tissues growing in a limited space were responsible for the form of the body. Later, Carey (1920a, 1920b, 1935) criticized the prevalent opinion among embryologists concerning the origin of muscular tissue. Whereas they asserted it was on self-differentiation without taking the environment into consideration, he explained that embryological development presents zones of unequal or differential growth, and he illustrated the cellular forces outside the differentiating zone. When it comes to muscle tissue, the tensional stress in the mesenchyme as a result of forces extrinsic to the zone of myogenesis was essential. The work of Blechschmidt (1948, 1954) was based on a major collection of accurate 3D

reconstructions of human embryos at different stages of development that are still on display in Göttingen (Germany). He explained the morphogenesis of the human body as a closed system with living cells as the active part, and biological, chemical and physical laws as the rules. His biomechanical and biodynamical approach introduces the ideas of developmental movements, growth forces, and metabolic field. He describes the latter as a region of cells with similar shape and metabolism that arise at a particular moment and are placed under unique biodynamic circumstances. Inside, spatially ordered metabolic movements take place, giving rise to cartilage in relation to pressure (densation field), to bone in relation to shearing forces (detraction field), and to muscle in relation to dilation forces (dilation field) (Blechschmidt, 1948, 2004). Blechschmidt illustrated the correlation between muscle fiber direction and the developmental movements of the underlying skeletal components with numerous examples: the direction and extension of the muscles responsible for eye motility and the expansion of the growing eyeball; the direction of the sternocleidomastoid muscles which reflects the growth of the cervical spine; the arm and leg muscles that run in an superior-inferior direction like the main bones underneath; the autochthonous muscles of the vertebrae that reflect the vertical, transverse and oblique expansion of each vertebra; and the trapezius muscle that shows the lateromedial expansion of the shoulder and the superior-inferior expansion of the upper vertebral column. He also illustrated the orientation of the masticatory muscles which reflects the growth vectors of the enlarging skull (Fig. 78.) (Blechschmidt, 1948, 2004).

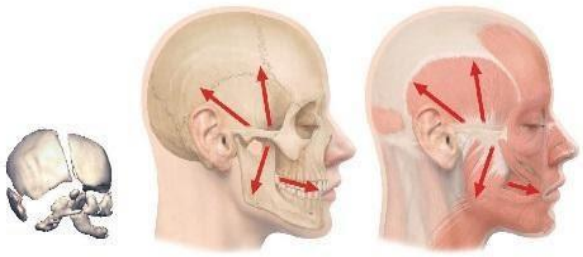

a **b** **c**

Fig. 78: Main vectors of growth of the skeletal elements are at the same time the main vectors of muscle fiber orientation.

The direction of the masticatory muscles fibers (arrows in **c**) matches the direction of growth of the skull (arrows in **b**) in the fetal cranium (**a**).

Depiction obtained from Radlanski (2018), modified after Blechschmidt (2004).

The formation of muscle tissue in dilation fields has been studied more recently by other authors like Goldspink (1999) and Radlanski et al., (2001). The former showed that the stretch of

mesenchymal tissue was an important mechanical sign that leads to formation of musculature by producing more actin and myosin filaments. The latter made evident the direction of muscles fibers of the floor of the mouth during early prenatal stages by performing 3D reconstructions, and he correlated the arrangement of these muscles with changes in form and size of the developing mandible.

Following the principle that mechanical stimulus plays a fundamental role in tissue differentiation and morphogenesis, we have also created 3D reconstructions in order to elucidate the exact timing and location of the regions where these forces take place during muscle formation. We have also gained knowledge about the process of development, growth, changes in proportions, spatial arrangement and relations with the surrounding structures. It is evident that the orientation of the fibers of the masticatory muscles reflects the direction of the growing underlying skeletal elements, in this case the mandible and the cranium. Using some fiducial landmarks, we could also corroborate Blechschmidt's principle of muscle differentiation: the region of the mandible anterior to the temporomandibular joint, where the masticatory muscles are situated, increased sixfold in size from stage E14.5 to stage P4. However, the region posterior to the temporomandibular joint, where we do not observe any muscle formation, but instead the bilaminar zone, increased twofold in size in the same period of development. Therefore, this observation provides strong evidence for the concept of Erich Blechschmidt that muscles form from mesenchymal tissue, which is dilated under the direct mechanical forces of the developing skull. This detailed information may help to bridge the gap between classic developmental mechanics and contemporary molecular biology and how they both lead to tissue differentiation.

D'Arcy Thompson (1860-1948) demonstrated in his highly cited book *On Growth and Form* (1917) that the shapes of related animals, or parts of them, could be transformed into each other by means of a simple graphic procedure, called the method of coordinates (Nieuwenhuys, 2009). This consists on a Cartesian coordinate grid projected onto the outline of an entire organ or organism. Next, the grid is submitted to some simple mathematical transformation, such as stretching or distorting, to produce the shape of another related organ or organism. The book was illustrated with the shape of many hand-drawn images, such as cells, tissues, shells, teeth, and bones (Wallace Arthur, 2006). The approach of D'Arcy Thompson has been criticized for oversimplification, and for a lack of causal explanation from a genetic and developmental point of view (Briscoe & Kicheva, 2017). Another limitation is that all forms shown in the book are from adult organisms (Wallace Arthur, 2006). However, his work has had, and continues to have, an enormous influence, and also beyond the biological community (Briscoe & Kicheva,

2017). In the last few years, modern computer image processing methods equivalent to coordinate transformation have been applied to understand facial configuration and shape in clinical genetics (DiLiberti, 1991), to analyze the structure of the brain stem of mammals (Nieuwenhuys, 2009), and to investigate the patterning and growth of the neural tube (Briscoe & Kicheva, 2017). The depictions obtained were more sophisticated and more complex than those of Thompson. Following this goal, we created detailed three-dimensional graphical reconstructions that accurately characterize the formation and development of the murine temporomandibular joint and its surrounding structures. This precise representation allows us to improve on the over-smoothly geometrical and even too idealistic drawings of Thompson. Apart from that, we should emphasize that our reconstructions have been performed only on one species, i.e. *Mus musculus*, whereas Thompson described changes between homologous structures in different species.

6.3.5 Muscle-bone interactions

Muscle and bone are linked genetically, molecularly, and mechanically. The close relationship between them already starts during embryonic development by sharing a common mesenchymal precursor, since both are formed from somites from the paraxial mesoderm, and it continues with similar genetic factors during organogenesis. Because the main function of the musculoskeletal system, which also includes tendons, ligaments, cartilage, joints and other connective tissues, is locomotion, this tight interdependence stretches on lifelong (Brotto & Bonewald, 2015).

It is accepted that the main interaction between muscles and bones is through mechanical stimuli from the muscles, which either have an active (weight-bearing load) or a passive (static load, i.e. the presence of muscular tissue alone) role in bone formation (Herring & Lakars, 1982; Hall, 2001). As early as 1947, Washburn identified three classes of morphological features in the skull that depend on muscle action: those that arose only in the presence of musculature (e.g. the temporal and mylohyoid lines), the self-differentiating structures that required the presence of muscle to maintain them (e.g. the coronoid process), and those which were independent of muscle presence (e.g. in the brain's case). Based on this classification, Avis (1959, 1961) confirmed that the coronoid and angular processes belonged to the second group, because they were self-differentiated, but needed the temporalis and masseter to maintain them, respectively. However, Spyropoulos (1977) examined human embryos and fetuses and concluded that the temporalis primordium appeared before the precursor of the coronoid process. This merited the further suggestion that the differentiation of this bony process was not self-differentiating but depended on muscular activity of the temporalis. Recently, the dependence of bone

development, in particular of the mandible, upon muscle has been studied in large part using double knock-out mice and *exo utero* surgery. Rot-Nikcevic et al. (2007) showed the abnormalities of the mandible in amyogenic mice and concluded that the posterior muscle attachment areas of the mandible were more affected than the tooth-bearing regions. The condyle was slender and some large ligaments had arisen to compensate the lack of musculature, while the coronoid process was significantly reduced in size, and the angular process was even absent. Their results led to the following conclusions. Firstly, the condylar process, apart from being an attachment site, was also part of the temporomandibular joint and thus received additional mechanical stimuli. Secondly, the embryonic origin and gene pattern played an essential role in the maintenance of the coronoid process. Thirdly, the angular process was the most dependent upon local muscle action (Hall, 2005). Habib et al. (2005, 2007) performed *exo utero* surgery in mice at stage E18.5 by fixing the mandible and the maxilla in order to restrict the fetal jaw movement, observing changes in the articular disc (shape, arrangement and volume of the mesenchymal cells changed), in the temporal bone, and in condylar cartilage development. Jahan et al. (2010) obtained similar results using the same technique and concluded that the mechanical stress caused by intrauterine jaw movement is an important factor, not only in muscle development, but also in the formation of the condyle and the articular disc, as such mechanical stimulation acts directly on cells.

As mentioned at the beginning of this section, bones and muscle cells communicate at biochemical and molecular levels beyond and complementary to mechanical interactions (Brotto & Bonewald, 2015). Back in 1955, Baume affirmed that muscles had an osteogenic effect due to a bone-forming organ rather than as part of their functioning. However, it was only at the end of the 1990s that skeletal muscles were recognized for their significant secretory capacity. Pedersen and colleagues (quoted after Brotto & Bonewald, 2015) were the first research group to use the term ‘myokines,’ and since then, several muscle secreted factors have been described.

In terms of our investigation, at stage 13.5 we identified the muscle primordium of the masseter and the first ossification centers of the mandible, but there was no attachment between them. However, only 24 hours later, at stage E14.5 all masticatory muscles and all parts of the mandible could be observed, and the very close proximity, which morphologically suggests a real attachment as good as histological sections, could be revealed. This information could be useful for future studies in the area of mechanical, molecular and genetic interactions between muscle and bone. This field of study is a popular area of research nowadays, due to the clinical significance of musculoskeletal diseases that have become more frequent in an increasingly aging population.

6.4 Conclusion and future perspectives

This work shows for the first time some complex aspects of murine craniofacial development.
Firstly, we have accurately characterized the morphogenesis of the temporomandibular joint, some selected structures, and the masticatory muscles, not only with descriptions but also with depictions. Therefore, our study provides a reference and educational resource for scientists, students and clinicians. The focus on the chronology is important in this investigation, and we thus conclude that one of the greatest turning points in murine craniofacial development occurs between stages E13.25 and E13.5, since many structures form within these 6 hours. After that, the time interval between specimens in our investigation was one or two days. For this reason, in further investigations, we see the necessity to additionally observe changes in craniofacial morphogenesis at every half or quarter day during the very early stages of development.
Secondly, we have performed morphometric studies to evaluate the hypothesis of Blechschmidt regarding muscle formation. Therefore, we consider that a molecular study using both morphometric and myogenetic markers would be meaningful.
Finally, we also conclude that although the recent expansion of molecular genetic technology has brought with it an improved knowledge of the regulatory mechanisms that control embryological development, understanding and updating the complex morphogenesis itself is crucial to extrapolate information from animal models to better understand normal and abnormal development in humans.

7 BIBLIOGRAPHY

1. Abe S, Hiroki E, Iwanuma O, Sakiyama K, Shirakura Y, Hirose D, Shimoo Y, Suzuki M, Ikari Y, Kikuchi R, Ide Y, Yoshinari M. Relationship between function of masticatory muscle in mouse and properties of muscle fibers. Bull Tokyo Dent Coll 2008;49(2):53-58.
2. Amin S, Tucker AS. Joint formation in the middle ear: Lessons from the mouse and guinea pig. Dev Dyn 2006;235(5):1326-1333.
3. Ankamreddy H, Min H, Kim JY, Yang X, Cho ES, Kim UK, Bok J. Region-specific endodermal signals direct neural crest cells to form the three middle ear ossicles. Development 2019;146(2) doi: 10.1242/dev.167965.
4. Anthwal N, Joshi L, Tucker AS. Evolution of the mammalian middle ear and jaw: Adaptations and novel structures. J Anat 2013;222(1):147-160.
5. Anthwal N, Peters H, Tucker AS. Species-specific modifications of mandible shape reveal independent mechanism for growth and initiation of the coronoid. Anthwal et al. EvoDevo 2015;6:35 doi: 10.1186/s13227-015-0030-6.
6. Anthwal N, Thompson H. The development of the mammalian outer and middle ear. J Anat 2016;228(2):217-232.
7. Arthur W. D'Arcy Thompson and the theory of transformations. Nat Rev Genet 2006;7(5):401-406.
8. Arthur W. D'Arcy Thompson and the theory of transformations. Nat Rev Genet. 2006;7(5):401-406.
9. Avis V. The relation of the temporal muscle to the form of the coronoid process. Am J Phys Anthropol 1959;17(2):99-104.
10. Avis V. The significance of the angle of the mandible: an experimental and comparative study. Am J Phys Anthropol. 1961;19(1):55-61.
11. Baume LJ, Holz J. Ontogenesis of the human temporomandibular joint. 2. Development of the temporal components. J Dent Res 1970;49(4):864-875.
12. Baume LJ. Muscle insertion and bone growth; its significance in functional orthodontics. SSO Schweiz Monatsschr Zahnheilkd 1955;65(1):18-27.
13. Baume LJ. Ontogenesis of the human temporomandibular joint. I. Development of the condyles. J Dent Res 1962;41:1327-1339.
14. Baverstock H, Jeffery NS, Cobb SN. The morphology of the mouse masticatory musculature. J Anat 2013;223(1):46-60.

15. Benigno MI, Azeredo RA, Lemos JL, König Júnior B, Liberti EA. The structure of the bilaminar zone in the human temporomandibular joint: a light and scanning electron microscopy study in young and elderly subjects. J Oral Rehabil 2001;28(2):113-119.
16. Bernick S. The vascular and nerve supply to the temporomandibular joint of the rat. Oral Surg Oral Med Oral Pathol 1962;15:488-498.
17. Bernuy NE. Morphological Differences of the Articulating Surfaces of Mandibular Condyles in C3H/HeJ and A/J Mice. Diss. Chapel Hill, 2013.
18. Bhaskar SN, Weinmann JP, Schour I. Role of Meckel's cartilage in the development and growth of the rat mandible. J Dent Res 1953;32(3):398-410.
19. Blechschmidt E. Der menschliche Embryo: Dokumentationen zur kinetischen Anatomie. The human embryo: documentation on kinetic anatomy. Stuttgart: Friedrich-Karl Schattauer-Verlag, 1963.
20. Blechschmidt E. Mechanische Genwirkungen Funktionsentwicklung I. Göttingen: Musterschmidt, 1948.
21. Blechschmidt E. Rekonstruktionsverfahren mit Verwendung von Kunststoffen. Ein Verfahren zur Ermittlung und Demonstration von Entwicklungsbewegungen. Z Anat Entwicklungsgesch 1954;118(2):170-174.
22. Blechschmidt E. The ontogenetic basis of human anatomy: a biodynamic approach to development from conception to adulthood. Freeman B, editor. Berkeley, CA: North Atlantic Books, 2004.
23. Born GJ. Die Plattenmodellier-Methode. Archiv für Mikroskopische Anatomie 1883;22(1):584-599.
24. Briscoe J, Kicheva A. The physics of development 100 years after D'Arcy Thompson's "On Growth and Form". Mech Dev 2017;145:26-31.
25. Brotto M, Bonewald L. Bone and muscle: Interactions beyond mechanical. Bone. 2015;80:109-114.
26. Byrd KE. Mandibular movement and muscle activity during mastication in the guinea pig (Cavia porcellus). J Morphol 1981;170:147-169.
27. Carey EJ. Studies in the dynamics of histogenesis : I. Tension of differential growth as a stimulus to myogenesis. J Gen Physiol. 1920a;2(4):357-372.
28. Carey EJ. Studies in the dynamics of histogenesis: II. Tension of differential growth as a stimulus to myogenesis in the esophagus. J Gen Physiol 1920b;3(1):61-83.

29. Carey EJ. Studies in the wave-mechanics of muscle form and function: II. The experimental biophysics of the external form and internal structure of cro-striated muscle and tendon. Anat Rec 1935;61:69.
30. Carpentier P, Yung JP, Marguelles-Bonnet R, Meunissier M. Insertions of the lateral pterygoid muscle: an anatomic study of the human temporomandibular joint. J Oral Maxillofac Surg 1988;46(6):477-482.
31. Carranza ML, Carda C, Simbrón A, Quevedo MC, Celaya G, de Ferraris ME. Morphology of the lateral pterygoid muscle associated to the mandibular condyle in the human prenatal stage. Acta Odontl Latinoam 2006;19(1):29-36.
32. Chai Y, Maxson Jr RE. Recent advances in craniofacial morphogenesis. Dev Dyn 2006;235(9):2353-2375.
33. Chappard D, Kün-Darbois JD, Mercier P, Guillaume B, Aguado E. Microcomputed tomography (microCT) and histology of the mandibular canal in human and laboratory animals. Morphologie 2018;102(339):263-275.
34. Chiego DJ Jr. The early distribution and possible role of nerves during odontogenesis. Int J Dev Biol 1995;39(1):191-194.
35. Cox PG, Jeffery N. Reviewing the morphology of the jaw-closing musculature in squirrels, rats, and guinea pigs with contrast-enhanced micro CT. Anatomical Rec (Hoboken) 2011;294(6):915-928.
36. Crompton AW. On the lower jaw of Diarthrognathus and the origin of the mammalian lower jaw. Proc Zool Soc London 1986;140:697-753.
37. Das SM. Studies of musculature of *Funambulus palmarum tristirtus.* J Zool Soc India 1955;7:57-82.
38. Davies AM. The trigeminal system: an advantageous experimental model for studying neuronal development. Development 1988;103(Suppl):175-183.
39. de Bakker BS, de Jong KH, Hagoort J, de Bree K, Besselink CT, de Kanter FE, Veldhuis T, Bais B, Schildmeijer R, Ruijter JM, Oostra RJ, Christoffels VM, Moorman AF. An interactive three-dimensional digital atlas and quantitative database of human development. Science. 2016;25;354(6315) doi: 10.1126/science.aag0053.
40. Dechow PC, Wang Q. Development, structure, and function of the zygomatic bones: What is new and why do we care? Anat Rec (Hoboken) 2016;299(12):1611-1615.
41. Dechow PC, Wang Q. Evolution of the jugal/zygomatic bones. Anat Rec (Hoboken) 2017;300(1):12-15.

42. Dergin G, Kilic C, Gozneli R, Yildirim D, Garip H, Moroglu S. Evaluating the correlation between the lateral pterygoid muscle attachment type and internal derangement of the temporomandibular joint with an emphasis on MR imaging findings. J Craniomaxillofac Surg 2012;40(5):459-463.
43. DiLiberti JH. Application of D'Arcy Thompson's coordinate transformation approach to clinical genetics photographs using image processing techniques. J Med Genet 1991;28(7):472-476.
44. Dixon AD. Structure and functional significance of the intra-articular disk of the human temporomandibular joint. Oral Surg Oral Med Oral Pathol 1962;15:48-61.
45. Domon M, Kurabayashi T. Postnatal development of the duct system in the mouse parotid gland. Anat Rec 1987;217(4):391-394.
46. Druzinsky RE, Doherty AH, De Vree FL. Mammalian masticatory muscles: homology, nomenclature, and diversification. Integr Comp Biol 2011;51(2):224-234.
47. DuBrul EL. Sicher and DuBrul's Oral Anatomy. Saint Louis: Ishiyaku EuroAmerica, 1988.
48. Duterloo HS, Jansen HW. Chondrogenesis and osteogenesis in the mandibular condylar blastema. Rep Congr Eur Orthod Soc 1969:109-118.
49. Fawcett E. Notes of the development of human sphenoid. J Anat Physiol 1910;44(3):207-222.
50. Frommer J, Margolies MR. Contribution of Meckel's cartilage to ossification of the mandible in mice. J Dent Res 1971;50(5):1260-1267.
51. Frommer J. Prenatal development of the mandibular joint in mice. Anat Rec 1964;150:449-462.
52. Garg A, Zhang X. Lacrimal gland development: From signaling interactions to regenerative medicine. Dev Dyn 2017;246(12):970-980.
53. Gaunt WA & Gaunt PN. Three-dimensional reconstruction in biology. London: Pitman Medical Publications, 1978.
54. Gaupp E. Die Reichertsche Theorie (Hammer-, Amboss-, und Kieferfrage). Arch Anat Physiol Suppl 1912:1-416.
55. Ginot S, Claude J, Hautier L. One skull to rule them all? Descriptive and comparative anatomy of the masticatory apparatus in five mouse species. J Morphol 2018;279(9)1234-1255.
56. Göbel Marlene. Das gleichzeitige Vorhandensein von primärem und sekundärem Kiefergelenk bei der Maus. Diss-Charité Universitätsmedizin Berlin, 2020, in preparation.

57. Goldspink G. Changes in muscle mass and phenotype and the expression of autocrine and systemic growth factors by muscle in response to stretch and overload. J Anat 1999;194(3):323-334.
58. Gu S, Wei N, Yu L, Fei J, Chen Y. Shox2-deficiency leads to dysplasia and ankylosis of the temporomandibular joint in mice. Mech Dev 2008;125(8):729-742.
59. Gu S, Wu W, Liu C, Yang L, Sun C, Ye W, Li X, Chen J, LONG F, Chen Y. BMPRIA mediated signaling is essential for temporomandibular joint development in mice. PLoS One. 2014;9(8):e101000.
60. Habib H, Hatta T, Rahman OI, Yoshimura Y, Otani H. Fetal jaw movement affects development of articular disk in the temporomandibular joint. Congenit Anom (Kyoto). 2007;47(2):53-57.
61. Habib H, Hatta T, Udagawa J, Zhang L, Yoshimura Y, Otani H. Fetal jaw movement affects condylar cartilage development. J Dent Res 2005;84(5):474-479.
62. Haiter-Neto F1, Hollender L, Barclay P, Maravilla KR. Disk position and the bilaminar zone of the temporomandibular joint in asymptomatic young individuals by magnetic resonance imaging. Oral Surg Oral Med Oral Pathol Oral Radiol Endod 2002;94(3):372-378.
63. Hall BK. Bones and cartilage: Development and evolutionary skeletal biology. Amsterdam: Elsevier, 2005.
64. Hall BK. Development of clavicles in birds and mammals. J Exp Zool 2001;15:153-161.
65. Hallgrímsson B, Lieberman DE. Mouse models and the evolutionary developmental biology of the skull. Integr Comp Biol 2008;48(3):373-384.
66. Harada Y, Ishizeki K. Evidence for transformation of chondrocytes and site-specific resorption during the degeneration of Meckel's cartilage. Anat Embryol (Berl)1998;197(6):439-450.
67. Hautier L, Saksiri S. Masticatory muscle architecture in the Laotian rock rat Laonastes aenigmamus (Mammalia, Rodentia): new insights into the evolution of hystricognathy. J Anat 2009;215(4):401-410.
68. Herring SW, Lakars TC. Craniofacial development in the absence of muscle contraction. J Craniofac Genet Dev Biol 1982;1(4):341-357.
69. Herring SW, Liu ZJ.Loading of the temporomandibular joint: anatomical and in vivo evidence from the bones. Cells Tissues Organs 2001;169(3):193-200.
70. Herring SW. Masticatory muscles and the skull: a comparative perspective. Arch Oral Biol 2007;52(4):296-299.

71. Herring SW. TMJ anatomy and animal models. J Musculoskelet Neuronal Interact 2003;3(4):391-394.
72. Hiiemae K, Houston WJB. The structure and function of jaw muscles in rat (*Rattus morvegicus* L.). Zool J Linn Soc 1971;50:75-99.
73. Hiiemae K. Masticatory function in the mammals. J Dent Res 1967;46:883-893.
74. Hinton RJ, Carlson DS. Response of the mandibular joint to loss of incisal function in the rat. Acta Anat (Basel) 1986;125(3):145-151.
75. Hirouchi H, Kitamura K, Yamamoto M, Odaka K, Matsunaga S, Sakiyama K, Abe S. Development characteristics of secondary cartilage in the mandibular condyle and sphenoid bone in mice. Arch Oral Biol 2018;89:84-92.
76. His W. Unsere Körperform und das physiologische Problem ihrer Entstehung. Leipzig: FCW Vogel, 1874.
77. Howell AB. Anatomy of the wood rat. Baltimore: Williams and Wilkins Co, 1926.
78. Hsu JC, Yamada KM. Salivary Gland Branching Morphogenesis – Recent Progress and Future Opportunities. Int J Oral Sci 2010; 2(3): 117–126.
79. Hwang K, Lee DK, Kim HJ, Shin YH, Chung IH. Zygomaticomandibularis muscle. J Craniofac Surg 2005;16(4):655-657.
80. IFAA (International Federation of Associations of Anatomists). Terminologia Anatomica. Kapstadt: 1998. TE PrePublication, 2010: accessed May 2014 at: http://www.unifr.ch/ifaa/
81. Ishizeki K, Saito H, Shinagawa T, Fujiwara N, Nawa T. Histochemical and immunohistochemical analysis of the mechanism of calcification of Meckel's cartilage during mandible development in rodents. J Anat 1999;194(2):265-277.
82. Jahan E, Matsumoto A, Udagawa J, Rafiq AM, Hashimoto R, Rahman OI, Habib H, Skine J, Otani H. Effects of restriction of fetal jaw movement on prenatal development of the temporalis muscles. Arch Oral Biol 2010;55(11):919-927.
83. Kantomaa T, Rönning O.The effect of electrical stimulation of the lateral pterygoid muscle on the growth of the mandible in the rat. Proc Finn Dent Soc 1982;78(5-6):215-219.
84. Kaufmann MH. Atlas of Mouse Development. New York: Academic Press, 1994.
85. Kelly RG. Core issues in craniofacial myogenesis. Exp Cell Ress 2010;316(18):3034-3041.
86. Kermack KA. The origin of mammals and the evolution of the temporomandibular joint. Proc R Soc Med 1972;65(4):389-392.

87. Kim HJ, Park KM, Tak HJ, Choi JW, Kang SH, Park W, Bertin H, Corre P, Lee SH. Skeletal unit construction of rat mandible based on the masticatory muscle anatomy and double microcomputed tomography. Anat Histol Embryol. 2018;47(5):417-427.
88. Kino K, Ohmura Y, Amagasa T. Reconsideration of the bilaminar zone in the retrodiscal area of the temporomandibular joint. Oral Surg Oral Med Oral Pathol 1993;75(4):410-421.
89. Kishi A, Yamamoto M, Kikuchi A, Iwanuma O, Watanabe Y, Ide Y, Abe S. Gene and protein expressions of vimentin and desmin during embryonic development of the mylohyoid muscle. Anat Sci Int 2012;87:126-131.
90. Kokot, Karolin. Zur Entwicklung des Ligamentum sphenomandilare bei der Maus. Histologische und morphologische Untersuchungen des Ligamentum sphenomandilare bei aberrantem Verlauf aus dem meckelschen Knorpel in den Stadien E13,25-P10. Diss Charité-Universitätsmedizin Berlin, 2020, in preparation.
91. Koyama E, Saunders C, Salhab I, Decker RS, Chen I, Um H, Pacifici M, Nah HD. Lubricin is Required for the Structural Integrity and Post-natal Maintenance of TMJ. J Dent Res 2014;93(7):663-670.
92. Lee JH, Park K, Kang TC, Choung YH. Three-dimensional anatomy of the temporal bone in normal mice. Anat Histol Embryo 2009;38(4):311-315.
93. Leonardi R, Rusu MC, Loreto F, Loreto C, Musumeci G. Immunolocalization and expression of lubricin in the bilaminar zone of the human temporomandibular joint. Acta Histochem 2012;114(1):1-5.
94. Liang W, Li Xihai, Gao B, Gan H, Lin X, Liao L, Li C. Observing the development of the temporomandibular joint in embryonic and post-natal mice using various staining methods. Exp and Ther Med 2016;11(2):481-489.
95. Louryan S. Development of the auditory ossicles in the human embryo: correlations with data obtained in mice. Bull Assoc Anat (Nancy) 1993;77(236):29-32.
96. Low A. Further observations on the ossification of the human lower jaw. J Anat Physiol 1909;44(1):83-95.
97. Mah, J. Histochemistry of the foetal human temporomandibular joint articular disc. Eur J Orthod 2004;26(4):359-365.
98. Márquez S, Pagano AS, Schwartz JH, Curtis A, Delman BN, Lawson W, Laitman JT. Toward Understanding the Mammalian Zygoma: Insights From Comparative Anatomy, Growth and Development, and Morphometric Analysis. Anat Rec (Hoboken) 2017;300(1):76-151.

99. Masuda Y, Honjo H, Naito M, Ogura Y. Normal development of the middle ear in the mouse: a light microscopic study of serial sections. Acta Med Okayama 1986;40(4):201-207.
100. Matsunaga K, Usui A, Yamaguchi K, Akita K An anatomical study of the muscles that attach to the articular disc of the temporomandibular joint. Clin Anat 2009;22(8):932-940.
101. Mattiske D, Sommer P, Kidson SH, Hogan BLM. The role of the forkhead transcription factor, Foxc1, in the development of the mouse lacrimal gland. Dev Dyn 2006; 235(4): 1074–1080.
102. McNamara JA Jr, Carlson DS.Quantitative analysis of temporomandibular joint adaptations to protrusive function. Am J Orthod 1979;76(6):593-611.
103. Mérida Velasco JR, Rodríguez JF, De la Cuadra C, Mérida JA, Sánchez I. The posterior segment of the temporomandibular joint capsule and its anatomic relationship. J Oral Maxillofac Surg 2007;65(1):30-33.
104. Mérida Velasco, JR, Rodríguez Vázquez JF, Mérida Velasco JA, Sánchez Montesinos I, Espín Ferra J, Jiménez Collado J. Development of the human temporomandibular joint. Anat Rec 1999;255(1):20-33.
105. Miyake T, Cameron AM, Hall BK. Detailed staging of inbred C57BL/6 mice between Theiler´s (1972) stages 18 and 21 (11-13 days of gestation) based on craniofacial development. J Craniofac Genet Dev Bio 1996;16(1):1-31.
106. Moffett BC. The prenatal development of the human temporomandibular joint. In: Contributions to embryology, 243(36). Washington, D.C; Carnegie Instn. Wash. Publ. 1957.
107. Mulisch M & Welsch U. Romeis Mikroskopische Technik. Heidelberg: Spektrum Akademischer Verlag, 2010.
108. Murakami K, Hoshino K. Regional anatomical nomenclature and arthroscopic terminology in human temporomandibular joints. Okajimas Folia Anat Jpn 1982;58(4-6):745-760.
109. Murray GM, Phanachet I, Uchida S, Whittle T. The human lateral pterygoid muscle: a review of some experimental aspects and possible clinical relevance. Aust Dent J 2004;49(1):2-8.
110. Murray PD, Drachman DB. The role of movement in the development of joints and related structures: the head and neck in the chick embryo. J Embryol Exp Morphol 1969;22(3):349-371.

111. Nagata M, Ohashi Y, Ozawa H. A histochemical study of the development of premaxilla and maxilla during secondary palate formation in the mouse embryo. Arch Histol Cytol 1991;54(3):267-278.
112. Nakanishi T, Iwai-Liao Y. Comparative histological contributions to the development of the ear-ossicular joints and the temporomandibular joint in the mouse. Okajimas Folia Anat Jpn 1990;67(5):381-391.
113. Nanci A und Ten Cate AR. Ten Cate's Oral Histology: Development, Structure, and Function. 9th ed. St. Louis: Elsevier, 2017.
114. Nieuwenhuys R. Analysis of the structure of the brain stem of mammals by means of a modified D'Arcy Thompson procedure. Brain Struct Funct 2009;214(1):79-85.
115. Nishizaki K, Anniko M. Developmental morphology of the middle ear. Auris Nasus Larynx 1997;24(1):31-38.
116. Noden DM (1991) Cell movements and control of patterned tissue assembly during craniofacial development. J Craniofac Genet Dev Biol 1991;11:192-213.
117. Noden DM, Francis-West P. The differentiation and morphogenesis of craniofacial muscles. Dev Dyn 2006;235(5):1194-1218.
118. Nowak I. Zur Entwicklung des Desmodonts im Zusammenhang mit dem peridentalen Knochen. Histologische und morphologische Untersuchungen der Molarenregion der Maus in den postnatalen Stadien P8-P40. Diss. Charité – Universitätsmedizin, 2016.
119. Oğütcen-Toller M, Keskin M. Computerized 3-dimensional study of the embryologic development of the human masticatory muscles and temporomandibular joint. J Oral Maxillofac Surg 2000;58(12):1381-1386.
120. Ohshima T, Yonezu H, Nishibori Y, Uchiyama T, Shibahara T. Morphological observation of process of mouse temporomandibular joint formation. Bull Tokyo Dent Coll 2011;52(4):183-190.
121. Pan Y, Carbe C, Powers A, Feng G-S, Zhang X. Sprouty2-modulated Kras signaling rescues Shp2 deficiency during lens and lacrimal gland development. Development 2010;137(7):1085–1093.
122. Patel NG. Functional morphology of the masticatory muscles of *Mus musculus.* Proc Indian Acad 1978;5:1-7.
123. Pedersen BK. Muscle as a secretory organ. Compr Physiol 2013; 3(3):1337–1362. Quoted after Brotto 2015.
124. Petrovic AG, Stuzman J, Oudet C. Control processes in the postnatal growth of the condylar cartilage of the mandible. In: McNamara JA (ed) Determinants of mandibular

form and growth. Monograph No. 4. Center for human growth and development, University of Michigan. Ann Arbor.

125. Piette E, Lametschwandtner A. The angioarchitecture of the rat mandibular joint bilaminar zone. Archives of Oral Biology 1995;40(6):499-505.
126. Pirlot P. Morfología evolutiva de los cordados. Barcelona: Ediciones Omega, 1976.
127. Purcell P, Joo BW, Hu JK, Tran PV, Calicchio ML, O'Connell DJ, Maas RL, Tabin CJ. Temporomandibular joint formation requires two distinct hedgehog-dependent steps. Proc Natl Acad Sci USA 2009;106(43)18297-18302.
128. Radlanski R, Renz H, Tabatabai A. Prenatal development of the muscles in the floor of the mouth in human embryos and fetuses from 6.9 to 76 mm CRL. Ann Anat 2001;183(6):511-518.
129. Radlanski RJ, Renz H, Klarkowski MC. Prenatal development of the human mandible. 3D reconstructions, morphometry and bone remodelling pattern, sizes 12-117 mm CRL. Anat Embryol (Berl) 2003;207(3):221-32.
130. Radlanski RJ, Renz H, Tsengelsaikhan N, Schuster F, Zimmermann CA. The remodeling pattern of human mandibular alveolar bone during prenatal formation from 19 to 270mm CRL. Ann Anat 2016;205:65-74.
131. Radlanski RJ, Renz H. An atlas of prenatal development of the human orofacial region. Eur J Oral Sci 2010;118(4)321-324.
132. Radlanski RJ, Renz H. Genes, Forces and Forms: Mechanical Aspects of Prenatal Craniofacial Development. Dev Dyn 2006;235(5):1219-1229.
133. Radlanski RJ. Oral structure and biology. USA: Quintessence Publishing, 2018.
134. Rafferty KL, Herring SW, Artese F. Three-dimensional loading and growth of the zygomatic arch. J Exp Biol 2000;203(14):2093-2104.
135. Rajeshwari MS, Pushpa M. Study of lateral pterygoid muscle and its insertion with the maxillary artery and buccal nerve and an anatomical classification based on its insertion. Int J Anat Res 2015;3(4):1680-1684.
136. Ramaesh T, Bard JBL. The growth and morphogenesis of the early mouse mandible: a quantitative analysis. J. Anat 2003;203(2):213-222.
137. Rayne J, Crawford GN. The development of the muscles of mastication in the rat. Ergeb Anat Entwicklungsgesch 1971;44(5):1-55.
138. Rees LA: The structure and function of the mandibular joint. Br Dent J 1954;96(6):125-133.

139. Reichert KB. Über die Visceralbogen der Wirbeltiere im Allgemeinen und deren Metamorphosen bei denReichert KB. Über die Visceralbogen der Wirbeltiere im Allgemeinen und deren Metamorphosen bei den Vögeln und Säugetieren. Arch Anat Physiol Wissensch Med 1837:120-220. Vögeln und Säugetieren. Arch Anat Physiol Wissensch Med 1837:120-220.
140. Rizzolo RJC, Madeira MC. Sistema articular. In: Anatomia Facial com Fundamentos de Anatomia Sistemica Geral. 5th ed. Sao Paulo: Ed Sarvier, 2005.
141. Roberts DS, Miller SA. Apoptosis in cavitation of middle ear space. Anat Rec 1998;251(3):286-289.
142. Robinson J, O'Brien A, Chen J, Wadhwa S. Progrenitor cells of the mandibular condylar cartilage. Curr Mol Biol Rep 2015;1(3):110-114.
143. Ródriguez JF, Mérida JR, Arráez L, et al. Morfología de la región posterior de la articulación temporomandibular en fetos humanos. Arch Esp Morfol 1999;4:25.
144. Rot-Nikcevic I, Downing KJ, Hall BK, Kablar B. Development of the mouse mandibles and clavicles in the absence of skeletal myogenesis. Histol Histopathol 2007;22(1):51-60.
145. Rot-Nikcevic I, Mardesic-Brakus S, Costain WJ, Saraga-Babic M, Kablar B. Role of skeletal muscle in mandible development. Histol Histopathol 2014;29(11):1377-1394.
146. Sano T. Recent developments in understanding temporomandibular joint disorders. Part 2: Changes in the retrodiscal tissue. Dentomaxillofac Radiol 2000;29:260-263.
147. Sato I, Miwa Y, Hara S, Fukuyama Y, Sunohara M. Tenomodulin regulated the compartments of embryonic and early postnatal mouse masseter muscle. Ann Anat 2014;196(6):410-415.
148. Satoh K. Comparative functional morphology of mandibular forward movement during mastication of two murid rodents, Apodemus speciosus (Murinae) and Clethrionomys rufocanus (Arvicolinae). J Morphol 1997;231(2):131-142.
149. Scapino RP. The posterior attachment: its structure, function and appearance in TMJ imaging studies. Part I. Journal of Craniomandibular Disorders and Facial and Oral Pain 1991;5(2):83-95.
150. Scheuer, L., & Black, S. Developmental Juvenile Osteology. San Diego, CA: Elsevier Academic Press, 2000.
151. Schmolke C. The relationship between the temporomandibular joint capsule, articular disc and jaw muscles. J Anat 1994;184:335-345.
152. Schumacher GH. Funktionelle Morphologie der Kaumuskulatur. Jena: VEB Gustav Fischer Verlag, 1961.

153. Shi HP, Gross MK, Kioussi. Muscle development: Forming the head and trunk muscles. Acta histochemica 2008;110:97-108.
154. Shibata S, Fujimori T, Yamashita Y. An in situ hybridization and histochemical study of development and postnatal changes of mouse mandibular angular cartilage compared with condylar cartilage. J Med Dent Sci 2006;53:41-50.
155. Shibata S, Sato R, Murakami G, Fukuoka H, Rodríguez-Vázquez JF. Origin of mandibular condylar cartilage in mice, rats, and humans: Periosteum or separate blastema? Journal of Oral Biosciences 2013;55:208-216.
156. Shibata S, Suda N, Fukada K, Ohyama K, Yamashita Y, Hammond VE. Mandibular coronoid process in parathyroid hormone-related protein-deficient mice shows ectopic cartilage formation accompanied by abnormal bone modeling. Anat Embryol (Berl) 2003;207(1):35-44.
157. Shibata S, Suzuki S, Tengan T, Ishii M, Kuroda T. A histochemical study of the developing condylar cartilage of the fetal mouse mandible using coronal section. Archs Oral Biol 1996;41:47-54.
158. Shibata S, Takahashi M, Fujikawa K. Histochemical and ultrastructural study of developing gonial bone with reference to initial ossification of the malleus and reduction of meckel's cartilage in mice. Anat Rec 2019;302(11):1916-1933.
159. Shih HP, Gross MK, Kioussi C. Cranial muscle defects of Pitx2 mutants result from specification defects in the first branchial arch. Proc Natl Acad Sci U S A 2007;104(14):5907-5912.
160. Siéssere S, Vitti M, de Sousa LG, Semprini M, Hallak Regalo SC. Bilaminar zone: anatomical aspects, irrigation, and innervation. Braz J Morphol Sci 2004;21(4):217-220.
161. Smeele LE. Ontogeny of relationship of middle ear and temporomandibular (squamomandibular) joint in mammals [corrected]. I. Morphology and ontogeny in man. Acta Anat (Basel) 1988;131(4):338-341.
162. Soft Imaging System GmbH. Analysis® User's guide 3D-Processing. Münster: Olympus Soft Imaging Solutions, 2008.
163. Sperber GH. Craniofacial Embryology. In: Dental Practitioner Handbook. 4th ed. Cambridge, England: University Press, 1989.
164. Sperber, G. Craniofacial development. Hamilton: Decker, 2001.
165. Spyropoulos MN. The morphogenetic relationship of the temporal muscle to the coronoid process in human embryos and fetuses. Am J Anat. 1977;150(3):395-409.

166. Stöckle M, Fanghänel J, Knüttel H, Alamanos C, Behr M. The morphological variations of the lateral pterygoid muscle: A systematic review. Annals of Anatomy 2019;222:79-87.
167. Strauss F, Christen A, Weber W. The architecture of the disk of the human temporomandibular joint. Helv Odontol Acta 1960;4:1–4.
168. Sugimoto T, Taya Y, Shimazu Y, Soeno Y, Sato K, Aoba T. Three-Dimensional visualization of developing neurovascular architecture in the craniofacial region of embryonic mice. Anat Rec 2015;298:1824-1835.
169. Suzuki A, Iwata J. Mouse genetic models for temporomandibular joint development and disorders. Oral Dis 2016;22(1):33-38.
170. Suzuki A, Nozawa-Inoue K, Ikeda N, Amizuka N, Ono K, Takagi R, Maeda T. Development of the articular cavity in the rat temporomandibular joint with special reference to the behavior of endothelial cells and macrophages. Anat Rec A Discov Mol Cell Evol Biol 2005;286(2):908-916.
171. Suzuki A, Sangani DR, Ansari A, Iwata J. Molecular mechanisms of midfacial developmental defects. Dev Dyn 2016;245(3):276-293.
172. Swiderski DL, Zelditch ML. The complex ontogenetic trajectory of mandibular shape in a laboratory mouse. J Anat 2013;223:568-580.
173. Symons NBB. The development of the human mandibular joint. J Anat 1952; 86(3): 326–332.
174. Tapia Contreras J, Cantín M, Zavando D, Suazo Galdames I. Percentage of lateral pterygoid muscle inserted in the disc of human temporomandibular joint. Int. J Morphol 2011;29(3):965-970.
175. Tengan T. Histogenesis and three-dimensional observation on condylar cartilage in prenatal mice. Kokubyo Gakkai Zasshi. 1990;57(1):32-57.
176. Thompson D'A.On Growth and Form.Cambridge: Cambridge University Press, 1917.
177. Troiano MF. New concept of the insertion of the lateral pterygoid muscle. J Oral Surg 1967;25(4):337-340.
178. Tsuchikawa K, Kumakura M, Kuwahara T, Ito Hidetoshi. Histological investigation of the development of the anlage of the mandibular condyle of mouse. Oral Science International 2010;7(2):66-71.
179. Tucker AS. Major evolutionary transitions and innovations: the tympanic middle ear. Philos Trans R Soc Lond B Biol Sci 2017;372(1713).1-11.
180. Turnbull WD. Mammalian masticatory apparatus. Fieldiana Geol 1970;18:149-356.

181. Uemura-Sumi M. The early development of the temporomandibular joint in the mouse. Hiroshima Daigaku Shigaku Zasshi 1985;17:304-310.
182. Urban DJ, Anthwal N, Luo Z-X, Maier JA, Sadier A, Tucker AS, Sears KE. A new developmental mechanism for the separation of the mammalian middle ear ossicles from the jaw. Proc R Soc B 2017;284:20162416.
183. Van der Linden EJ, Burdi AR, de Jongh HJ. Critical periods in the prenatal morphogenesis of the human lateral pterygoid muscle, the mandibular condyle, the articular disk, and medial articular capsule. Am J Orthod Dentofacial Orthop 1987;91(1):22-28.
184. Vinkka-Puhakka H, Thesleff I. Initiation of secondary cartilage in the mandible of the syrian hamster in the absence of muscle function. Arch Oral Biol 1993;38:49-54.
185. Vora SR, Camci ED, Cox TC. Postnatal Ontogeny of the Cranial Base and Craniofacial Skeleton in Male C57BL/6J Mice: A Reference Standard for Quantitative Analysis. Front Physiol 2016;6:417.
186. Washburn SL. The relation of temporal muscle to the form of the skull. Anat Rec 1947;99:239-248.
187. Wish-Baratz S, Ring GO, Hiss J, Shatz A, Arensburg B. The microscopic structure and function of the vascular retrodiscal pad of the human temporomandibular joint. Archives of Oral Biology 1993;38(3):265-268.
188. Wood AE, White RR 3rd. The myology of the chinchilla. J Morphol 1950;86(3):547-597.
189. Wood AE. Grades and clades among rodents. Evolution 1965;19:115-130.
190. Wyganowska-Świątkowska M, Kawala B, Kozanecka A, Kurlej W. Observations on muscular attachments to human developing mandible. Adv Clin Exp Med. 2012;21(4):447-454.
191. Yamaki Y, Tsuchikawa K, Nagasawa T, Hiroyasu K. Embryological study of the development of the rat temporomandibular joint: highlighting the development of the glenoid fossa. Odontology 2005;93(1):30-34.
192. Yamamoto M, Cho KG, Choi SS, Rodríguez-Vázquez JF, Murakami G, Abe S. Individual variations in the vascular content of retrodiscal tissue in the temporomandibular joint: a study using histological sections of human fetuses and magnetic resonance images of adults without pathology. Folia Morphol 2014a;73(2):153-158.
193. Yamamoto M, Kitamura K, Kasahara M, Serikawa M, Katumura S, Yoshimoto T, Matubayashi T, Odaka K, Matsunaga S, Abe S. Histological study of the developing pterygoid process of the fetal mouse sphenoid. Anat Sci Int 2017;92(3):364-372.

194. Yamamoto M, Shinomiya T, Kishi A, Yamane S, Umezawa T, Ide Y, Abe S. Desmin and nerve terminal expression during embryonic development of the lateral pterygoid muscle in mice. Archives of Oral Biology 2014b;59(9):871-879.
195. Yamane A. Embryonic and postnatal development of masticatory and tongue muscles. Cell Tissue Res 2005;322(2):183-189.
196. Yang RT, Zhang C, Liu Y, Zhou HH, Li ZB. Autophagy prior to chondrocyte cell death during the degeneration of Meckel's cartilage. Anat Rec 2012;295(5):734-741.
197. Yokohama-Tamaki T, Maeda T, Tanaka TS, Shibata S. Functional analysis of CTRP3/cartducin in Meckel's cartilage and developing condylar cartilage in the fetal mouse mandible. J Anat 201;218(5):517-533.
198. Zenker W. Das retroarticuläre plastische Polster des Kiefergelenkes und seine mechanische Bedeutung. Z Anat Entgesch 1956;119:375.
199. Zhang H, Zhao X, Zhang Z, Chen W, Zhang X. Immunohistochemistry study of Sox9, Runx2, and Osterix expression in the mandibular cartilages of newborn mouse. Biomed Res Int 2013;2013:265380 doi: 10.1155/2013/265380.
200. Zhang L, Yoshimura Y, Hatta T, Otani H. Myogenic determination and differentiation of the mouse palatal muscle in relation to the developing mandibular nerve. J Dent Res 1999;78(8):1417-1425.

8 AFFIDAVIT

“I, Esther María Fernández Rubio, by personally signing this document in lieu of an oath, hereby affirm that I prepared the submitted dissertation on the topic “Concerning the lack of a muscular antagonist to the lateral pterygoid. Morphogenetic and morphological investigations of the murine temporomandibular joint and masticatory muscles from stages E13.25 to P4”, independently and without the support of third parties, and that I used no other sources and aids than those stated.

All parts, which are based on the publications or presentations of other authors, either in letter or in spirit, are specified as such in accordance with the citing guidelines. The sections on methodology (in particular regarding practical work, laboratory regulations, statistical processing) and results (in particular regarding figures, charts and tables) are exclusively my responsibility.

My contributions to any publications to this dissertation correspond to those stated in the below joint declaration made together with the supervisor. All publications created within the scope of the dissertation comply with the guidelines of the ICMJE (International Committee of Medical Journal Editors; http://www.icmje.org) on authorship. In addition, I declare that I shall comply with the regulations of Charité – Universitätsmedizin Berlin on ensuring good scientific practice.

I declare that I have not yet submitted this dissertation in identical or similar form to another Faculty.

The significance of this statutory declaration and the consequences of a false statutory declaration under criminal law (Sections 156, 161 of the German Criminal Code) are known to me.”

Date Signature

9 CURRICULUM VITAE

My curriculum vitae does not appear in the electronic version of my paper for reasons of data protection.

10 LIST OF PUBLICATIONS

1. Fernández Rubio EM, Kokot K, Göbel M, Renz H, Radlanski RJ. Why is there no antagonist muscle to the lateral pterygoid? 50. Jahrestagung der Arbeitsgemeinschaft für Grundlagenforschung (AfG) der DGZMK, Mainz 11.-12. Jan 2018.

2. Göbel M, Fernández Rubio EM, Kokot K, Renz H, Radlanski RJ. Das gleichzeitige Vorhandensein von primärem und sekundärem Kiefergelenk bei der Maus. 50. Jahrestagung der Arbeitsgemeinschaft für Grundlagenforschung (AfG) der DGZMK, Mainz 11.-12. Jan 2018.

3. Kokot K, Göbel M, Fernández Rubio EM, Renz H, Radlanski RJ. Herkunft des Ligamentum sphenomandibulare bei der Maus. 50. Jahrestagung der Arbeitsgemeinschaft für Grundlagenforschung (AfG) der DGZMK, Mainz 11.-12. Jan 2018.

11 ACKNOWLEDGEMENTS

First and foremost, I would like to express my sincere gratitude to my thesis supervisor, Prof. Dr. Dr. Ralf Johannes Radlanski, for his continuous support, patience, motivation, and immense knowledge. His guidance helped me all the time of research and writing and it will surely remain of greatest value for my future.

Besides my supervisor, I would like to thank Dr. Herbert Renz for his insightful comments, hard questions and critical input. I have gained a lot of knowledge from the seminar discussions.

My sincere thanks also go to the medical technicians Frau Irene Schwarz and Frau Barbara Danielowski for preparing the histologic specimens and for their help during the 3D reconstruction process. I am also very grateful to Frau Beate Lion for her organizational assistance. Without the precious work of these women, it would not have been possible to conduct this research.

I would also like to acknowledge my PhD colleagues, Marlene Göbel and Karolin Kokot, who made this journey more enjoyable. Thank you for your help, discussions, and constructive criticisms.

I wish to express my gratitude to Arnold Jansen and Dr. Dr. J. Thomas Neisius for their empathy. It is a great pleasure to work with both of you.

To my friends in Madrid, Berlin and those around the world who were always there when I needed to drown my sorrows or share my happiness.

To my grandparents for their unconditional love. I am happy that you are with me.

To my sisters for sharing laughs every day and because your endless encouragement made all challenges easy to beat.

To my parents for their enormous effort to make education the cornerstone of our lives. Your love and support made me who I am, who I will be. This thesis is dedicated to you.